RIPENING OF PAH AND TPH POLLUTED SEDIMENTS

Determination and Quantification of Bioremediation Parameters

Promotor

Prof. dr. ir. W.H. Rulkens
Hoogleraar Milieutechnologie

Copromotor

Dr. ir. J.T.C. Grotenhuis
Universitair Docent bij de sectie Milieutechnologie

Samenstelling promotiecommissie

Dr. J. Harmsen	Wageningen Universiteit en Researchcentrum
Dr. ir. J. Joziasse	TNO Bouw en Ondergrond, Utrecht
Prof. dr. C.J. Ritsema	Wageningen Universiteit
Prof. dr. ir. T.S. Steenhuis	Cornell University, Ithaca NY, USA
Prof. dr. ir. S.E.A.T.M. van der Zee	Wageningen Universiteit

Dit onderzoek is uitgevoerd binnen de onderzoekschool SENSE (Socio-Economic and Natural Sciences of the Environment)

RIPENING OF PAH AND TPH POLLUTED SEDIMENTS

Determination and quantification of bioremediation parameters

Johan Vermeulen

Proefschrift

ter verkrijging van de graad van doctor
op gezag van de rector magnificus
van Wageningen Universiteit,
Prof. dr. M.J. Kropff,
in het openbaar te verdedigen
op woensdag 17 januari 2007
des namiddags te vier uur in de Aula

Vermeulen J, 2007. Ripening of PAH and TPH polluted sediments – Determination and quantification of bioremediation parameters

PhD-Thesis Wageningen University, Wageningen, The Netherlands – with references – with summaries in English and Dutch

ISBN: 90-8504-577-0

opgedragen aan mijn vader
W. Vermeulen (1927 – 1981)
en moeder
N.J. Vermeulen - Gideonse (1928 – 1998)

ABSTRACT

Vermeulen J, 2007. *Ripening of PAH and TPH polluted sediments. Determination and quantification of bioremediation parameters*. PhD-thesis Wageningen University. Wageningen.

Ripening is a process of initial soil formation that results from drainage of disposed water-logged sediments. Ripening can be subdivided into physical, chemical and biological ripening. Physical ripening irreversibly converts water-saturated clayey sediment into aerated (unsaturated), structured clayey soil by desiccation. Chemical ripening changes the chemical composition of sediments by oxidation processes like the conversion of reduced sulfur into sulfate. Biological ripening consists of the development of aerobic (micro)organisms and their effect on, for instance, soil organic matter (SOM) mineralization and degradation of organic pollutants. Ripening can be deployed as a bioremediation technique for dredged sediments that are polluted with polycyclic aromatic hydrocarbons (PAH) and total petroleum hydrocarbons (TPH).

In this study, bioremediation parameters were determined and quantified for different clayey dredged sediments. On the average, clay, soil organic carbon, and reduced sulfur contents of the studied sediments were 22, 7.6, and 1.2%, respectively. All sediments were heavily polluted with PAH and slightly to heavily polluted with TPH. The different sub-processes of physical ripening, chemical ripening, and biological ripening – including PAH and TPH degradation – were studied in several independent laboratory experiments. First, physical ripening was studied independently from chemical and biological ripening in artificial sediment aggregates that were physically ripened in specially designed microdepots. Furthermore, biological and chemical (biochemical) ripening processes were studied during an incubation experiment with slurried sediments that were optimally supplied with oxygen. In this way, the biochemical ripening processes could be studied independently from physical ripening. The effects of oxygenation on PAH and TPH degradation in slurried and consolidated sediments were quantified. Finally, the extent of oxygenation in a layer of clayey dredged sediments with average characteristics was calculated for different stages of field scale ripening using an oxygen diffusion model for aggregated soils.

It was concluded that matric potentials lower than -16,000 hPa are needed for complete physical ripening of dredged sediments. For a good description of physical ripening, not only information is needed on the lowest past matric potential, but also on the aggregate size distribution. Oxygen uptake rates of biochemically ripening sediments can completely be explained by oxidation of reduced sulfur and mineralization of SOM. Oxygen uptake for the degradation of PAH and TPH played only a negligible role in the total oxygen uptake. Fractions of sulfur and SOM that were oxidized and mineralized during biochemical ripening were 5 to 35% and 5 to 10%, respectively. PAH and TPH fractions that were degraded during biochemical ripening amounted up to 10 to 60% of the initial amounts of PAH and TPH. Relative PAH and TPH degradation rates are in the same order of magnitude as relative SOM mineralization rates. The model results showed that the maximum layer thickness of 'average' clayey dredged sediments that can be completely oxygenated increases from a few millimeters to 1.10 meter as a result of the combination of physical and biochemical ripening. Each doubling of oxygen uptake rates decreases the layer thickness that can be completely oxygenated with a factor 1.4.

The research described in this thesis increased the insight into the individual processes of physical ripening, biochemical ripening – including PAH and TPH degradation – that result from drainage of disposed water-logged sediments. This increased insight can be used to optimize conditions for ripening of dredged sediments at upland sediment disposal sites.

Key words: bioremediation, degradation, dredged sediments, mineralization, mineral oil, oxygen diffusion, oxidation, polycyclic aromatic hydrocarbons (PAH), ripening, soil formation, soil organic matter (SOM), sulfur, total petroleum hydrocarbons (TPH)

TABLE OF CONTENTS

1

GENERAL INTRODUCTION

Waar een gewoon en bondig antwoord mogelijk was,
maak je een eindeloze omweg.
De vraag over klei bijvoorbeeld had ik gewoon,
kort kunnen afdoen met te zeggen
dat klei met vocht vermengde aarde is,
zonder in te gaan op de toepassing.

Theaitetos – Plato

1.1 Dredged sediments

Worldwide, the water management and nautical functions of surface waters are threatened by settling sediments. To ensure sufficient water depth, huge amounts of sediments have to be dredged. It is estimated that in The Netherlands alone, 40×10^6 m^3 of sediments have to be dredged annually during the current decennium. 50% of this volume originates from freshwater (AKWA 2001).

For centuries, the dredged sediments have been used to raise the land and as natural fertilizers because of their nutrient content (Van Egmond 1971). Dredged material was a sought-after product. In the late 1970s, it appeared that urban and agricultural areas where dredged material had been utilized were heavily contaminated. We now know that 40% of the Dutch freshwater sediments are heavily polluted with a 'cocktail' of contaminants (AKWA 2001). Therefore, nowadays the dredged material that has been removed from channels and harbors is seen as an unwanted heritage from the past and no longer as a useful material (Huisman 2004).

Until the middle of the 1980s, large quantities of polluted dredged sediment were dumped into the North Sea. The Dutch government decided to stop this dumping as a first step to avoid negative effects on the marine environment. It was decided that the sediments had to be stored under controlled conditions. For this reason, a permanent disposal facility (the 'Slufter') was built near the North Sea coast in 1985. During the last decennia, several additional sediment disposal sites have been constructed. However, the costs of these permanent facilities are high and their capacity is limited (Huisman 2004). Therefore, dredging activities decline and vast amounts of polluted dredged sediments are stored temporarily at disposal sites located throughout The Netherlands. Through the years, this temporary upland disposal has become the most widely adopted alternative for dredged sediments worldwide (Singh et al. 1998).

1.2 Remediation of polluted sediments

In the Environmental Management Act of the Netherlands, dumping and storing in permanent disposal facilities are considered as the least desired alternatives to solve the problem of polluted dredged sediments (Ministerie van VROM 1992). Therefore, research into clean-up (remediation) and utilization of polluted dredged sediments has been stimulated by research programs of governmental organizations like the Dutch Directorate for Public Works and Water Management (e.g. POSW 1997, AKWA 1999a), water boards (e.g. GOBZ 1998, Stowa 1998), and research institutes (e.g. TNO-MEP 1997, CUR/NOBIS 1997).

In addition to these applied research programs, biological, chemical and physical remediation processes for sediments were also evaluated in different, more fundamental research projects of Wageningen University. For instance, Noordkamp (1999), Bonten (2001), Cuypers (2001), Mulleneers (2001), and Harmsen (2004) carried out research with sediments that were polluted with the widespread pollutants PAH (Polycyclic Aromatic Hydrocarbons) and mineral oil (characterized as TPH (Total Petroleum Hydrocarbons)). This research has contributed to a better insight into the processes that play a role in remediation of sediments.

Recently, insight among remediation specialists has grown that – from an ecotoxicological point of view – it is not necessary to completely remove the pollutants during remediation of soils and sediments. Only the potentially (bio)available fraction of the pollutants needs to be removed to reduce the risk for environment and humans to acceptable levels (Grotenhuis et al. 2004, Smit et al. 2005). Therefore, extensive remedation methods that aimed at total clean-up and have been studied and developed in the past (e.g. Noordkamp 1999 and Bonten 2001) will be applied less and less frequently. In the final report of the Dutch development programme for treatment processes for contaminated sediments (POSW 1997), it was concluded that immobilization and less extensive techniques like sand separation (possibly combined with polishing or flotation), landfarming and ripening – both typical examples of off-site remediation techniques – are the most promising of the currently available remediation techniques.

1.3 Ripening of PAH and TPH polluted dredged sediments

Ripening is a soil formation process that irreversibly converts waterlogged clayey sediment into aerated soil by the action of desiccation and structure development (Pons and Zonneveld 1965). During ripening at least part of the aerobically degradable contaminants will degrade to harmless products like carbon dioxide and water. The product of ripening is a diggable clay that depending on the physical and chemical composition can be deployed as a construction material (POSW 1997).

Ripening can either be seen as a first step in the processing of sediments through landfarming (Harmsen 2004), or as a more independent processing method, through which fine, clayey types of sediments are processed (POSW 1997). *In this thesis, we regard ripening as an independent bioremediation technique for PAH and TPH polluted sediments that are stored at upland disposal sites.* If sediments could be successfully remediated by ripening during temporary disposal space needed for permanent disposal facilities is not needed. Therefore, ripening is not only a promising remediation technique, but it also complies with the goals of the Dutch Environmental Management Act (section 1.2).

Numerous studies have confirmed that ripening has potential as a bioremediation technique for sediments that are polluted with organic pollutants like PAH and TPH (POSW 1995, 1997a, 1997b, GOBZ 1998, CUR/NOBIS 1999a, CUR/NOBIS 1999b, Harmsen 2004). In these studies, non-optimal removal of pollutants was attributed to a combination of limited bioavailability of the pollutants and limited availability of oxygen. However, most of these (field) studies could not separate the effect of the individual processes on the success of bioremediation because of the complex relationships between the different ripening processes and bioremediation. It was concluded in several studies that the available knowledge was not sufficient to guarantee optimal ripening during temporary upland disposal and that more fundamental research was needed (e.g. PHB 1996, TNO-MEP 1997, CUR/NOBIS 1997). In such fundamental research, the different aspects of ripening of dredged sediments – including degradation of PAH and TPH – should be studied independently (see also chapter 2 of this thesis).

1.4 Objective and outline of this thesis

Ripening of sediments is complex. Numerous interacting processes take place. Many are not well understood. The objective of this thesis is therefore to optimize bioremediation conditions in dredged sediments during temporary storage by better defining the individual ripening processes – including PAH and TPH degradation – and its interactions.

In chapter 2, a literature review is presented on the different aspects of ripening of clayey dredged sediments. Special attention is given to the subdivision into physical, biological and chemical ripening. The relevance of the ripening process as bioremediation technique for PAH and TPH polluted sediments is demonstrated. It is shown that more fundamental research is needed to quantify the different processes that are at work during upland disposal.

In chapter 3, all relevant physical process parameters are quantified for two sets of clayey dredged sediments at different stages of physical ripening. The first set of sediments was artificially ripened in the laboratory, using specially designed microdepots (Vermeulen et al.. 2000). The second set of sediments had undergone naturally ripening at field disposal sites that were extensively described by Harmsen (2004). The chapter includes the quantification of parameters governing shrinkage, swelling, moisture retention, hydraulic conductivity, oxygen diffusion, and structure development. Using the microdepots, physical ripening could be studied independently from chemical and biological ripening.

In chapter 4, the mineralization kinetics of soil organic matter (SOM) in dredged sediments is described with a double exponential model. Besides, information is given about nitrogen, phosphorus and sulfur mineralization. In chapter 5, the kinetics of PAH and TPH degradation in the five same sediments as the sediments of chapter 4 are described with a double exponential model and compared with the SOM mineralization kinetics of chapter 4. The biological and chemical (biochemical) ripening processes that are described in chapters 4 and 5 were studied in an incubation experiment with five types of slurried sediments that were optimally supplied with oxygen (Bonten et al. 1999). In this way, the biochemical ripening processes could be studied independently from physical ripening.

In the last part of chapter 5, measurements of oxygen penetration into consolidated sediment (aggregates) and PAH and TPH degradation in this consolidated sediment are presented.

In chapter 6, the extent of oxygenation in a layer of clayey dredged sediments at different stages of ripening is calculated for a field scale using an oxygen diffusion model for aggregated soils (Smith 1980). All values that were used for the model's input parameters origin, or were derived from, preceding chapters of this thesis. The relative importance of the different input parameters is shown for ripening of PAH and TPH polluted sediments that are stored at upland disposal sites.

Summaries and general conclusions of the thesis are presented in chapters 7 (English) and 7' (Dutch).

1.5 Research material

This thesis deals with ripening of *clayey* sediments because they are most widespread in delta areas like The Netherlands (AKWA 1999b) and because only sediments with clay contents higher than 8% and/or a SOM content higher than 3% exhibit substantial physical ripening (Pons and Zonneveld 1965). All sediments that were used in this study were collected from the bottoms of water bodies in The Netherlands. Their clay and SOM content ranged from 8 to 26% and 5 to 17%, respectively. They therefore roughly represent the 'standard sediment' (containing 25% clay and 10% SOM) that was defined in Dutch legislative texts that are used to assess the severity of cases of soil and sediment contamination (e.g. Ministerie van VROM 2000).

All studied sediments were heavily polluted with PAH (40 – 100 mg kg^{-1}) and slightly to heavily polluted with TPH (450 – 9,100 mg kg^{-1}).

2

RIPENING OF DREDGED SEDIMENTS

Literature review

Met de hand verzamelen ze slijk
dat ze meer door de wind dan door de zon laten drogen
en met deze turf verwarmen ze hun voedsel
en hun door de noordenwind verkleumde lichamen.

Naturalis historia – Plinius

This chapter is based on a paper that was originally published in the Journal of Soils and Sediments (Vermeulen et al. 2003)

Abstract

In The Netherlands about 40 million m^3 of sediment has to be dredged annually for both maintenance and environmental reasons. Temporary upland disposal is the most widely adopted alternative for dredged sediments worldwide. For good management of temporary disposal sites, knowledge is needed on the processes controlling the behavior of the sediments during disposal. Therefore, a review of the literature was made to get an integrated overview about processes that take place during temporary disposal.

After disposal of clayey sediments, the following spontaneous dewatering processes can be distinguished: sedimentation, consolidation, and ripening. Sedimentation and consolidation are relatively fast processes, whereas ripening can take up to several years. From a remediation perspective, the ripening of sediments is the most important dewatering process. Ripening, which may be subdivided into physical, chemical, and biological ripening, transforms sediment into soil. Physical ripening is the irreversible loss of water and results in the formation of soil prisms separated by shrinkage cracks. Continuing water loss causes a breaking up of the prisms into aggregates. The aggregates produced by this ongoing desiccation process usually remain quite large (> 50 mm) and can only be further broken down by weathering processes like wetting and drying or by tillage. As a result of the aeration caused by physical ripening, also chemical and biological ripening take place. Chemical ripening can be defined as the changes in chemical composition due to oxidation reactions and leaching of soluble substances. Biological ripening is the result of the activity of all kinds of soil fauna and flora that develop as a result of aeration, including both the larger and the microscopic forms of life. Decomposition and mineralization of soil organic matter caused by micro-organisms can be seen as the most important aspect of biological ripening. Many interactions exist between the different ripening processes.

Oxygenation of dredged sediment is improved as a result of the natural ripening processes: the air-filled porosity increases, the aggregate size decreases, and the initially high respiration rates caused by chemical and biological ripening decreases. Therefore, conditions in the disposal site become more favorable for aerobic biodegradation of organic pollutants like Polycyclic Aromatic Hydrocarbons (PAH) and mineral oil. It is concluded that the naturally occurring process of ripening can be used as a bioremediation technique. Ripening in an upland disposal site is an off-site technique, and therefore, the process could be enhanced by means of technological interference. However, it is concluded that the knowledge currently available about upland disposal is not sufficient to distinguish critical process steps during the ripening of PAH and mineral oil polluted sediments because of the complex relationships between the different ripening processes.

2.1 Introduction

Enormous volumes of sediments have to be dredged worldwide for both maintenance and environmental reasons. In The Netherlands, for example, 40×10^6 m^3 of sediment have to be dredged annually. 50% of this volume originates from freshwater. 40% of the freshwater sediment is heavily polluted with a 'cocktail' of contaminants (AKWA 2001). Sediments that are polluted with hydrocarbons like Polycyclic Aromatic Hydrocarbons (PAH) and mineral oil can potentially be remediated during temporary upland disposal. Because temporary upland disposal is easy and cost-effective, it is the most widely adopted disposal alternative worldwide. If the quality of the dewatered sediments that remains after temporary disposal meets the legal standards, they can be used in landscaping, agriculture, construction, restoration of previous industrial sites, the ceramic industry and as confining layers in and on landfills (Willet 1985, Singh et al. 1998). In delta areas like The Netherlands, the majority of dredged sediments is clayey (AKWA 1999b) and the dredged material in upland disposal facilities consequently consists primarily of clayey material.

For good management of temporary disposal sites, knowledge is needed on the processes controlling the behavior of the sediments during disposal. International literature about dredged sediments in upland disposal sites mainly focuses on chemical aspects and the potential risks for the environment (e.g. Singh et al. 1998 and Brandsch et al. 2001). Literature about dewatering processes and their relationship with aerobic biodegradation of organic pollutants is scarce or has not been directed toward the description of the processes taking place in the relatively thin layers of dredged sediment that are stored in an upland disposal facility (PHB 1997). Therefore, the aims of this review are: (i) to present an integrated overview of literature of geotechnique, soil science, and environmental technology about processes that take place after clayey dredged material is disposed, (ii) to show the relevance of these processes for biodegradation of PAH and mineral oil polluted dredged material, and (iii) to show where there is a lack of knowledge about the use of temporary upland disposal as a remediation technique.

In The Netherlands, the knowledge level about the topic is relatively high. Therefore, much of the data presented in this review originates from Dutch research. Other research in Europe is conducted in countries with large areas of surface waters like United Kingdom, Germany and Belgium. The Dutch conditions are more or less comparable with the conditions in the rest of Western Europe. Under different (climatic) conditions, the same processes occur, but their magnitude may be different.

2.2 Sedimentation, consolidation and ripening

The water content of dredged sediments that are transported through pipelines and disposed of in an upland disposal site is over 70% of the total weight. This water is removed from the disposal site by runoff (horizontally), drainage (downward) or evapo(transpi)ration (upwards). During this dewatering, sedimentation, consolidation, and ripening can be distinguished as processes that affect the intrinsic biodegradation of PAH and mineral oil (Fig. 2.1).

Sedimentation of the sediment particles takes place immediately after disposal of dredged material. If sediment particles can fall freely without hindrance, Stokes' law governs their settling rate. However, when solid concentrations are high, as in dredged material, hindered settling is usually observed (Imai 1980). Coarse particles composed of gravel and sand settle almost instantaneously. Particles smaller than 2 μm in diameter (clay minerals) have a very small settling rate. However, they are liable to collide and flocculate into flocs resulting in higher settling rates. Flocculation is a function of particle and electrolyte concentration: saltwater results in faster flocculation than freshwater. Even in freshwater, electrolyte concentrations are usually sufficiently high to cause flocculation (Hough 1957). Sedimentation of clayey material results in a honeycomb structure of clay platelets (Pons and Van der Molen 1965). In this honeycomb structure, much of the clay particles are dispersed and organized in a so called 'edge-to-edge or edge-to-face flocculated' association (Van Breemen and Buurman 1998, Grossman 1983, Van Olphen 1977). Sedimentation is a relatively fast process that takes place within hours or days. In general, coarse or high-density particles have higher sedimentation rates than small or low-density particles.

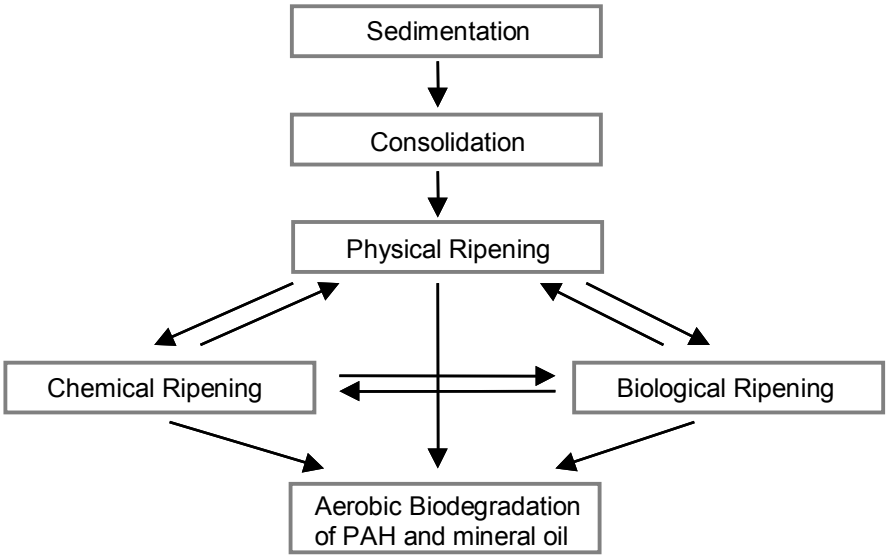

Fig 2.1 Intrinsic processes during temporary upland disposal of dredged material and their mutual relationships

Sedimentation is followed by a stage where the settling rate of the particles decreases significantly. During this phase, the flocs which are formed during sedimentation form bonds and 'self-weight consolidation' starts. The weight of overlying sediment forces out the pore water and the honeycomb structure collapses slowly at the bottom (Partheniades 1965). Different forms of consolidation can be distinguished including 'consolidation by overburden pressure' and 'consolidation by desiccation'. However, in this review we reserve the term 'consolidation' solely for 'consolidation by overburden pressure', whereas the term 'physical ripening' is used for 'consolidation by desiccation' (section 2.4.1). The driving force for 'consolidation by overburden pressure' is the pressure caused by the weight of overlying sediment (see also Appendix 3). The volume will only be reduced if water is able to drain, either upward or downward, from the sediment layer (Terzaghi and Peck 1967). Therefore, slow permeable sediment layers with a thickness of several meters may require consolidation periods of several decades. Rijniersce (1983) found permeability values for water of 1.7×10^{-4} m d^{-1} in a wide range of clay, and organic matter contents and pore volumes. However, Kim et al. (1993a) and Wichman (1999) measured different permeabilities for different degrees of consolidation, which is more likely. They report values from 1.0×10^{-5} to 3.0×10^{-2} m d^{-1} for void ratios (for definition, see chapter 3) ranging from 2.0 to 4.5 cm^3 cm^{-3}. Thin layers of sediment (< 2 m) result in consolidation periods on the order of months (AKWA 1999a). A linear relationship exists between the logarithm of the overburden pressure and the resulting void ratio (Bradford and Gupta 1986).

From a remediation perspective, the desiccation of dredgings is a more important compaction process. In soil science, this process is known as 'ripening'. This denotes the initial soil formation processes that render a soft alluvial deposit suitable for agricultural use. Hence, ripening is the very first stage of 'maturation' in the pedological sense (Pons and Zonneveld 1965). The term was coined as an analogy to the traditional term of 'ripening' used for cheese (Van Breemen and Buurman 1998). According to Pons and Van der Molen (1973), ripening may be subdivided into physical, chemical, and biological ripening. Although the three ripening processes proceed simultaneously and interact with

each other (Pons and Van der Molen 1973), physical ripening can be considered as the driving force of the whole ripening process.

In The Netherlands, the ripening process has been the object of extensive study during reclamation of the IJssel-Lake polders and ample Dutch literature is available on the subject (Rijniersce 1983). The processes taking place during dewatering of dredgings in an upland disposal site change soft anaerobic sediment into an aerated soil with structure. Therefore, the use of the term 'ripening' is also widely accepted to describe these processes in The Netherlands (Willet 1972, De Waard and Van de Velde 1981, Dekker 1981, Willet and Cavelaars 1981, Van Tol 1985, De Haan et al. 1998, Zevenbergen et al. 1999, Vermeulen et al. 2000, Harmsen 2001).

2.3 Physical ripening

Physical ripening can be summarized as follows: "physical ripening is a soil forming process by which a sediment that is exposed to drier hydrological conditions than those with which it can maintain equilibrium is practically irreversibly converted into more compact, aerated, more permeable material, the physical properties of which depend on the new hydrological conditions and which can be designated by the name soil" (Rijniersce 1983). Physical ripening consists of dehydration and shrinkage, increase of permeability, change from a soft to a friable or hard consistency (see also Appendix 2), and subsidence of the surface of the sediment, resulting in the formation of soil prisms separated by shrinkage cracks (Pons and Van der Molen 1973). Sediments that have no colloidal particles will not exhibit physical ripening phenomena. In practice, only sediments with a clay content higher than 8% and/or an organic matter content higher than 3% exhibit physical ripening (Pons and Zonneveld 1965).

2.3.1 Desiccation

The process of drying sediment is different from the normal drying of clayey soils. Under normal drying, clay platelets in a face-to-face orientation approach each other as a result of increasing capillary forces. Upon wetting, the distance between the platelets increases again and clayey aggregates regain their original volume (Bronswijk and Evers-Vermeer 1990). However, during physical ripening, the major part of shrinkage caused by an increase in capillary forces is irreversible (Kim et al. 1993b). This irreversibility is caused by a telescoping of the individual clay platelets in the honeycomb structures that remain after sedimentation (Pons and Zonneveld 1965). Due to this telescoping, individual clay platelets assume a face to face orientation (are 'stacked'). The process of telescoping results in irreversibly contracted honeycomb structures in which the clay platelets are more and more aggregated (Van Breemen and Buurman 1998, Van Olphen 1977). Only mechanical disturbance of the ripened material under wet conditions like 'puddling' can reverse this process (Pons and Zonneveld 1965). After a period of desiccation, the colloidal particles that have moved towards new positions of higher free energy will gradually rearrange their positions and orientations back towards a minimum free energy configuration. This process, that may occur if the soil stays at constant water content, is

called 'age-hardening by particle rearrangements' and results in an extra increase in strength of the soil (Dexter et al. 1988).

Rather than shrinking entirely in a vertical direction (consolidation) or uniformly in all three directions (three-dimensional isotropic shrinkage) the soil may show a distribution of cracking and subsidence which lies somewhere between these two extremes depending on the degree of physical ripening, strength and overburden load. Crack formation can occur only if the soil is firm enough to bear the load without flowing (Rijniersce 1984). Horizontal shrinkage is caused by the capillary attraction stress of pore water. A physical measure for this stress is the matric pressure (Baver et al. 1972, Appendix 3). A crack is initiated when the total stress at any point is equal to the tensile strength of the soil. Stresses of this magnitude are reached at matric pressures lower than about -200 hPa (Konrad and Ayad 1997). Primary cracks tend to form a hexagonal-type pattern on the surface, but in a vegetated surface they may run halfway through the rows of plants where the soil is wettest and hence weakest. When primary cracks reach a certain width, drying of the soil from the vertical crack faces occurs and horizontal secondary cracks may be induced (Dexter 1988). Further drying can produce vertical tertiary cracks. Fig. 2.2a (section 2.3.3) gives a schematic representation of primary, secondary, and tertiary cracks. Slow drying tends to produce wide cracks at large spacings, whereas rapid drying tends to produce more but narrower cracks at smaller spacings. On the average, distances between the primary cracks are about 50 cm (Selley 1976, Chertkov 2000). However, depending on the granular composition, distances between primary cracks range from 25 (Yaalon and Kalmar 1984) to 100 cm (Dasog et al 1988).

In cracked bare soils the greater part of evaporation occurs from the shrinkage cracks (Ritchie and Adams 1974, PHB 1997) whereas evaporation from cracks is negligible in cropped soils (Bronswijk 1991). Due to cracking, the permeability for water increases from the values mentioned in section 2.2 up to several hundred meters per day and is related solely to the 'crack permeability' (Rijniersce 1983). As their void ratio decreases gradually during shrinkage, the permeability of the formed soil prisms decreases. Physical ripening causes a higher degree of compaction than is brought about by consolidation, because the magnitude of matric pressures caused by evapo(transpi)ration can be much larger (up to thousands of hPa) than the overburden pressure caused by the overlying mass of sediments (up to hundreds of hPa). Data provided by Kim (1993a) suggest that a soil is almost completely physically ripened if a matric pressure lower than -1,000 hPa is reached.

The time needed to physically ripen a layer of sediments in a disposal site depends on different factors. If initial water contents are high, more water needs to be removed before physical ripening is complete. In The Netherlands – with an average annual evaporation surplus in the summer season of about 60 mm (Rijniersce 1983) – matric pressures in the (top)soil as low as -16,000 hPa can be reached (Bronswijk and Evers-Vermeer 1990). Under these humid climatic circumstances, a one-m thick layer of clayey sediments vegetated with natural vegetation can be physically ripened within six years. At a cultivated disposal site with dredged sediments, about two years are needed for this process (Harmsen 2001). Ripening can be enhanced by the construction of trenches of

the application of sediments in ridges. Also creation of permeable sand layer in between layers of dredged sediments can be advantageous. The presence of a (vacuum) tile drainage system can enhance downward water removal during consolidation (PHB 1997). Injection of sand slurry into the clayey dredged material to create thin internal drainage layers has been proved to be successful; attempts to apply electro-osmotic were not (Haliburton TA 1979). Cultivation of sediments creates new wet surfaces from which maximum evaporation can occur. Evaporation can also be stimulated by increasing the temperature, by vegetation, or by forced ventilation (Harmsen 2001). Under drier climatic conditions, the desiccation process can be much faster (Rijniersce 1983).

2.3.2 Ripening index

The stage of physical ripening can be described with a quantitative ripening index, called n-value. The n-value is an empirical measure of the water-binding capacity of the material at a certain ripening stage and is therefore closely related to the total porosity of the material. In the literature, the n-value is defined in several different ways (Pons and Zonneveld 1965, Pons and Van der Molen 1973, Soil Survey Staff 1975, Rijniersce 1983, Van Breemen and Buurman 1998). We here give the most widely used definition:

$$n_{rip} = \frac{w_{sat} - pR}{L + bH} \tag{2.1}$$

where:

n_{rip}	= n-value (g water g^{-1} clay)
w_{sat}	= saturated moisture ratio (g water (100 g)$^{-3}$ D.M.)
p	= water-storing capacity of non-colloidal parts (g water g^{-1} R)
R	= sand + silt content (g sand + silt (100 g)$^{-1}$ D.M.)
L	= clay content (g clay (100 g)$^{-1}$ D.M.)
b	= ratio between water adsorption of 1 g organic matter compared to that of 1 g clay (-)
H	= organic matter content (g organic matter (100 g)$^{-1}$ D.M.)

In soils with well-humified organic matter and illite-clay, a *b*-factor of 3 is valid. As most Western European clays mainly consist of illite and, except for peaty dredged material, most organic matter in dredged material has a high humification, it is also permissible to use a *b*-factor of 3 for dredged materials in Western Europe. The *b*-factor for partly disintegrated organic matter fluctuates between 3 and 9. The n-value ranges from 3.0 – 2.0 (unripe, recently deposited sediment) via 2.0 – 1.4 g g^{-1} (consolidated, but practically unripe), 1.4 – 1.0 g g^{-1} (half-ripe), and 1.0 – 0.7 g g^{-1} (nearly ripe) to < 0.7 g g^{-1} (ripe, normal soil). Generally, a *p*-factor of 0.2 g g^{-1} is used. However, for very sandy material this figure might be somewhat higher and in very clayey sediment somewhat lower (Pons and Zonneveld 1965). At several places in the literature, it is suggested to use a *p*-factor of 0.3 g g^{-1} for dredged sediments (Willet 1972, De Waard and Van de Velde 1981, PHB 1995). The n-value for soils with clay minerals other than illite, can be estimated if the ratio between the cation exchange capacity (CEC) of the clay mineral in question and the CEC of illite is known (Pons and Zonneveld 1965, Appendix 2).

Table 2.1 provides the values of several characteristics of clayey dredgings after sedimentation (n_{rip} < 3 g g^{-1}), after consolidation (n_{rip} < 2 g g^{-1}), and after physical ripening

(n_{rip} < 0.7 g g^{-1}). All values (see also appendix 1) in this table are calculated and based on the n-values.

Table 2.1 Characteristics of clayey dredged material with different n-values (n_{rip}): saturated moisture ratio on mass (w_{sat}) and volume basis (ϑ_{sat}), dry matter content (*D.M.*), wet bulk density ($^b\rho_w$), dry bulk density ($^b\rho_d$), and relative layer thickness (*Z*) after sedimentation, after consolidation, and after physical ripening

Stage	w_{sat} [b] (mass-%)	ϑ_{sat} [cd] (cm^3 cm^{-3})	*D.M.* (mass-%)	$^b\rho_w$ [d] (g cm^{-3})	$^b\rho_d$ [d] (g cm^{-3})	*Z* (-)
sedimented, n_{rip} < 3 g g^{-1} [a]	< 178	< 4.46	> 36	> 1.28	> 0.46	< 1.00
consolidated, n_{rip} < 2 g g^{-1} [a]	< 123	< 3.08	> 45	> 1.37	> 0.61	< 0.75 [e]
ripe, n_{rip} < 0.7 g g^{-1} [a]	< 52	< 1.29	> 66	> 1.66	> 1.09	< 0.61 [f]

[a] n_{rip} = n-value (Eq. (2.1))

[b] $w_{sat} = n_{rip}(L+3H) + 0.2R$ (derived from Eq. (2.1)) with L = 25%, H = 10%, and R = 65% (typical values for Dutch sediments)

[c] ϑ = volume water / volume solids

[d] ϑ_{sat}, $^b\rho_w$, and $^b\rho_d$ are calculated assuming a particle density of 2.51 g cm^{-3}

[e] calculated with $^b\rho_d$ before and after consolidation: Z = 1(0.46 / 0.61)1 (no crack formation, 1-dimensional subsidence)

[f] calculated with $^b\rho_d$ before and after ripening: Z = 0.75(0.61 / 1.09)1/3 (crack formation, 3-dimensional isotropic shrinkage)

2.3.3 Structure development

Desiccation causes polygonal fractures at the surface forming a very coarse prismatic structure (Fig. 2.2a). The soil prisms are subsequently broken down into coarse angular or subangular blocky and thick platy aggregates (Wilding and Hallmark 1984). Blocky aggregates may be found in the surface layers, whereas platy aggregates exist in the subsurface layers due to overburden pressure (Ahmad 1983). At the same time, the coarse prismatic structure may be formed deeper in the profile (Fig. 2.2b).

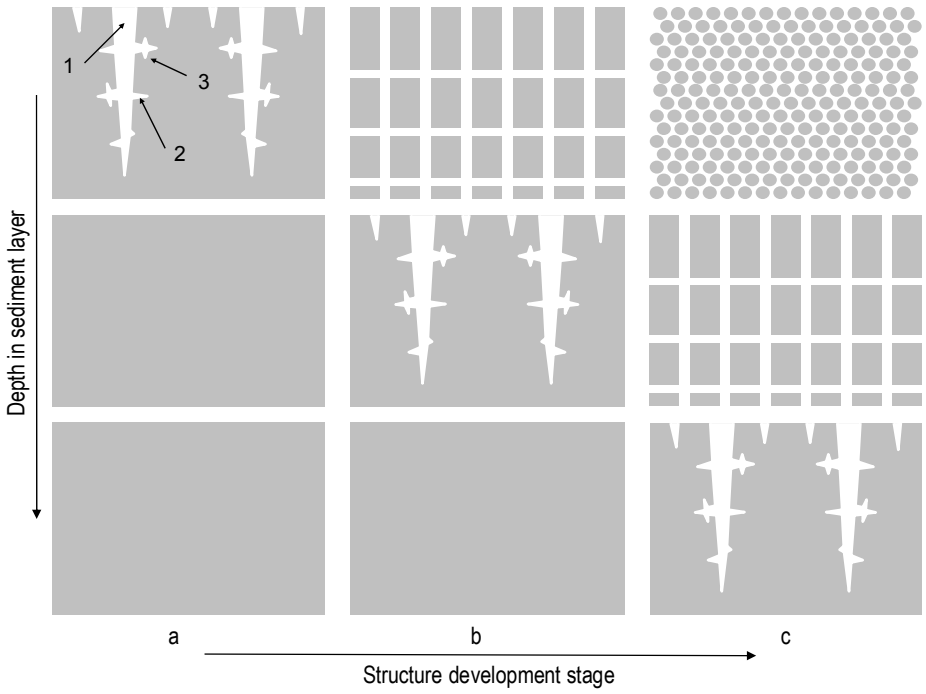

Fig. 2.2 Schematic cross section of a layer of dredged material at different stages of structure development (After Baver et al. 1972, Dexter, 1988 and Vervoort et al. 1999). a = very coarse prismatic structure with primary (1), secondary (2), and tertiary cracks (3); b = coarse blocky and platy aggregates on very coarse prismatic structure; c = medium and fine aggregates on coarse blocky and platy aggregates and very coarse prismatic structure

The blocky aggregates are quite large (> 50 mm, Baver et al. 1972) and can be further broken down to medium and fine aggregates (< 50 mm) by applying mechanical stresses, externally by tillage, internally by weathering processes (wetting/drying or freezing/thawing) or by a combination of the two (Dexter 1988, Baver et al. 1972). The more intensively soils are dried, and the more often they are rewetted, the smaller the average aggregate diameter becomes. Only soils with over 15% clay tend to form stable aggregates (Horn et al. 1994). Provided that the layer of dredged material is thick enough, a soil profile as described by Southard and Buol (1988) and Vervoort et al. (1999) is formed (Fig. 2.2c). The thickness of the different layers depends on evapo(transpi)ration surplus and the amplitude of the groundwater level.

The process of reduction in aggregate size is called 'mellowing' (Utomo and Dexter 1981a) and simultaneously causes an increase in bulk density and strength of the resulting aggregates (Hadas 1990). The degree of the dependence between strength and aggregate size has been developed as a measure of soil friability (Utomo and Dexter 1981b). Dexter et al. (1984) found extreme high values of friability in young soils from reclaimed polders, meaning that aggregates can be broken down easily by weathering processes. Since these young soils are still in the process of physical ripening, this is also an indication that aggregates which are formed in a disposal site for dredged material are easily broken down into smaller aggregates. Friability is positively correlated with increasing organic carbon content, decreasing sand content, increasing hydraulic conductivity, and decreasing bulk density (Watts and Dexter 1998). The friability of a given soil tends to increase as a result of wetting and drying, freezing and thawing, and the addition of lime, gypsum or phosphoric acid (Watts and Dexter 1998, Chan et al. 1999).

The geometric mean diameter (*GMD*) and the log standard deviation ($\sigma_{log\ d}$) can be useful to quantify the structure development process (Allmaras et al. 1965). During a laboratory experiment with a reworked (= unripe) clay soil, Shiel et al. (1988) found that the *GMD* decreased from 44.7 mm after the second wet/dry cycle to 0.8 mm after the eighth cycle. $\sigma_{log\ d}$ decreased from 1.0 to 0.3. The aggregate decay rates decreased with falling aggregate size, suggesting that an equilibrium aggregate size distribution was approached.

Thus, the stability of the formed aggregates depends on the amount of previous wet/dry cycles. Besides, chemical processes (section 2.4) are also involved in aggregate stabilization. 'Age-hardening by cementation' (Dexter et al. 1988) occurs if chemical bonds between soil particles are formed by agents like $CaCO_3$, Al and Fe-oxides, divalent cations, and humus (Koorevaar et al. 1983). Furthermore, aggregate stabilization by biologically produced agents (section 2.5), like extracellular metabolic products of colonies of bacteria and root exudates, has been observed (Horn et al. 1994).

2.3.4 Aeration

Since oxygen diffusion into the layer of sediments is largely determined by the presence of continuous air-filled macropores (Bronswijk 1991), aeration is enhanced by the formation of structure. Soil aeration is governed by the transport of oxygen from the atmosphere into the soil and consumption of oxygen by biological respiration or by chemical

reactions (Horn et al. 1994). Most soil physicists support the hypothesis that diffusion rather than convection is the more important mechanism of soil aeration. However, convection can contribute significantly to soil aeration in certain circumstances (Hillel et al. 1998). Diffusion rates through the air-filled cracks (macropores) into the soil system are relatively high, whereas diffusion rates through water-filled pores in the aggregates (micro-pores) are relatively low (Smith 1980). However, if aggregate size decreases, the transport of oxygen into the bed of aggregates is inhibited due to an increase in tortuosity of the macropores (see Fig. 2.2). It was shown by Bronswijk (1991) that inter-aggregate diffusion rates in a well-structured clay soil can be 70% lower than the diffusion rate in a cracked, poorly structured clay soil due to an increase in tortuosity of macropores. So, the requirements for inter- and intra-aggregate aeration are in conflict, but if respiration rates and inter and intra-aggregate diffusion coefficients are known, it is possible to estimate the aggregate size range and thickness of the aggregate bed that prevents the onset of anoxic conditions (Braunack and Dexter 1989).

In agricultural soils, diffusion coefficients within aggregates range from about 1.4×10^{-7} for water-saturated to 1×10^{-2} cm^2 s^{-1} for very dry aggregates (Smith 1980, Sextone et al. 1985, Sierra et al. 1995, Rappoldt 1995), whereas inter-aggregate diffusion coefficients range from about 8×10^{-6} to 8×10^{-2} cm^2 s^{-1} (Smith 1980, Bronswijk 1991). Complete oxygenation of soil aggregates can be expected only when pores within the aggregates become filled with air or when micro-cracks start to develop (Bakker and Bronswijk 1993) as a result of ongoing desiccation. Heavy clay soils can have anaerobic centers even at matric pressures of -16,000 hPa (Braunack and Dexter 1989). In these soils, only reduction of aggregate size by weathering or tillage may lead to complete oxygenation.

Calculations made by Smith (1980) show that 65% (at the surface) to 90% (at 1 m depth) of the total volume is anoxic in a soil profile with air-filled macropores and water-saturated aggregates (GMD = 10 cm; $\sigma_{log\ d}$ = 1) and a respiration rate of the aggregate matrix (Q) of 2×10^{-7} cm3 O_2 s^{-1} cm^{-3}. A GMD of 10 cm and a $\sigma_{log\ d}$ of 1 are valid for dredged material in an initial stage of structure development (section 2.3.3). However, it is expected that chemical and biological ripening processes in dredged material cause a higher respiration rate than the respiration rate used by Smith. Therefore, larger fractions of the total volume are expected to be anoxic in a temporary disposal site.

2.4 Chemical ripening

Oxidation combined with chemical changes as a result of the improved aeration by physical ripening causes the following processes: "oxidation of soil components that are stable only under reduced conditions, change of ionic composition and concentration of the soil solution, weathering of less stable minerals, change of ratios of adsorbed ions, and the formation of new minerals and precipitates" (Pons and Van der Molen 1973).

Conversion of reduced sulfur compounds plays an important role during chemical ripening. In general, inorganic sulfur compounds dominate in industrialized environments (Tack et al. 1997). In the IJssel-Lake polders in The Netherlands, one year of chemical ripening of the top layer led to a sulfide decrease of 30%. After 15 years, a reduction of

60% was reached. Initially, FeS was oxidized to $Fe(OH)_3$ and H_2SO_4, which is a chemical process. In a later stage, also the more stable FeS_2 (pyrite) can be oxidized (De Glopper et al. 1992). The last oxidation proceeds slowly, but can be enhanced by a factor of 10^6 by the microorganism *Thiobacillus ferrooxidans* at pH values lower than 4.5 (Evangelou 1998). Tack et al. (1997) found no conversion of pyrite during 30 days of drying and oxidizing contaminated dredged material with a pH of 7.6. Other sulfides were completely converted to sulfate.

One of the effects of oxidation is a drop in pH, which is mainly due to the formation of sulfuric acid. Also (biological) oxidation of soil organic matter produces acid (Singh et al. 1998). In low-buffered sediments, this leads to a mobilization of trace metals, particularly Cd and Zn compared to Cu and Pb (Calmano et al. 1993). Stephens et al. (2001) and Singh et al. (2000) showed that the leachability of Zn, Cd, Cr, Cu, Ni, Pb, and As increases during drying and oxidation of a dredged canal sediment. Most dredged material in The Netherlands – except dredgings from peatland waters – contains an excess of calcite, and therefore seems not to be vulnerable to acidification (Zevenbergen et al. 1999). However, also in well-buffered sediments, mobilization of trace metals during oxidation cannot be excluded (Calmano et al. 1993). The mobilization and transfer of toxic trace metals from a disposal site can be an environmental concern. Uptake by plants and animals and transport by runoff and through percolating water are the major sources of metal migration from upland disposed dredged materials into the environment. Before disposing dredged material in an unconfined upland disposal site, a combination of chemical and biological methods is needed to acquire a complete picture of the potential environmental impact (Singh et al. 1998). After this, a decision can be made concerning what measures should be taken to prevent metals from migrating into the environment.

Contrary to the behavior of the above mentioned trace metals, Mn and Fe-mobility is lowered during oxygenation. The lower solubility of iron can be explained by the conversion to insoluble iron oxyhydroxides (Singh et al. 1998). Also a part of the previously water-soluble P-complexes with Ca, Mg, Al, and Fe can precipitate (Glinski and Stepniewski 1985). Precipitates can improve the structure stability, as was already discussed in section 2.3.3.

The buffering by calcite results in decalcification. Within four years of ripening, calcite concentrations can decrease from 10 to about 9%. Excess amounts of calcite together with oxidation of sulfides result in a relatively high amount of adsorbed calcium cations on the soil complex which is favorable for the development of a good soil structure (De Glopper et al. 1992). If no calcite is available in clayey dredged material, clay particles become dispersed and Acid Sulfate Soils or Solonchak Soils may develop which are characterized by a poor soil structure. Acid Sulfate Soils can develop in dredgings with high amounts of reduced sulfur (Pons and Van der Molen 1973, Van Mensvoort and Dent 1997), whereas Solonchak Soils can develop in dredgings with relatively high amounts of Na (Pons and Van der Molen 1973, Van Breemen and Buurman 1998). In saltwater dredgings, the NaCl concentration decreases depending on the precipitation surplus in winter. Complete desalinization from 6 g to concentrations lower than

0.5 g NaCl l^{-1} can take up to 16 years. During chemical ripening, significant amounts of potassium can leach (De Glopper et al. 1992).

The visible result of chemical ripening is a change from a nearly black color of the reduced material to mostly lighter, brownish or yellowish gray colors. The change in color is caused by the oxidation of FeS to $Fe(OH)_3$. The redox potential (Eh) is generally accepted as being the best indicator for evaluating the degree of oxidation in soils (Glinski and Stepniewski 1985). As a result of aeration, Eh increases from -300 to -250 mV to +400 to +700 mV (Patrick et al. 1996). During the increase of redox potential, reduced components are oxidized in the following sequence: organic matter → CO_2, S^{2-} → SO_4^{2-}, Fe(II) → Fe(III), NH_4^+ → NO_2^- and NO_3^-, Mn(II) → Mn(IV).

Beside the pyrite oxidation mentioned, numerous other chemical processes are biologically catalyzed. The conversion of NH_4^+ to NO_2^- and NO_3^- is an enzyme-driven reaction and can therefore only be carried out by specialized microorganisms like *Nitrosomonas* and *Nitrobacter* (Evangelou 1998). Several researchers classify the decomposition and mineralization of organic components also as a chemical ripening process (Pons and Zonneveld 1965, Pons and Van der Molen 1973, Buol et al. (1973). However, we prefer to classify this last process as biological and it will therefore be discussed in section 2.5.

2.5 Biological ripening

Biological activity develops best in a humid climate, in soils that are not extremely wet or dry. Therefore, physical ripening makes it possible for biological activity to flourish (biological ripening). "Biological ripening is the result of activity of all kinds of soil fauna and flora, including both the larger and the microscopic forms of life, but not including the direct activity of man" (Pons and Zonneveld 1965).

2.5.1 Development of soil fauna and flora

In the first stage of ripening, aerobic bacteria can develop. At matric pressures lower than -5,000 hPa, conditions become more favorable for fungi (Parr et al. 1981). During dewatering and subsequent oxygenation of an unripe soil in a polder in The Netherlands, the number (plate counts) of aerobic microorganisms increased from 1.0×10^6 (at the moment that the water had been pumped out) via 5.0×10^6 (after one year of dewatering) and 5.0×10^7 (after two years) to 6.5×10^7 (after four years) per gram soil. In old arable soil in the neighborhood of this polder, 9.0×10^7 microorganisms per gram soil were found (Van Schreven 1962). Development of microorganisms during temporary upland disposal of sediments shows the same pattern, more or less. Harmsen and Bouwman (2002) found that, during the land farming of polluted sediments, time and tillage positively affected bacterial biomass, and the numbers and diversity of nematodes.

If desiccation proceeds, aerobic microbial activity might be limited by a lack of moisture. Different attempts have been made to quantify the effect of moisture on the microbial activity in soils (Parr et al. 1981). Rijtema et al. (1999) summarized data found in the

literature in a reduction factor for moisture stress conditions: at matric pressures higher than -250 hPa, moisture is optimal for microbial activity, whereas activity is inhibited for 80% at matric pressures lower than -16,000 hPa. Matric pressures lower than -16,000 hPa do not occur in The Netherlands (Bronswijk and Evers-Vermeer 1990). Therefore, complete inhibition of microbial activity due to moisture limitation is not expected. Intermittent drying and wetting, and freezing and thawing, cause not only a further breakup of aggregates (section 2.3.3), but can also have a positive effect on microbial activity (Ross 1989).

Worms, that preferably live in wet soils and can even survive in entirely anaerobic sediments, are the most important member of the macro fauna that is involved in ripening of dredged material (Bal 1982). Other fauna prefers moist to dry soil and is therefore not discussed in this review. Worms can appear in ripening sediments by different mechanisms: by cocoons that are disposed with the sediment, by birds which carry cocoons, or by natural horizontal dispersion which is 4 – 10 meters per year, on the average (Bal 1982).

During dewatering, so-called 'pioneer vegetation' develops. Three stages can be distinguished during this development: supply of seeds by wind and birds, germination of the seeds, and competition between species (Van Duin 1976). Some months after polders fell dry in The Netherlands, they were occupied by a vigorous vegetation of the marsh fleawort (*Senecio congestus*), celery leaved buttercup (*Ranunculus sceleratus*), sea club-rush (*Scirpus maritimus*), and knotgrass (*Polygonum nodosum*). To accelerate physical ripening and to keep down weeds, large areas of the polders were sown with common reed (*Phragmites australis*) some years after they had fallen dry (Bal 1982). Natural vegetation also fully covered temporary disposal sites that were filled with PAH and mineral oil polluted sediments within one to two years (Harmsen 2001). Usually, plant growth will not be limited by a lack of nutrients, because dredged sediments are rich in both organic and mineral nutrients.

2.5.2 Effects of soil fauna and flora

One of the results of microbial activity is the complete decomposition of some components of soil organic matter (SOM) and the partial conversion of other components to compounds of intermediate complexity. These may reunite to form new, more stable organic substances: humus. Anaerobic microorganisms that are present in unripe sediments are able to degrade organic matter. However, this process is 100 to 1,000 times slower than the process under aerobic conditions (Rijtema et al. 1999).

The rate of SOM decomposition depends on its 'quality'. This quality depends on the amount of lignin and the relationship between the energy (C) in the SOM and its nutrient content (N and P). In general, the decomposition rate depends more on the amount of lignin than on the other factors (Ross 1989). Carbohydrates are by far the most important degrading fractions of SOM in sediments (Conrad 1999). Initially, there is a rapid breakdown of these carbohydrates, resulting in a more resistant material. Because of this, overall SOM degradation rates decrease with time (Janssen 1984). Due to the different

mentioned reasons, SOM degradation rates vary over an order of magnitude (Middelburg 1989). Janssen (1984) reports aerobic degradation rates (k) between 2.0 y^{-1} for fresh, labile SOM like leaves and other plant residues and 0.02 y^{-1} for well-humified, stable SOM.

Sediments that contain much fresh SOM can have a relatively high C/N ratio (≈ 20 g g^{-1}). However, these high C/N ratios will decrease to values close to 10 g g^{-1} as a result of biological ripening (Pons and Zonneveld 1965). If SOM is degraded, organic N and P are transformed into inorganic nutrients. Part of these nutrients is immobilized through the biomass-synthesis. Depending on the C/N and C/P ratios of the original SOM, net mineralization or immobilization can take place (Rijtema et al. 1999). When C/N ratios are less than 20, net N-mineralization occurs, whereas in systems with C/N ratios above 30 – 35 g g^{-1}, net N-immobilization takes place. Generally, if C/P is less than 200 g g^{-1}, net mineralization of phosphorus occurs, whereas when C/P is above 300 g g^{-1}, net immobilization occurs (Evangelou 1998). There are indications, however, that the phosphorus mineralization and immobilization, compared with the nitrogen mineralization, is less dependent on the mineralization of organic phosphates, due to the availability of relatively large quantities of inorganic phosphates (Rijtema et al. 1999).

The oxidation of SOM by microorganisms affects the course of physical and chemical ripening. Metabolites that are formed during SOM degradation can increase the aggregate stability (Wilding and Hallmark 1984). During SOM degradation, the CEC increases, whereas the water absorption capacity (b-factor in Eq. (2.1)) decreases (Pons and Zonneveld 1965). Many chemical processes (section 2.4) are catalyzed by the activity of microorganisms.

By the activity of macro fauna that enters the sediment after conditions are improved, stratified sediments are mixed (Pons and Van der Molen 1973). The blocky aggregates formed by weathering processes (section 2.3.3) can be transferred into granular aggregates when larger fauna-species ingest soil and produce excreta, and when biopores are formed (Oades 1993). Although earthworms prefer a wet environment, they have the ability to crack soil by tensile stresses (McKenzie and Dexter 1988). Annually, worms may work 5 to 120 tons of soil per hectare and may translocate this through the soil. Worms move down to greater depths when they are forced to do so for various reasons, for instance due to heating, desiccation or freezing. For this reason earthworms which usually live at or near the surface can be found down to 1 – 2 m depths (Bal 1982). Earthworms produce mainly vertical pores up to 1 cm in diameter, sometimes to depths of several meters (Van Bremen and Buurman 1998). The ingestion of soil by earthworms can promote the decomposition of soil organic matter. The importance of worms was already recognized by Darwin (1881), who observed that they consume soil, which is often excreted at the soil surface in the form of worm casts. The activity of earthworms develops a granular sponge-like soil structure that promotes high infiltration, high water-holding capacity and good aeration.

Roots of vegetation attract extra water which enhances desiccation (section 2.3.1) of the sediment. Roots also have the ability to mix the soil particles (Pons and Zonneveld 1965). Some plants are able to extract water from totally reduced sediment layers (Pons and

Zonneveld 1965). Because roots of these plants penetrate into the unripe dredged sediment and extract water at depth, physical ripening can take place deeper in vegetated sediment than in non-vegetated sediment. Although roots grow mainly in moist soils with low tensile strengths, and even then prefer to grow in pores rather than through aggregates, plant roots have the ability to crack soil by tensile stresses (Misra et al. 1986). Monocotyledonous plants such as grasses have numerous fine roots which dry the soil at countless sites, thus creating many non-oriented cracks which give rise to a granular, crumb structure (Oades 1993). As already mentioned in section 2.3.3, the production of root metabolites favors the formation and stability of a granular structure (Wilding and Hallmark 1984). Some wetland plants possess a root ventilation system that can produce downward oxygen fluxes between 0.5 (basket willow, *Salix viminalis*) and 8 g m^{-2} d^{-1} (common reed, *Phragmites australis*) which may enhance chemical and biological oxidation in the area surrounding the roots (Trapp and Karlson 2001).

2.6 Aerobic biodegradation of PAH and mineral oil

PAH and mineral oil biodegradation has been discussed extensively (e.g. Wilson and Jones 1993). Here, we will discuss the topic briefly to identify its relationship with ripening of sediments during temporary upland disposal. PAH and mineral oil can be biodegraded under both aerobic and anaerobic conditions. However, like the biodegradation of SOM, anaerobic biodegradation of PAH and mineral oil is about a factor 1,000 slower than aerobic biodegradation (Van Agteren et al. 1998). Therefore, oxygen can be seen as the first prerequisite for bioremediation of PAH and mineral oil polluted sediments. In general, an air-filled pore space > 10% and a redox potential > 50 mV are assumed to be sufficient for aerobic microbial activity. Furthermore, the microbial activity is dependent on other chemical and physical conditions in the soil, such as pH, nutrient availability and moisture (Table 2.2).

Table 2.2 Environmental conditions affecting biodegradation of organic contaminants in soil (After Wilson and Jones 1993)

Parameter	Optimal conditions for aerobic microbial activity
Oxygen content	air filled pore space > 10%
Redox potential	> 50 mV (aerobes), < 50 mV (anaerobes)
Soil moisture	25 – 85% of water-holding capacity (matric pressure ≈ -300 hPa)
Nutrient content	C:N:P 120:10:1, Salts < 4%
Soil pH	5.5 – 8.5
Temperature	15 – 45 °C

In The Netherlands, with its temperate climate and typically well-buffered, nutrient-rich sediments, conditions for temperature, soil pH, and nutrient content in ripened sediments are expected to meet the requirements mentioned in Table 2.2. Obviously, microbial activity and therefore aerobic biodegradation will be inhibited during wintertime. Furthermore, biodegradation of PAH and mineral oil may be influenced by oxygen limitation, if the sediment is still unripe, or by moisture limitation if the sediment has dried out too much.

Even in a ripe soil, anoxic centers of aggregates can result in anoxic conditions in 65% of the total volume at the surface to 90% at 1 m depth (section 2.3.4). In unripe, dredged

sediments, chemical and biological ripening processes cause a higher respiration rate than the respiration rate used by Smith (1980). Therefore, even larger fractions of the total volume are expected to be anoxic in a temporary disposal site. Complete oxygenation of the aggregates – and therefore optimal conditions for aerobic biodegradation – is expected only when pores within the aggregates become filled with air or when micro-cracks start to develop, both as a result of ongoing desiccation. Nocentini and Pinelli (2001) proved experimentally that PAH degradation in the interior of wet aggregates is indeed limited by oxygen availability. If desiccation proceeds too far, aerobic microbial activity might be limited by lack of moisture. However, in The Netherlands, complete inhibition of microbial activity due to moisture limitation is not expected (section 2.5.1).

The presence of contaminants that are toxic, such as trace metals and cyanides, may hinder degradation by microorganisms (Wilson and Jones 1993). However, the effect of this seems to be negligible in general, because of their relatively low availability in soil (Riis et al. 2002). Other limiting factors are soil properties like SOM, texture and structure, and the biodegradability of the specific PAH and the mineral oil. Finally, the indigenous microorganisms must be able to degrade the pollutant.

It should be stressed that only the bioavailable part of the contaminants can be biodegraded (Cuypers et al. 2000). The fraction of PAH that is bioavailable depends on different sediment characteristics and decreases with time, which is called 'aging'. Among other factors, aging is enhanced by the wetting and drying cycles (White et al. 1997) that occur during ripening. In many cases, the non-available part of the pollutant causes hardly any risk (Cuypers 2001), and only the bioavailable part of the pollution needs to be removed during remediation.

2.7 Ripening as bioremediation technique

The naturally occurring process of ripening can be used as a bioremediation technique during temporary disposal of PAH and mineral oil polluted sediments. Ripening is an off-site technique and it is therefore possible to enhance the process by means of technological interference like installation of a tile drainage system, stimulation of plant growth, addition of oxygen release compounds (Koenigsberg and Sandefur 2001), addition of soil conditioners that increase the friability (Watts and Dexter 1998, Chan et al. 1999), tillage, mechanical ventilation, heating (Harmsen and Bouwman 2002), and active introduction of earthworms (Ma et al. 1995). Active introduction of specific plants as a remediation technique (phytoremediation) may be successful not only by influencing physical factors, but also by influencing chemical (enzymes, Eh, pH, complexing agents) and biological (roots, microorganisms, mycorrhiza) factors (Trapp and Karlson 2001). If matric pressures are monitored and controlled, moisture conditions during temporary disposal can be optimized with respect to maximum physical ripening and maximum microbial activity.

Active introduction of (genetically engineered) microorganisms is often proposed. However, microorganisms that are introduced may have difficulty adapting to the specific ecological conditions in the disposal site (Wilson and Jones 1993). Also, the introduction

of white-rot fungus, which have the potential to degrade compounds that will not pass through bacteria cell walls, seems not to enhance the biodegradation process in soils (Kotterman et al. 1999 and Harmsen 2001). Finally, addition of surfactants can enhance desorption and solubilization and, consequently, the biodegradation of hydrocarbons (Wilson and Jones 1993).

Possibly, ripening can also be used as a remediation technique for trace metal polluted sediments. Löser et al. (1999) and Löser et al. (2000) showed that ripening could change an impermeable muddy-paste into a permeable, soil-like material that was suitable for (bio)leaching. As a result of chemical ripening, pH decreased from 7.0 to 5.6. Addition of 1% S° − that was oxidized to H_2SO_4 by the indigenous microorganisms − could create weakly acidic conditions through which significant Zn, Ni and Cd could be leached. Addition of 2% S° also dissolved Cu and Cr. Pb was practically immobile even after the addition of 5% S° (pH 2). Additions of S° greater than 2% led to an undesired mobilization of Fe, Al, and Ca, which corroborates the findings of Tichý et al. (1996). They concluded that removal of trace metals using acids should always be optimized with respect to maximum metal removal at minimum soil damage.

Ripening in temporary disposal sites can require several years and relatively large areas of land. Therefore, in densely populated areas like The Netherlands, a combination of this technique with another type of land use like production of a biomass fuel might be advantageous (Breteler et al. 2001).

2.8 Conclusions and outlook

After dredged material is disposed in a temporary disposal site, conditions for aerobic biodegradation of PAH and mineral oil are poor, because of a lack of oxygen. As shown in this review, several conditions affecting oxygenation improve in clayey dredgings as a result of the natural ripening processes: the air-filled porosity increases, the aggregate size decreases, and the initially high respiration rate caused by chemical and biological ripening decreases. Therefore, we conclude that the conditions for aerobic biodegradation of organic micro-pollutants like PAH and mineral oil improve as ripening proceeds. Therefore we conclude that ripening can be seen as a cost effective bioremediation technique for PAH and mineral oil polluted sediments.

Data provided by De Haan et al. (1998), Zevenbergen et al. (1999), and Harmsen (2001) support our conclusion. Their experiments at field scales show that ripening changes an anaerobic layer of dredgings into an aerobic soil within two to six years. Physical ripening could be enhanced by cultivation, vegetation or increasing the temperature in a greenhouse. Non-optimal biodegradation was attributed to a combination of limited bioavailability of the pollutants and limited availability of oxygen. However, these field studies were not suitable to distinguish the influence of the individual relevant processes on the success of bioremediation because of the complex relationships between the different ripening processes (see Fig. 2.1).

To quantify the relevance of the different processes taking place during temporary disposal, more fundamental research is needed in which the effects of the different ripening processes (including degradation of PAH and mineral oil) are studied independently. We anticipate that the increased insight into these specific processes can be used to identify the critical process steps to be able to improve this bioremediation technique.

Acknowledgements

We thank Marjorie Aelion of the University of South Carolina for her critical comments on the English of the manuscript. The research was supported by and performed within the Research Centre on Soil, Sediment and Groundwater Management and Remediation WUR/TNO.

3

PHYSICAL RIPENING OF DREDGED SEDIMENTS

Quantification of physical properties

O land van mest en mist, van vuilen, kouden regen,
Doorsijperd stukske grond, vol killen dauw en damp,
Vol vuns, onpeilbaar slijk en ondoorwaadbre wegen,
Vol jicht en parapluies, vol kiespijn en vol kramp!

Boutade – P.A. de Génestet

This chapter is based on a paper that was originally published in *Geoderma* (Vermeulen et al. 2005)

Abstract

The soil formation process ripening can be used as a bioremediation technique for dredged sediments that are polluted with organic chemicals. Currently, data are lacking that quantify the effects of physical ripening on parameters that affect aerobic biodegradation. We quantified the effects of physical ripening on shrinkage, swelling, moisture retention, hydraulic conductivity, and oxygen diffusion for three freshly dredged sediments using specially designed pressure chambers. We also quantified the effect of physical ripening on structure development by measuring aggregate size distributions for four half-ripe and four ripe sediment samples that were collected from field sediment disposal sites. Using the data and information developed in this study the course of physical ripening and the aerobic biodegradation process of sediments at above ground (upland) disposal sites can be predicted with a combination of existing water- and oxygen transport and ripening models.

3.1 Introduction

Large amounts of sediments are dredged for both maintenance and environmental reasons worldwide. For example, 400×10^6 m^3 of sediment are dredged annually by the United States Army Corps of Engineers or their permit recipients (Linkov et al. 2002), and about 40×10^6 m^3 of sediment are dredged annually in the Netherlands (Chapter 2). A substantial proportion of these dredged sediments is held temporarily at an above ground (upland) disposal facility. Upland disposal is a relatively easy, cost-effective alternative for dredged materials and is therefore a widely adopted sediment management practice.

Following the application of clayey dredged sediments to a temporary upland disposal site, the compaction processes of consolidation and ripening are initiated. Consolidation is caused by the 'overburden pressure' resulting from the weight of the overlying sediment (Terzaghi and Peck 1967 and Appendix 3). Ripening is a soil formation process that irreversibly converts waterlogged sediments into aerated soil by desiccation and structure development (Pons and Van der Molen 1973, Chapter 2). The soil profile that results from ripening, roughly exists of four zones with different extents of structure development: (i) unripe, consolidated soil below the water table, (ii) half-ripe soil with a coarse to very coarse prismatic structure, (iii) nearly ripe soil with coarse aggregates, and (iv) ripe soil with medium to fine aggregates at the top (Chapter 2).

Ripening of dredged sediments consists of physical, chemical, and biological processes. In Chapter 2, we described these three sub-processes extensively and concluded that ripening can be used as a bioremediation technique for temporarily disposed dredgings that are polluted with organic pollutants like Polycyclic Aromatic Hydrocarbons (PAH) and mineral oil (Total Petroleum Hydrocarbons (TPH)). It is known that ripening of a one-meter thick layer of dredgings can take up to 3 to 6 years. (Harmsen 2001). However, it is currently not possible to predict the exact course of ripening of dredged material during temporary disposal because of the complex relationships (coupling effects) between ripening and biodegradation of organic pollutants (Chapter 2). Therefore, the development of a mathematical model that describes the different processes and their coupling effects would be useful. Such a combined model would need sediment specific input data. Because the different coupling effects have been studied only rarely (Vulliet et al. 2002, Horn 2003), sufficient data on parameters that affect aerobic biodegradation during ripening are lacking.

Therefore, we carried out this study to quantify: (i) the shrinkage and swelling behavior of dredged sediments, (ii) the effect of physical ripening on the moisture retention and hydraulic conductivity characteristics, (iii) the oxygen diffusion coefficients of desiccating dredged sediments, and (iv) the effect of physical ripening on structure development. We quantified (i) – (iii) with three freshly dredged, clayey sediments that were artificially ripened in the laboratory. For (iv) we used samples of sediments that had been subjected to natural ripening at field disposal sites.

In this study, we only consider the physical aspects of ripening. Biological and chemical processes typically play an important role in structure development (Dexter 1988, Horn et al. 1994, Chapter 2), however, we consider physical ripening to be the most important and the driving mechanism of the whole ripening process.

3.2 Quantification and modeling of physical ripening

The n-value as defined by Pons and Van der Molen (1973) can be used as an empirical measure of the degree of desiccation of dredged sediments (Chapter 2):

$$n_{rip} = \frac{w_{sat} - 0.2R}{L + 3H} \tag{3.1}$$

where:

n_{rip} = n-value (g water g^{-1} clay)
w_{sat} = saturated moisture ratio in (g moisture (100 g)$^{-1}$ dry matter (D.M.))
R = sand + silt content (g sand + silt (100 g)$^{-1}$ D.M.)
L = clay content (g clay (100 g)$^{-1}$ D.M.)
H = organic matter content (g organic matter (100 g)$^{-1}$ D.M.)

Using n_{rip}, Pons and Van der Molen (1973) defined five classes of physical ripening (Table 3.1). Structure development cannot be described directly by Eq. (3.1) because this process is not only governed by desiccation but also by the intensity and number of wet/dry cycles (Chapter 2). However, in general, low values of n_{rip} correspond with a high degree of structure development.

Table 3.1 Classification of sediment material according to the degree of physical ripening

n_{rip} g g^{-1}	Designation
3.0 – 2.0	Unripe, recently deposited sediment
2.0 – 1.4	Consolidated, but practically unripe
1.4 – 1.0	Half ripe
1.0 – 0.7	Nearly ripe
< 0.7	Ripe, normal soil

Eq. (3.1) gives only a static description of physical ripening. To describe the dynamics of physical ripening, different mathematical models have been developed in the past decennia (Rijniersce 1983, Kim et al. 1992a). Kim et al. (1992a) included an overburden potential into Richards' equation (Richards 1931) to describe water transport, consolidation, and physical ripening in a single model. Their model describes both one-dimensional water transport and three-dimensional deformation (consolidation and physical ripening) of the soil in a Lagrangian coordinate frame. This coordinate frame is mathematically more convenient for the description of water transport in a shrinking and

swelling soil than the more familiar Eulerian coordinate frame is (Garnier et al. 1997). Kim's model only considers water movement in a soil matrix excluding shrinkage cracks from the flow domain. To describe ripening of sediments at a disposal site, his model should be combined with a model that simultaneously considers water movement through cracks and matrix in the vadose zone (e.g. Bronswijk 1988 or Van Dam 2000).

For the description of oxygen diffusion and respiration in an aggregated soil with the occurrence of anoxic aggregate interiors, different oxygen diffusion models have been developed (Leffelaar 1979, Smith 1980, Rappoldt 1990). All these models are based on Ficks diffusion law (Fick 1855) and divide the aggregated soil profile into two distinct domains, each having their own diffusion characteristics: micro-pores within the soil matrix and macro pores between this matrix. Besides, assumptions are made about the aggregate size distribution.

A combination of a water transport model (Van Dam 2000), a physical ripening model (Kim et al. 1992a), and an oxygen diffusion model (Smith 1980), could describe the coupling effects between hydraulics, mechanics and biology (HMB coupling), both in the absence of air (water-saturated sediment) and in the presence of air (unsaturated soil).

3.3 Materials and methods

3.3.1 Types of dredged sediment

To study the consolidation and physical ripening process in the laboratory, we collected three types of dredged sediment at different places in the Netherlands: from a ditch in Rotterdam (ROSL), a canal in Woerden (WOGR), and a river in Leeuwarden (LERI). The collected dredgings were transported to the laboratory in airtight containers, sieved to pass a 2 mm-screen, and stored anaerobically (under water) at 4 °C before use. Table 3.2 presents some properties of the dredgings.

Table 3.2 Properties of freshly dredged sediments

	dry matter [a] (mass-%)	Particle density (g cm^{-3})	< 2 μm [b c] (mass-%)	< 50 μm [b] (mass-%)	$CaCO_3$ [d] (mass-%)	Organic matter [d e] (mass-%)
ROSL	27	2.40	16	74	10	16
WOGR	22	2.52	25	62	14	10
LERI	30	2.55	25	62	4	11

[a] in percentage of wet weight
[b] in percentage of mineral part
[c] *L* (Eq. (3.1)) can be calculated by multiplying with: (1 - fraction of organic matter)
[d] in percentage of dry weight
[e] is equal to *H* in Eq. (3.1)

To characterize structure development during physical ripening, we also collected samples of aggregates (≈ 20 dm^3) of eight types of dredged sediment from field disposal facilities. We collected four samples (OH1 – OH4) of half-ripe aggregates (n_{rip} ≈ 1.2 g g^{-1}) at the facility "Oostwaardhoeve" that is located near Slootdorp, the Netherlands. The sediments had been held at the disposal site for only a few months. Besides, we collected four samples (PH, WM, GH, and ZZ. These sediments were extensively studied by

Harmsen (2004)) of ripe aggregates ($n_{rip} \approx 0.7$ g g^{-1}) at the facility "Kreekraksluizen" near Bergen op Zoom, the Netherlands. These sediments had been ripened at the disposal site for 8 to 12 years. Clay and organic matter contents of the different types of dredged sediment from the disposal sites were in the range of 8 – 26% and 5 – 10%, respectively.

3.3.2 Laboratory physical ripening (desiccation)

We used specially designed pressure chambers (hereafter referred to as microdepots, Vermeulen et al. 2000) to consolidate and ripen the dredged material at specific pneumatic pressure levels. After one day of consolidation at a gas pressure of 100 hPa the pressure was set at the desired level to simulate the physical ripening process. To achieve dredged material with different degrees of physical ripening five pressure levels were applied: 100, 333, 1,000, 2,000, and 16,000 hPa. The nylon filter material used in the microdepots (S&S Nytran®, pore size 0.45 μm) had a bubbling pressure of 2,500 hPa. To apply the pressure of 16,000 hPa, we transferred the samples from the microdepots into a pressure chamber as described by Klute (1986).

We allowed the physical ripening process in the microdepots and pressure chamber to proceed until outflow of water had ceased (2 to 7 days). According to Klute (1986), equilibrium between the applied pressure (P_{gas}) and the potential of the water in the dredged material can be assumed after this period. Neglecting the small difference in pressure between the sample and the discharging water, the resulting matric potential of the water is $\psi_m = -P_{gas}$ (Koorevaar et al. 1983). To keep anoxic conditions in the samples during consolidation and ripening, we applied all pressure levels with nitrogen. We achieved samples with a matric potential of -1,000,000 hPa after equilibrating them with a N_2-atmosphere with 50% relative humidity, which is known as the 'vapor equilibrium method' (Klute 1986).

With the above described procedure we achieved homogeneous circular model aggregates (all in triplicate) of approximately equal size (diameter ≈ 45 mm, height ≈ 20 mm, hereafter referred to as pellets) that were different in matric potential, matrix porosity, and air-filled porosity.

To determine matrix porosity (ϕ_{matrix}) and air-filled porosity ($\phi_{a,matrix}$) we used the method as described by Brasher et al. (1966). We briefly immersed the pellets in a resin (SARAN-F310™ (DOW) to Methyl Ethyl Ketone ratio 1:4). The resin was air-dried, after which we determined weight and volume of the pellets by weighing and under water weighing. Finally, we determined the oven dry weight of the coated pellets (24 h at 105 ºC) and we determined the loss on ignition (3 h at 550 ºC) from which we calculated the moisture content and organic matter content H (H = loss on ignition (%) - 0.07 × L (%)). We used the measured mass and known density of the fresh and air-dry resin and the density of the oven-dry resin to correct the results, assuming that the resin was completely lost during ignition. We calculated the density of the solid phase (Table 3.2) for all pellets using the pedotransfer function that was suggested by Poelman (1975):

$$\rho_p = \frac{100}{\frac{H}{1.47} + \frac{L}{2.88} + \frac{R}{2.66}} \tag{3.2}$$

where:

ρ_p = particle density (g cm^{-3})

We verified the validity of Eq. (3.2) for our sediments with the submersion method (Blake and Hartge 1986).

We characterized shrinkage of the pellets by changes in their moisture and void ratios, which are defined as (Bronswijk 1988):

$$\vartheta = \frac{V_w}{V_s} \tag{3.3}$$

$$e = \frac{V_p}{V_s} \tag{3.4}$$

where:

ϑ = moisture ratio (cm^3 cm^{-3})
e = void ratio (cm^3 cm^{-3})
V_w = water volume (cm^3)
V_s = solid volume (cm^3)
V_p = pore volume (cm^3)

In shrinking and swelling soils ϑ and e are more suitable to express water content and matrix porosity than the commonly used volumetric moisture content (θ) and the matrix porosity (ϕ_{matrix}). If needed they can simply be converted into each other:

$$\theta = \frac{\vartheta}{1+e} \tag{3.5}$$

$$\phi_{matrix} = \frac{e}{1+e} \tag{3.6}$$

where:

θ = volumetric moisture content (cm^3 cm^{-3})
ϕ_{matrix} = matrix porosity (cm^3 cm^{-3})

We calculated dry matter content (*D.M.*), wet bulk density ($^b\rho_w$), dry bulk density ($^b\rho_d$), matrix porosity (ϕ_{matrix}), air-filled porosity ($\phi_{a,matrix}$), void ratio (e), volumetric moisture content (θ), and moisture ratio (ϑ). We determined the 'initial void ratio' e_i – that is the void ratio at the transition from sedimentation to consolidation (ψ_m = 0 hPa) – by taking a sample of dredged material that had settled in a beaker for two weeks.

In a separate experiment, we ripened pellets at different specified pressures. After ripening, we cut the resulting pellets into two parts after which one part was rewetted and swollen on a suction table (Klute 1986) that was adjusted at a matric potential of -5 hPa. After one week, swelling was complete and we measured the resulting saturated moisture ratios (ϑ_{sat}).

Finally, we calculated n-values (n_{rip}) with Eq. (3.1). We used ϑ_{sat} that we had derived with the swelling function (section 3.3) to calculate the saturated moisture ratio (w_{sat}) of Eq. (3.1).

3.3.3 Shrinkage characteristics and swelling functions

To describe shrinkage, swelling, crack volume and crack depth in a clay soil, soil shrinkage characteristics can be used. Shrinkage characteristics describe the relationship between the void ratio (e) and the moisture ratio (ϑ). Usually three stages can be distinguished in a shrinkage characteristic (Bronswijk 1988, Van Dam 2000):

- normal shrinkage. Volume decrease of soil aggregates is equal to water loss. The aggregates remain fully water-saturated;
- residual shrinkage. Upon drying the volume of the aggregates still decreases, but water loss exceeds volume decrease. Air enters the pores of the aggregates;
- zero shrinkage. The soil particles have reached their densest configuration. Upon further water extraction, the volume of aggregates stays constant. Water loss is practically equal to the increase of air volume in the aggregates.

Air can enter a ripening layer of sediments through the shrinkage cracks that are formed during normal shrinkage (Bronswijk 1991). However, complete oxygenation of formed aggregates will only be possible during residual shrinkage, during which air enters the soil matrix and micro-cracks can develop within the aggregates (Bakker and Bronswijk 1993). In large field samples, containing more than one structural unit, sometimes a fourth shrinkage phase can be distinguished: structural shrinkage. The conditions in the microdepots prevented structural shrinkage during the artificial desiccation process and therefore we consider our pellets to be built up of soil matrix only, not containing any (micro)-crack.

Different equations to describe shrinkage characteristics are reported in the literature (Kim et al. 1992c, Olsen and Haugen 1998, Crescimanno and Provenzano 1999, Groenevelt and Grant 2002). However, these equations either have many parameters that are strongly correlated or lead to physically impossible representations of the shrinkage characteristic. Therefore, we used a restricted version of the equation of Groenevelt and Grant (2002) that is two times continuously differentiable at the air entry point and has only two fitting parameters, both having a physical meaning (Eq. (3.7)).

$$e = e_0 \left\langle 1 + \frac{1}{N} \exp\left\{ \frac{e_a}{e_0} \left[1 - \left(\frac{e_a}{\vartheta} \right)^N \right] \right\} \right\rangle \qquad \text{for } 0 < \vartheta < e_a \qquad (3.7a)$$

$$e = \vartheta \qquad \text{for } \vartheta \geq e_a \qquad (3.7b)$$

where:

e_0 = e at $\vartheta = 0$ ($cm^3\ cm^{-3}$)
e_a = e at the air entry point ($cm^3\ cm^{-3}$)
N = $e_0 / (e_a - e_0)$ (-)

We obtained the parameters for the shrinkage characteristic (Eq. (3.7)) by a non-linear regression in SPSS® 10.1 between the measured e and ϑ.

Bronswijk and Evers-Vermeer (1990) assumed that shrinkage in a (ripe) soil is a completely reversible process. However, this assumption is only valid for the part of the shrinkage process that is caused by face-to-face oriented clay platelets that approach each other (Chapter 2). During physical ripening the honeycomb structure that remains after sedimentation is contracted (Pons and Zonneveld 1965) and the clay platelets assume a face-to-face orientation (Chapter 2). This reorientation of the clay platelets and destruction of the contacts between the clay platelets cause irreversible shrinkage (Basma et al. 1996, Baumgartl 1998, Baumgartl and Horn 1999). The ratio between irreversible shrinkage and reversible shrinkage in ripening soil material can be identified using the concept of the swelling function (Kim et al. 1992a). We obtained this function (Eq. (3.8)) by relating the moisture ratio after dewatering at different pressures (ϑ_{min}) to the moisture ratio after swelling (ϑ_{sat}) at ψ_m = -5 hPa.

$$\vartheta_{sat} = c_1 \vartheta_{min} + c_2 \tag{3.8}$$

where:

ϑ_{sat} = moisture ratio at saturation (cm^3 cm^{-3})
ϑ_{min} = threshold moisture ratio below which irreversible shrinkage (= physical ripening) occurs (cm^3 cm^{-3})
c_1 = empirical fitting parameter (-)
c_2 = empirical fitting parameter (-)

The matric potential below which irreversible shrinkage occurs ($\psi_{m,min}$) has the same order of magnitude as the 'predesiccation stress' that was introduced by Baumgartl and Horn (1999). After rearranging Eq. (3.8), the moisture ratio below which irreversible drying occurs can be calculated for any given saturated moisture ratio:

$$\vartheta_{min} = \frac{\vartheta_{sat} - c_2}{c_1} \tag{3.9}$$

3.3.4 Moisture retention and hydraulic conductivity characteristics

Usually the volumetric moisture contents (θ) at various matric potentials (ψ_m) are used to construct moisture retention characteristics. However, using these parameters to describe the behavior of ripening soils is mathematically inconvenient and can lead to erroneous results due to changes in the volume of the soil matrix (Kim et al. 1992b, Garnier et al. 1997). Therefore, we used moisture ratios (ϑ) for constructing the moisture retention characteristics. Such moisture retention characteristics can be used in mathematical models that describe water transport and shrinkage and swelling in a Lagrangian coordinate frame.

Van Genuchten (1980) described the moisture retention characteristic with Eq. (3.10).

$$\vartheta = \vartheta_r + \frac{\vartheta_{sat} - \vartheta_r}{\left(1 + \left|\alpha \psi_m\right|^n\right)^m} \tag{3.10}$$

where:

ϑ_r = residual moisture ratio (cm^3 cm^{-3})
α = empirical shape factor which is related to the matric potential at the first inflection point (hPa^{-1})
ψ_m = matric potential (hPa)
n = empirical shape factor related to the steepness of the moisture retention characteristic at very low ψ_m (-)
m = 1 - 1/n (-)

We obtained the Van Genuchten parameters for the unripe dredged sediments ($\psi_{m,min}$ = 0 hPa) using the RETC code (Van Genuchten et al. 1991).

Physical ripening results in a change in moisture retention characteristic. To quantify this change, Kim et al. (1993a) proposed a mathematical relation between the parameters α and ϑ_{sat} of a ripening soil matrix:

$$\alpha = 10^{(c_3 \vartheta_{sat} - c_4)} \tag{3.11}$$

where:
c_3 = empirical fitting parameter (-)
c_4 = empirical fitting parameter (-)

To estimate c_3 and c_4 of Eq. (3.11), we constructed moisture retention characteristics for different values of ϑ_{sat} – that is different degrees of physical ripening – using the RETC code. We did this for the values of ϑ_{sat} belonging to $\psi_{m,min} \geq$ -2,000 hPa. After this, we performed a linear regression between the resulting values for α and ϑ_{sat}.

Because the parameters ϑ_r and n of Eq. (3.10) don't change significantly as a result of physical ripening (Kim et al. 1993a), we used fixed values for both of these parameters: ϑ_r was set at 0 by the RETC code and for n we used the value that was estimated for the unripe sediments.

Although it has been believed that physical ripening increases the hydraulic conductivity (Pons and Van der Molen 1973), this is mainly true for material consisting of both shrinkage cracks and soil matrix such as field ripening sediments but not for our pellets that consist of soil matrix only (Kim et al. 1993a). Laboratory measurements of hydraulic conductivity (K_{sat}) in a ripening soil matrix by Kim et al. (1993a) revealed that the decrease in ϑ_{sat} can almost completely describe the decrease in K_{sat} of the matrix in a ripening marine clay soil. They described this effect by a log-linear relationship between K_{sat} and ϑ_{sat}:

$$\log(K_{sat}) = c_5 \vartheta_{sat} - c_6 \tag{3.12}$$

where:
K_{sat} = saturated hydraulic conductivity (cm d^{-1})
c_5 = empirical fitting parameter (-)
c_6 = empirical fitting parameter (-)

Yong et al. (1983) and Wichman (1999) found similar relationships for consolidating clays. The slope (c_5) is more or less the same for different types of material, but the intercept (c_6) can fluctuate considerably. We measured the saturated hydraulic conductivity (K_{sat}) of pellets with $\psi_{m,min}$ = -100 hPa using the constant head method as described by Klute and Dirksen (1986) and derived sediment specific relationships like Eq. (3.12) for the three sediments, assuming a fixed value of 0.78 for c_5 (Kim et al. 1993a). We calculated saturated hydraulic conductivities for unripe ($\psi_{m,min}$ = 0 hPa) pellets and ripe ($\psi_{m,min}$ = -16,000 hPa) pellets with the resulting relationships.

Van Genuchten et al. (1991) described the hydraulic conductivity characteristic for unsaturated flow with Eq. (3.13).

$$K = K_{sat} S_e^{\lambda} \left[1 - \left(1 - S_e^{\frac{1}{m}} \right)^m \right]^2 \quad (3.13)$$

where:
K = unsaturated hydraulic conductivity (cm d^{-1})
λ = empirical shape parameter that is related to the connectivity of the pore system (-)
S_e = relative saturation (-), defined as:

$$S_e = \frac{\vartheta - \vartheta_r}{\vartheta_{sat} - \vartheta_r} \quad (3.14)$$

Based on a very weak correlation between λ and ϑ_{sat}, Kim et al. (1993a) claimed that λ increases linearly with decreasing ϑ_{sat}. An increase in λ would indicate a decrease in pore connectivity and therefore a decrease of K at matric potentials lower than 0 hPa (Eq. (3.13)). Horn et al. (1996) observed that K increases with decreasing ϑ_{sat}, suggesting that λ decreases. Wösten and Van Genuchten (1988) measured hydraulic conductivity characteristics for a large number of soils in the Netherlands and found lower values for λ of clayey samples compared to λ of sandy samples. For fine to medium textured soils, they found an average value for λ of -5. We concluded that λ is stronger related to textural characteristics than to ϑ_{sat} and used a fixed value of -5 for λ to construct the hydraulic conductivity characteristics for both unripe sediments ($\psi_{m,min}$ = 0 hPa) and ripe soils ($\psi_{m,min}$ = -16,000 hPa).

3.3.5 Intra-aggregate oxygen diffusion coefficients

Oxygen diffusion coefficients in soils can be expressed as a function of air-filled porosity and tortuosity factor in mathematical models. Penman (1940) used Eq. (3.15) that relates the diffusion coefficient (D_s) with the air-filled porosity (ϕ_a) and a tortuosity factor (f).

$$D_s = f \phi_a D_0 \quad (3.15)$$

where:
D_s = diffusion coefficient through the soil ($cm^2\ s^{-1}$)
D_0 = diffusion coefficient of oxygen in the atmosphere ($cm^2\ s^{-1}$)
f = intra-aggregate tortuosity factor (-)
ϕ_a = air-filled porosity ($cm^3\ cm^{-3}$)

Penman (1940) concluded that in dry soils, a value of 0.66 is valid for f. This value is widely used to make estimates of diffusion coefficients in soils. However, a value of 0.66 is only valid for a limited range of variation in air-filled porosity. Values of the parameter f ranging from 0.005 to 0.8 are reported in the literature (Hillel 1998). The value of f not only depends on the air-filled porosity, but also on other soil characteristics like the moisture retention characteristic. This moisture retention characteristic changes continuously during physical ripening (section 3.4). To avoid these issues, we performed direct measurements of the intra-aggregate oxygen diffusion coefficients ($D_{s,matrix}$).

We used the method described by Sextone et al. (1985) for the pellets at high matric potential values (-100, -333, -1,000 and -2,000 hPa). We monitored the oxygen concentration at a depth of 0.5 mm (+/- 0.01 mm) in the pellet with time (240 s) after we abruptly had changed the atmosphere outside the pellets from water-saturated air to water-saturated nitrogen. We measured the oxygen concentration with a cathode-type

microelectrode, built in a stainless steel needle (Visscher et al. 1991) combined with an Inlab302® Ag/AgCl reference electrode. We calculated $D_{s,matrix}$, with the method proposed by Sextone et al. (1985).

Our microelectrodes performed well down to matric potential values of -2,000 hPa. Probably the required moisture film at the electrode tip is not present at lower matric potentials (Van Doren and Erickson 1966). Therefore, we used a diffusion chamber as described by Rolston (1986) for the lower matric potentials (-16,000, and -1,000,000 hPa), using argon instead of oxygen. Argon has approximately the same diffusion coefficient and solubility in water as does O_2, but has the advantage that it is relatively unreactive. We monitored the change of N_2-concentration in the diffusion chamber (volume = 0.3 dm^3) every 10 to 20 min for 1 (ψ_m = -1,000,000 hPa) to 3 h (ψ_m = -16,000 hPa) by collecting 100 µl gas samples with a Hamilton syringe. We measured the N_2-concentration of the samples with a gas chromatograph (Interscience 8340) and handled the data obtained with the method proposed by Taylor (1949) to calculate values for $D_{s,matrix}$.

We applied both methods at a temperature of 30 ºC. Finally, we calculated air-filled porosities ($\phi_{a,matrix}$) with ϕ_{matrix} and θ, and values for f (Eq. (3.15)).

3.3.6 Inter-aggregate oxygen diffusion coefficients

Inter-aggregate diffusion coefficients ($D_{s,layer}$) at different stages of ripening could not be measured and were therefore calculated with Eq. (3.16) (Bronswijk 1991) that relates the diffusion coefficient with the fraction air-filled cracks and a tortuosity factor (F).

$$D_{s,layer} = F\left[1-\left(1-\phi_{a,cracks}\right)^{1-\frac{1}{r_s}}\right]D_0 \qquad (3.16)$$

where:

$D_{s,layer}$ = inter aggregate diffusion coefficient ($cm^2\ s^{-1}$)
F = inter-aggregate tortuosity factor (0.3 to 1.0) (-)
$\phi_{a,cracks}$ = volume fraction cracks, including the 'volume' of subsidence ($cm^3\ cm^{-3}$)
r_s = geometry factor (-)
D_0 = diffusion coefficient of oxygen in the atmosphere ($cm^2\ s^{-1}$).

In case of subsidence only (consolidation) the geometry factor (r_s) is equal to 1, indicating that no cracks are formed. Soil strength and depth in the soil profile affect the shrinkage geometry. During physical ripening, the soil becomes firmer and cracks can be formed, resulting in a value for r_s that gradually changes from 1 to 3 (Rijniersce 1984, Kim et al. 1992c). In ripe clayey soils, r_s has a constant value of 3, indicating three dimensional isotropic shrinkage (Bronswijk 1990). For this study, we assumed one-dimensional shrinkage (r_s = 1) for matric potentials from 0 to -100 hPa, and three-dimensional isotropic shrinkage (r_s = 3) for the lower matric potentials. We calculated the volume fraction of cracks ($\phi_{a,cracks}$ in Eq. (3.16)) occurring in the field with:

$$\phi_{a,cracks} = 1-\frac{{}^{b}\rho_{d,1}}{{}^{b}\rho_{d,2}} \qquad (3.17)$$

where (see next page):

$^{b}\rho_{d,1}$ = dry bulk density before shrinkage (g cm^{-3})
$^{b}\rho_{d,2}$ = dry bulk density after shrinkage (g cm^{-3})

We calculated values of $D_{s,layer}$ for sediments at initial crack formation conditions and for completely ripe, well structured soil for which we used values for F of 1.0 and 0.3, respectively. These values were suggested by Bronswijk (1991) for a poorly structured and a well structured clay soil, respectively.

3.3.7 Field physical ripening (structure development)

In the laboratory, we prepared samples for aggregate size measurements by air drying half-ripe and ripe field aggregates (section 3.1) at 30 °C. This procedure might have caused further crumbling of the aggregates and therefore an underestimation of the aggregate sizes. However, according to our visual observations, crumbling of the aggregates did not happen extensively during drying, which is consistent with the theory that aggregate size reduction is mainly caused by wet/dry cycles and not by drying alone (Shiel et al. 1988, Chapter 2).

After passing the aggregates trough sieves with circular openings of 40, 20, 10, 5 and 2.5 mm, we calculated the weight of the sieve fractions and constructed log-probability plots as suggested by Allmaras et al. (1965). From the plotted data, we derived the geometric mean diameter (*GMD*) and log-standard deviation ($\sigma_{log\ d}$) values. We also measured the diameter of of the largest aggregates in the samples to be able to construct a truncated lognormal distribution (Rappoldt and Crawford 1999). We expected values of both *GMD* and $\sigma_{log\ d}$ to decrease due to the forces of physical ripening (Chapter 2).

3.4 Results and discussion

3.4.1 Laboratory physical ripening (desiccation)

The pellet properties at different matric potentials are given in Table 3.3. Because of ongoing desiccation, the dry matter content (*D.M.*) increased from about 35% at initial conditions (ψ_m = 0 hPa) to more than 95% after air-drying (ψ_m = -1,000,000 hPa). The wet bulk density ($^{b}\rho_w$) increased from 1.24 to 1.63 g cm^{-3} down to matric potentials of about -2,000 hPa. This point of maximum wet bulk density is called the 'pycnostatic point' in the literature (Philip 1969). At lower matric potentials, we observed a slight decrease because of air entry in the pellets. The dry bulk density ($^{b}\rho_d$) increased from 0.41 g to 1.44 g cm^{-3}. Values of ROSL pellets were slightly smaller because of its relatively high organic matter content. Matrix porosities (ϕ_{matrix}) decreased from 0.84 to 0.43 cm^3 cm^{-3}. The initial void ratios (e_i) ranged from 4.56 to 5.22 cm^3 cm^{-3} and can be compared with values of Yong et al. (1983) who reported a value of 5.92 cm^3 cm^{-3} and Wichman (1999) who found a value of 4.84 cm^3 cm^{-3}.

The n-values (n_{rip}) decreased from 2.90 – 3.66 to 0.30 – 0.41 g g^{-1} as a result of desiccation (Table 3.3). According to Table 3.1, the initial values (ψ_m = 0 hPa) are typical for recently deposited sediments. An n-value of 1.4 to 1.0 g g^{-1} indicates that a sediment is half ripe. In our sediments, these values were reached at a matric potential of about -333 hPa (≈ 'field

Table 3.3 Dry matter content (*D.M.*), wet bulk density ($^{b}\rho_w$), dry bulk density ($^{b}\rho_d$), matrix porosity (ϕ_{matrix}), void ratio (e), volumetric water content (θ), moisture ratio (ϑ), calculated saturated moisture ratio after swelling (ϑ_{sat}), and n-value (n_{rip}) of the soil matrix at different matric potentials (ψ_m). Values are averages of triplicate measurements (± standard deviation), except for the values at ψ_m = 0 hPa

	ψ_m (hPa)	*D.M.* (mass-%)	$^{b}\rho_w$ (g cm^{-3})	$^{b}\rho_d$ (g cm^{-3})	ϕ_{matrix} (cm^3 cm^{-3})	e (cm^3 cm^{-3})	θ (cm^3 cm^{-3})	ϑ (cm^3 cm^{-3})	ϑ_{sat} (cm^3 cm^{-3})	n_{rip} [a] (g g^{-1})
ROSL	0	34	1.25	0.43	0.82	4.56	0.82	4.56	4.56	2.90
	-100	50 (0.30)	1.39 (0.01)	0.69 (0.01)	0.71(0.00)	2.47 (0.05)	0.71 (0.01)	2.42 (0.03)	2.54 (0.02)	1.52 (0.03)
	-333	54 (0.31)	1.43 (0.00)	0.77 (0.01)	0.69 (0.00)	2.25 (0.02)	0.66 (0.00)	2.23 (0.02)	2.27 (0.02)	1.32 (0.00)
	-1,000	63 (0.61)	1.53 (0.01)	0.97 (0.02)	0.59 (0.01)	1.47 (0.03)	0.56 (0.01)	1.39 (0.03)	1.77 (0.02)	0.92 (0.02)
	-2,000	67 (3.05)	1.53 (0.02)	1.03 (0.03)	0.57 (0.01)	1.33 (0.07)	0.49 (0.05)	1.16 (0.16)	1.61 (0.12)	0.84 (0.07)
	-16,000	74 (2.96)	1.52 (0.02)	1.13 (0.03)	0.53 (0.02)	1.12 (0.10)	0.39 (0.05)	0.83 (0.14)	1.36 (0.10)	0.67 (0.11)
	-1,000,000	97 (0.23)	1.24 (0.01)	1.20 (0.01)	0.49 (0.01)	0.97 (0.03)	0.04 (0.00)	0.08 (0.01)	0.81 (0.00) [b]	0.30 (0.01)
WOGR	0	33	1.24	0.41	0.84	5.22	0.84	5.22	5.22	3.66
	-100	48 (0.29)	1.40 (0.00)	0.67 (0.01)	0.73 (0.00)	2.75 (0.03)	0.73 (0.00)	2.73 (0.03)	2.96 (0.02)	1.93 (0.01)
	-333	53 (0.50)	1.46 (0.01)	0.78 (0.01)	0.69 (0.01)	2.25 (0.07)	0.69 (0.00)	2.23 (0.05)	2.57 (0.04)	1.53 (0.05)
	-1,000	64 (0.13)	1.58 (0.02)	1.01 (0.02)	0.60 (0.00)	1.49 (0.03)	0.57 (0.01)	1.43 (0.01)	1.96 (0.00)	1.11 (0.05)
	-2,000	70 (1.15)	1.63 (0.01)	1.14 (0.02)	0.55 (0.00)	1.21 (0.03)	0.45 (0.02)	1.08 (0.06)	1.69 (0.04)	0.93 (0.02)
	-16,000	78 (2.57)	1.54 (0.02)	1.20 (0.02)	0.52 (0.01)	1.08 (0.04)	0.34 (0.04)	0.72 (0.10)	1.41 (0.08)	0.71 (0.05)
	-1,000,000	96 (0.44)	1.49 (0.00)	1.44 (0.00)	0.43 (0.00)	0.75 (0.01)	0.05 (0.01)	0.10 (0.01)	0.94 (0.01)	0.41 (0.01)
LERI	0	34	1.26	0.43	0.83	4.95	0.83	4.95	4.95	3.36
	-100	51 (0.31)	1.43 (0.00)	0.73 (0.01)	0.71 (0.00)	2.48 (0.04)	0.70 (0.00)	2.44 (0.03)	2.60 (0.03)	1.76 (0.04)
	-333	54 (0.38)	1.46 (0.00)	0.79 (0.01)	0.69 (0.00)	2.22 (0.03)	0.67 (0.00)	2.17 (0.03)	2.39 (0.03)	1.47 (0.02)
	-1,000	66 (0.61)	1.62 (0.00)	1.07 (0.01)	0.58 (0.01)	1.38 (0.04)	0.55 (0.01)	1.31 (0.05)	1.73 (0.04)	0.99 (0.08)
	-2,000	72 (0.01)	1.61 (0.01)	1.16 (0.01)	0.54 (0.00)	1.19 (0.01)	0.50 (0.01)	1.00 (0.00)	1.49 (0.00)	0.80 (0.00)
	-16,000	75 (1.54)	1.59 (0.01)	1.19 (0.02)	0.53 (0.01)	1.13 (0.04)	0.39 (0.03)	0.83 (0.07)	1.37 (0.05)	0.72 (0.04)
	-1,000,000	97 (0.42)	1.44 (0.01)	1.39 (0.00)	0.45 (0.00)	0.81 (0.01)	0.05 (0.01)	0.09 (0.01)	0.79 (0.01) [b]	0.31 (0.01)

[a] calculated with Eq. (3.1), with $w_{sat} = (\vartheta_{sat} / \rho_p) \times 100$

[b] $\vartheta_{sat} < e$, which is physically impossible, most probably the swelling function is not valid for very low values of ϑ_{min}

capacity'). At a matric potential of -16,000 hPa (≈ 'wilting point') – which is more or less the lowest potential that can be expected under Dutch climatic conditions (Bronswijk and Evers-Vermeer 1990) – all three sediments showed values for n_{rip} close to 0.7 g g^{-1}, which indicates that the sediments were completely ripe. n_{rip} is closely related to the lowest matric potential ($\psi_{m,min}$) to which the sediments have been subjected. We believe that $\psi_{m,min}$ would be a more physically based and therefore better ripening index than n_{rip}. Kim et al. (1993b) also proposed a more physically based ripening index that was based on the swelling function (Eq. (3.8)). However, determination of $\psi_{m,min}$ or Kim's ripening index are both rather difficult and laborious, if possible at all. We therefore recommend using Eq. (3.1) for practical purposes. n_{rip} decreased down to values of 0.30 to 0.41 g g^{-1} after air drying (ψ_m = -1,000,000 hPa). Pons and Zonneveld (1965) found n_{rip} values down to 0.20 to 0.25 g g^{-1} for topsoils in a Dutch polder. Probably such low values can only be achieved after a process of repeated rewetting and drying, which causes an extra decrease in ϑ_{sat} (Baumgartl 1998, Baumgartl and Horn 1999). However, the decrease of n_{rip} in ripening sediments that is caused by desiccation is much larger than the extra decrease that could be caused by wet/dry cycles.

3.4.2 Shrinkage characteristics and swelling functions

The parameters e_0 and e_a describing the shrinkage characteristics (Eq. (3.7)) are listed in Table 3.4. A plot of the shrinkage characteristics of ROSL is given as an example in Fig. 3.1. Our characteristics range to > 4.5 cm^3 cm^{-3}. In general, the range of the moisture ratio in shrinkage characteristics varies from 2 cm^3 cm^{-3} for ripe soils (Bronswijk and Evers-Vermeer 1990, Olsen and Haugen 1998, Groenevelt and Grant 2001) to 4 cm^3 cm^{-3} for unripe soils (Kim et al. 1992c).

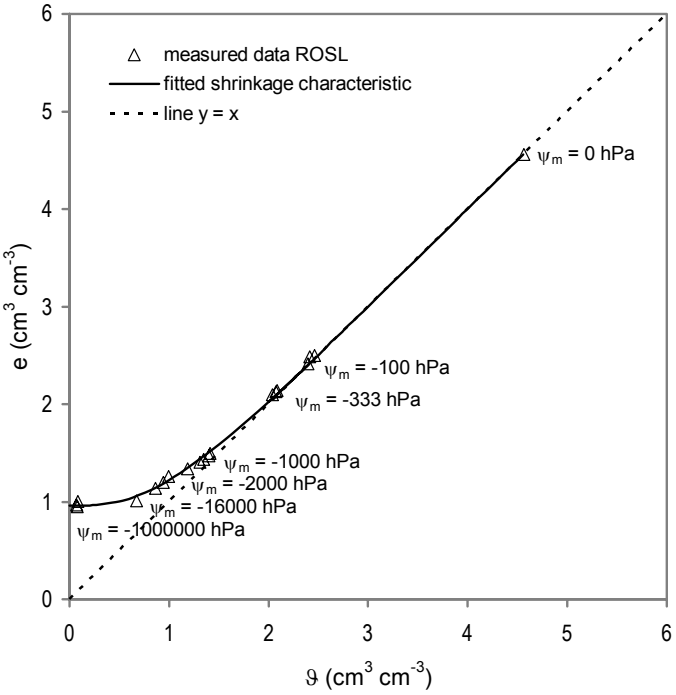

Fig. 3.1 ROSL shrinkage characteristic

Table 3.4 Parameters of the shrinkage characteristic (e_0 and e_a) and swelling function (c_1 and c_2) for ROSL, WOGR and LERI (95% confidence intervals of the estimated parameters are given between brackets)

	e_0 (cm^3 cm^{-3})	e_a (cm^3 cm^{-3})	c_1 (-)	c_2 (-)
ROSL	0.96 (0.93 – 0.99)	3.25 (2.92 – 3.57)	0.74 (0.61 – 0.86)	0.75 (0.50 – 1.00)
WOGR	0.77 (0.72 – 0.82)	3.92 (3.19 – 4.66)	0.77 (0.59 – 0.94)	0.86 (0.50 – 1.23)
LERI	0.81 (0.78 – 0.85)	3.88 (3.44 – 4.32)	0.77 (0.69 – 0.84)	0.73 (0.58 – 0.87)

Table 3.5 Van Genuchten parameters of the moisture retention (ϑ_r, ϑ_{sat}, α, and n), hydraulic conductivity characteristic (K_{sat} and λ) for ROSL, WOGR and LERI (95% confidence intervals of the estimated parameters are given between brackets), and parameters for the K_{sat} – ϑ_{sat} relation (c_5 and c_6)

	Moisture retention characteristic				Hydraulic conductivity			
	ϑ_r (cm^3 cm^{-3})	ϑ_{sat} (cm^3 cm^{-3})	α (hPa^{-1})	n (-)	K_{sat} (cm d^{-1})	λ (-)	c_5 (-)	c_6 (-)
Unripe ($\psi_{m,min}$ = *0 hPa)*								
ROSL	0	4.56 (4.45 – 4.67)	0.10 (0.04 – 0.17)	1.25 (1.21 – 1.29)	4.83	-5.00	0.78	2.89
WOGR	0	5.22 (5.12 – 5.31)	0.08 (0.05 – 0.11)	1.29 (1.26 – 1.33)	4.91	-5.00	0.78	3.39
LERI	0	4.95 (4.81 – 5.07)	0.12 (0.03 – 0.20)	1.27 (1.22 – 1.31)	3.87	-5.00	0.78	3.29
Ripe ($\psi_{m,min}$ = *-16,000 hPa)*								
ROSL	0	1.36	0.0007	1.25	0.0151	-5.00	0.78	2.89
WOGR	0	1.41	0.0012	1.29	0.0052	-5.00	0.78	3.39
LERI	0	1.37	0.0012	1.27	0.0061	-5.00	0.78	3.29

Our values for e_0 are 0.77 (WOGR) to 0.96 $cm^3\ cm^{-3}$ (ROSL). Bronswijk and Evers-Vermeer (1990) found values ranging from 0.4 to 0.8 $cm^3\ cm^{-3}$ for ripe soils and about 1.1 $cm^3\ cm^{-3}$ for unripe soils. Olson and Haugen (1998) found values between 0.5 and 0.8 $cm^3\ cm^{-3}$ and Groenevelt and Grant (2001) found values between 0.4 and 0.7 $cm^3\ cm^{-3}$. Kim et al. (1992c) found a value of about 1.0 $cm^3\ cm^{-3}$ for a ripening marine clay soil. Based on our measurements and the values found in the literature, we expect that the mechanism of rewetting and drying – which plays a role under field conditions – would not only cause a decrease of n_{rip} (section 4.1), but consequently also a decrease of e_0 (Bronswijk and Evers-Vermeer 1990). Differences between e_i and e_0 (shrinkage potential) are extremely high: 4.45 (WOGR), 4.14 (LERI), and 3.60 $cm^3\ cm^{-3}$ (ROSL). Obviously, this is a typical feature of ripening sediments.

Our values for e_a are between 3.25 (ROSL) and 3.92 $cm^3\ cm^{-3}$ (WOGR) and compare well with the results of Kim et al. (1992c), who found a value of about 3 $cm^3\ cm^{-3}$ for a ripening marine clay soil. The relatively low value for ROSL can be explained by the high value for 'L+3H' (Eq. (3.1)) that is a measure for the total water-absorbing capacity of clay and organic matter (Pons and Van der Molen 1973). For completely ripe topsoils, Bronswijk and Evers-Vermeer (1990) found values for e_a that are lower than 1.2 $cm^3\ cm^{-3}$, whereas they found values up to 2.1 $cm^3\ cm^{-3}$ for the less ripe subsoils. So, both e_0 and e_a are expected to decrease as a result of physical ripening, e_0 as a result of wet/dry cycles and e_a as a result of ongoing desiccation. We anticipate that these effects can be easily incorporated in a mathematical model describing physical ripening.

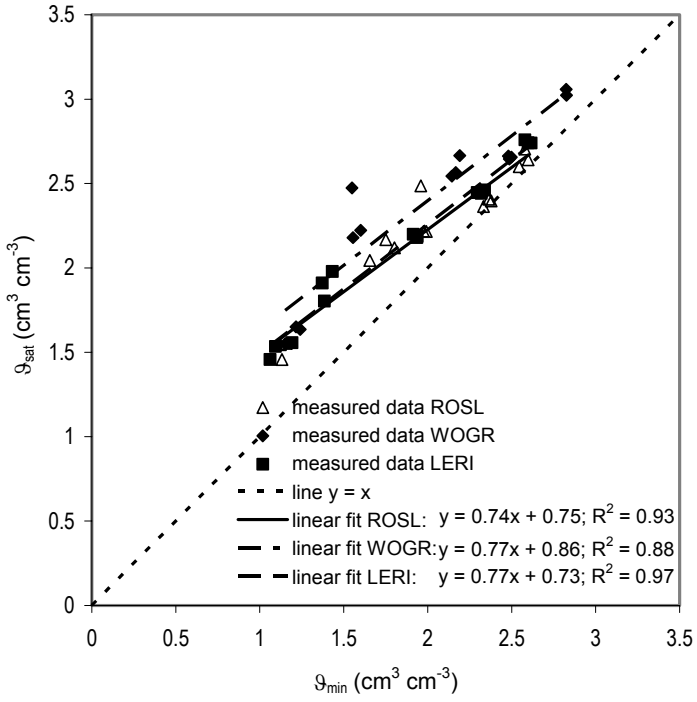

Fig. 3.2 Swelling functions of ROSL, WOGR, and LERI

Fig. 3.2 shows a plot of the swelling function (Eq. (3.8)) for the different dredged sediments. It can be seen that the swelling potential of the sediments increases while desiccation (= decrease in ϑ_{min}) proceeds. This agrees with the observations done by

Kim et al. (1992a) and can most probably be attributed to the relatively larger fraction of clay platelets that have assumed a face-to-face orientation after being desiccated. Basma et al. (1996) also found an increase in swelling potential when soils were fully shrunk; however, they found a decrease in the swelling ability when soils where alternately wetted and partially shrunk. The parameters c_1 and c_2 of the swelling function are 0.75 and 0.75 (ROSL and LERI) to 0.86 (WOGR), respectively (Table 3.4). WOGR's relatively high value for c_2 might be attributed to the relatively high initial void ratio of this sediment. Our values for c_1 compare well with the value given by Kim et al (1992a), whereas our values for c_2 are clearly lower, which might be attributed to the lower clay contents of our sediments. The swelling functions cross the line y = x, at a moisture ratio between 2.87 (ROSL) and 3.71 $cm^3\ cm^{-3}$ (WOGR). We speculate that these values – that are approximately equal to our values for e_a – correspond with critical moisture ratios at which horizontal shrinkage of the pellets was initiated and would indicate that horizontal shrinkage in the pellets is initiated at matric potentials (ψ_m) between 0 and -100 hPa (see Table 3.3).

3.4.3 Moisture retention and hydraulic conductivity characteristics

The Van Genuchten parameters describing the moisture retention characteristics of unripe sediments ($\psi_{m,min}$ = 0 hPa) are listed in Table 3.5. Fig. 3.3 gives a plot of the moisture retention characteristic of ROSL as an example.

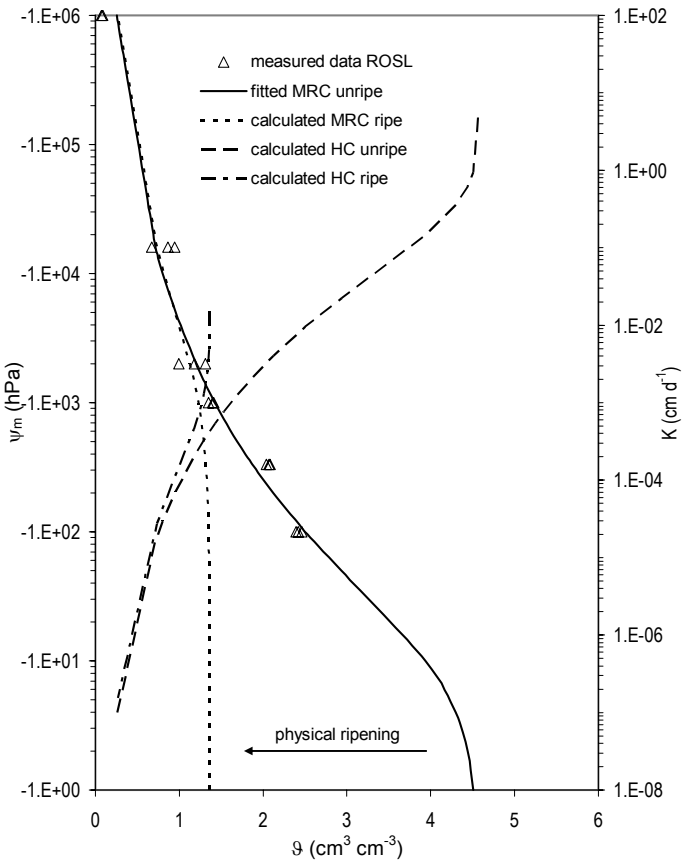

Fig. 3.3 ROSL moisture retention characteristics (MRC) and hydraulic conductivity characteristics (HC) of unripe sediment ($\psi_{m,min}$ = 0 hPa) and ripe soil ($\psi_{m,min}$ = -16,000 hPa)

The moisture retention characteristics of the three sediments are very similar. The only clear difference between the different sediments is that ϑ_{sat} of the unripe WOGR characteristic is higher than ϑ_{sat} of the other sediments. The values for the shape factors α and n are in the same order of magnitude as the values given by Kim et al. (1993a).

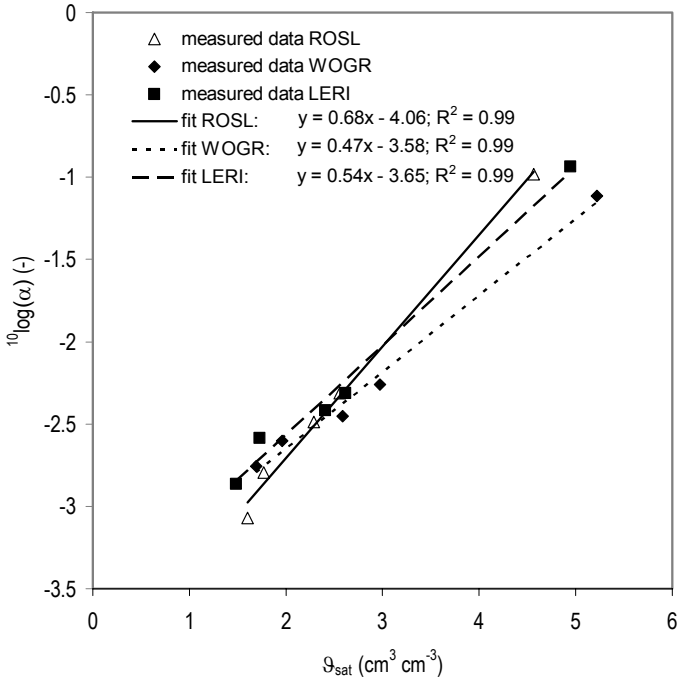

Fig. 3.4 Relations between the Van Genuchten parameters α and ϑ_{sat} of ROSL, WOGR, and LERI

Plots of the relations between α and ϑ_{sat} can be found in Fig. 3.4. Values for parameters c_3 and c_4 (Eq. (3.11)) are 0.47 to 0.68 and 3.58 to 4.06, respectively. Kim et al. (1993a) found similar values for c_3 en c_4. The relation for ROSL has the largest slope (c_3), whereas the relation for WOGR has the smallest slope, indicating that desiccation has a relatively large effect on the moisture retention characteristic of ROSL and a relatively small effect on the characteristic of WOGR. ROSL has also the highest value for 'L+3H' (Eq. (3.1)), whereas WOGR has the lowest value for this parameter. 'L+3H' is a measure for the total water-absorbing capacity of clay and organic matter (Pons and Van der Molen 1973). Also Horn et al. (1996) reported dependencies between α and ϑ_{sat} for samples from different texture classes. However, from their data we were not able to draw univocal conclusions about any effect of the water-absorbing capacity on the relation between α and ϑ_{sat}. The Van Genuchten parameters describing the moisture retention characteristic of the complete ripe sediments ($\psi_{m,min}$ = -16,000 hPa) are also listed in Table 3.5 (see Fig. 3.3 for a plot of ROSL).

The values for the parameters c_5 and c_6 of Eq. (3.12), the saturated hydraulic conductivity (K_{sat}) that we derived with this Eq., and the (fixed) connectivity parameter of the hydraulic conductivity characteristic (λ, Eq. (3.13)), can be found in Table 3.5. Plots of the resulting hydraulic conductivity characteristics for the unripe and ripe sediment ROSL are shown in Fig. 3.3. K_{sat} values for the matrix of unripe dredged sediments ranges from 3.87 (LERI) to 4.91 (WOGR) cm d^{-1}. K_{sat} for ripe sediments ranges from 0.0052 (WOGR) to

0.0151 (ROSL) cm d^{-1}, which is about 3 orders of magnitude lower than values that we found in the literature for comparable bulk soil (Wösten and Van Genuchten 1988). Horn (1990) found similar discrepancies between K_{sat} of single aggregates and K_{sat} of the bulk soil. K_{sat} for the ripe pellets of WOGR and LERI are about the same, whereas the value for ROSL is clearly higher. We assume that this difference is attributed to the relatively low clay contents of ROSL. All our values for K_{sat} are higher than the values reported by Kim et al. (1993a). Their lower values might be a result of the relatively high clay contents in the soil they studied (46%). Generally, a larger variation in K_{sat} is observed in field samples from different types of soil because K_{sat} in such samples is largely controlled by soil structural features, or macropores (Jarvis et al. 2002). Different textural properties cause different soil structural features. However, soil structure and macropores did not influence the hydraulic properties of the pellets because the formation of (micro-)cracks during physical ripening in the microdepots could be prevented. Therefore, we measured only small difference in K_{sat} between sediments having a different texture.

Moisture retention characteristics and hydraulic conductivity characteristics for sediments at intermediate ripening stages can be calculated with the methods that were described by Kim et al. (1993a).

3.4.4 Intra-aggregate oxygen diffusion coefficients

We successfully measured oxygen diffusion coefficients ($D_{s,matrix}$) in desiccating pellets of dredged sediment that had a moisture content from nearly water-saturated to air dry. Published diffusion coefficients usually cover the range from an air-filled porosity of about 5% to air-filled porosities equal to total porosities (Troeh et al. 1982, Moldrup et al. 1997). Only little data was published about diffusion coefficients in nearly saturated soil (Sextone et al. 1985, Zausig et al. 1993, Rappoldt 1995, Sierra et al. 1995). To our knowledge, measurements that cover the complete range from nearly saturated (unripe) sediments to air dry (ripe) soils have never been published before. Our measured $D_{s,matrix}$ ranges from 8.11×10^{-6} to 2.06×10^{-5} cm^2 s^{-1} at a matric potential of -100 hPa to 8.80×10^{-3} to 1.69×10^{-2} cm^2 s^{-1} at a matric potential of -1,000,000 hPa (Table 3.6).

The ROSL pellets show the highest values for $D_{s,matrix}$, whereas the WOGR pellets show the lowest values. The differences can be attributed to differences in clay content. The tortuosity factor f in Eq. (3.15) is not a constant value, but is low for matric potentials between -100 and -2,000 hPa (0.005 to 0.02) and relatively high for matric potentials between -16,000 and -1,000,000 hPa (0.04 to 0.17). These values are in the same order of magnitude as those reported by Grable and Siemer (1968) who found values for f of 0.02 at air-filled porosities around 10% and Lemon and Erickson (1952) who found values for f of 0.005 at air-filled porosities of about 5%. However, all our values for f that are representative for soil matrix are much lower than the value of 0.66, which was suggested by Penman (1940) for bulk soil.

Table 3.6 Measured inta-aggregate air-filled porosity ($\phi_{a,matrix}$), oxygen diffusion coefficient ($D_{s,matrix}$), and intra-aggregate tortuosity factor (f) and calculated inter-aggregate air-filled porosity ($\phi_{a,cracks}$) and oxygen diffusion coefficients ($D_{s,layer}$) for two tortuosity factors (F), all at different matric potentials (ψ_m). $\phi_{a,matrix}$ and $D_{s,matrix}$ are averages of triplicate measurements (± standard deviation)

	ψ_m (hPa)	$\phi_{a,matrix}$ ($cm^3\ cm^{-3}$)	$D_{s,matrix}$ ($cm^2\ s^{-1}$)	f (-)	$\phi_{a,cracks}$ [a] ($cm^3\ cm^{-3}$)	$D_{s,layer}$, F=1 [b] ($cm^2\ s^{-1}$)	$D_{s,layer}$, F=0.3 [b] ($cm^2\ s^{-1}$)
ROSL	0	0	n.m.	-	0	-	-
	-100	0.0120 (0.0073)	2.06×10^{-5} (9.81×10^{-7})	0.0108	0	-	-
	-333	0.0182 (0.0007)	4.03×10^{-5} (1.73×10^{-5})	0.0104	0.10	1.45×10^{-2}	4.35×10^{-3}
	-1,000	0.0330 (0.0109)	9.75×10^{-5} (7.42×10^{-5})	0.0145	0.29	4.37×10^{-2}	1.31×10^{-2}
	-2,000	0.0600 (0.0389)	1.36×10^{-4} (1.59×10^{-4})	0.0071	0.33	5.01×10^{-2}	1.50×10^{-2}
	-16,000	0.1377 (0.0270)	9.13×10^{-4} (3.06×10^{-4})	0.0325	0.39	6.01×10^{-2}	1.80×10^{-2}
	-1,000,000	0.4536 (0.0045)	1.69×10^{-2} (8.18×10^{-4})	0.1739	0.43	6.69×10^{-2}	2.01×10^{-2}
WOGR	0	0	n.m.	-	0	-	-
	-100	0.0056 (0.0007)	8.11×10^{-6} (3.97×10^{-6})	0.0070	0	-	-
	-333	0.0060 (0.0061)	1.61×10^{-5} (1.04×10^{-5})	0.0050	0.14	2.05×10^{-2}	6.14×10^{-3}
	-1,000	0.0235 (0.0109)	7.33×10^{-5} (5.86×10^{-5})	0.0180	0.34	5.18×10^{-2}	1.55×10^{-2}
	-2,000	0.0902 (0.0144)	8.78×10^{-5} (7.99×10^{-5})	0.0073	0.41	6.35×10^{-2}	1.90×10^{-2}
	-16,000	0.1771 (0.0361)	5.88×10^{-4} (4.25×10^{-4})	0.0173	0.44	6.86×10^{-2}	2.06×10^{-2}
	-1,000,000	0.3724 (0.0036)	8.80×10^{-3} (1.25×10^{-3})	0.1104	0.53	8.46×10^{-2}	2.54×10^{-2}
LERI	0	0	n.m.	-	0	-	-
	-100	0.0106 (0.0018)	1.85×10^{-5} (7.70×10^{-6})	0.0085	0	-	-
	-333	0.0167 (0.0028)	2.67×10^{-5} (1.44×10^{-6})	0.0075	0.07	1.01×10^{-2}	3.03×10^{-3}
	-1,000	0.0327 (0.0020)	4.46×10^{-5} (2.06×10^{-5})	0.0064	0.31	4.69×10^{-2}	1.41×10^{-2}
	-2,000	0.0732 (0.0049)	1.31×10^{-4} (8.39×10^{-5})	0.0070	0.37	5.67×10^{-2}	1.70×10^{-2}
	-16,000	0.1375 (0.0183)	1.83×10^{-3} (1.56×10^{-3})	0.0443	0.39	6.01×10^{-2}	1.80×10^{-2}
	-1,000,000	0.4010 (0.0027)	9.54×10^{-3} (1.04×10^{-3})	0.1113	0.48	7.56×10^{-2}	2.27×10^{-2}

[a] calculated with Eq. (3.17), we assumed $\phi_{a,cracks}$ = 0 for matric potentials from 0 to -100 hPa
[b] calculated with Eq. (3.16), with D_0 = 0.214 $cm^2\ s^{-1}$
n.m. = not measured

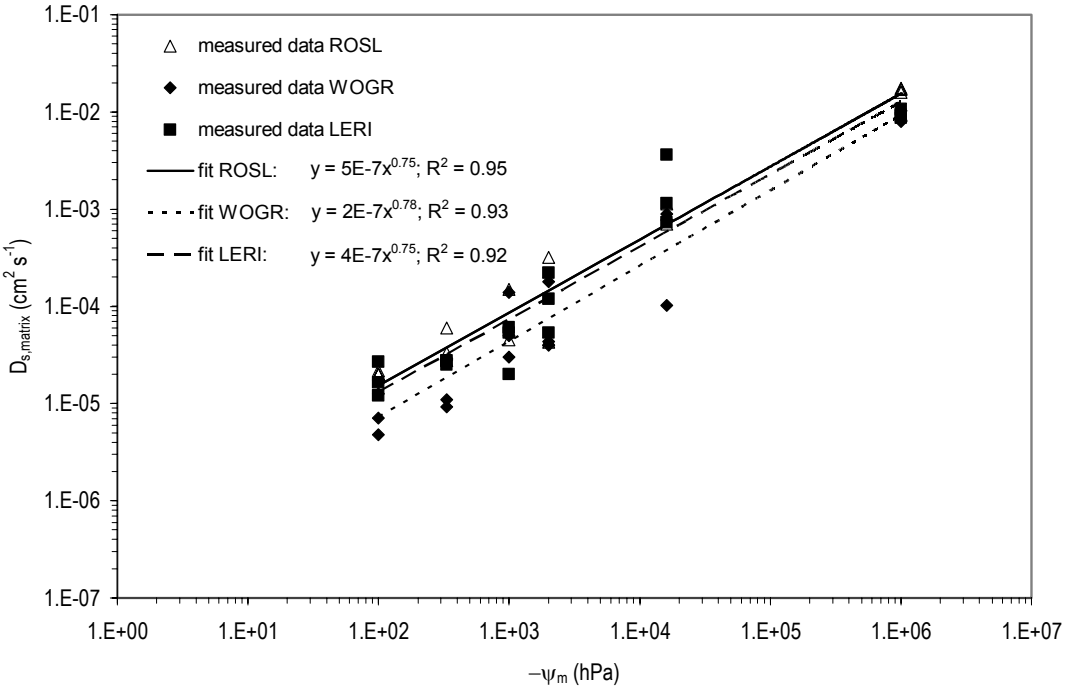

Fig. 3.5 Intra-aggregate oxyen diffusion coefficient ($D_{s,matrix}$) vs. -matric potential ($-\psi_m$) of ROSL, WOGR, and LERI

$D_{s,matrix}$ is positively correlated with $\phi_{a,matrix}$. However, using fixed parameters, none of the models described in the literature (Troeh et al. 1982, Moldrup et al. 1997, Moldrup et al. 1999), can relate $D_{s,matrix}$ with $\phi_{a,matrix}$ for the whole range of our measurements from wet to dry pellets. Zausig et al. (1993) concluded that an increasing connectivity of air-filled pores is more important than the total volume of air-filled pores and the only exact measure of oxygen diffusion properties is the diffusion coefficient itself. They found a nearly linear relation between $D_{s,matrix}$ and ψ_m in the a small range of matric potentials (ψ_m = 0 hPa to -70 hPa) and suggested using ψ_m as an indirect parameter to predict the aeration status of nearly saturated aggregates. We copied the ideas of Zausig et al. (1993) and could derive a linear relationship between the logarithm of $D_{s,matrix}$ and the logarithm of ψ_m for the whole range of ψ_m from -100 hPa to -1,000,000 hPa (Fig. 3.5). Extrapolation of our measurements up to a matric potential of -1 hPa, results in values for $D_{s,matrix}$ between 2×10^{-7} and 5×10^{-7} cm^2 s^{-1} (Fig. 3.5). Our values that were measured at a temperature of 30 °C, compare well with measurements reported in the literature: 1.4×10^{-7} at water-saturation (Sierra et al. 1995), 4.6×10^{-7} cm^2 s^{-1} at ψ_m = -10 hPa to 7.5×10^{-7} cm^2 s^{-1} at ψ_m = -70 hPa (Zausig et al. 1993), 8.5×10^{-6} cm^2 s^{-1} at 'field capacity' (Sextone et al. 1985), and 9×10^{-6} cm^2 s^{-1} under 'locally saturated' conditions (Rappoldt 1995). These literature values were measured at temperatures between 20 and 23 °C.

3.4.5. Inter-aggregate oxygen diffusion coefficients

The calculated values for $D_{s,layer}$ can be found in Table 3.6 and range from 1.01×10^{-2} to 8.46×10^{-2} cm^2 s^{-1} (F = 1) and 3.03×10^{-3} to 2.54×10^{-2} cm^2 s^{-1} (F = 0.3). We calculated the highest values for WOGR, whereas we calculated the lowest values for ROSL. Because

we used Eq. (3.16) to calculate $D_{s,layer}$, the resulting values are completely dependent on the shrinkage behavior of the sediments and therefore they are not surprising as WOGR has the largest shrinkage potential (section 4.2). Bronswijk (1991) reported measured maximum values for $D_{s,layer}$ of 3×10^{-2} cm^2 s^{-1} in a clayey soil with a poor structure and 2×10^{-2} cm^2 s^{-1} in a well structured clayey soil. Smith (1980) used a maximum value of 1×10^{-2} cm^2 s^{-1} to calculate oxygen profiles in a well structured clayey soil. These maximum values are in the same order of magnitude as our values. For F = 0.3, $D_{s,layer}$ is 1 to 3 times higher than $D_{s,matrix}$. For F = 1.0, $D_{s,layer}$ is 4 to 10 times higher than $D_{s,matrix}$. These last ratios correspond with indirect measurements of Currie (1965), who showed that the within-crumb coefficient was about one-fifth of the between-crumb coefficient for a given air space.

3.4.6 Field physical ripening (structure development)

The log-probability plots of the aggregate diameter distributions of samples from the different field disposal sites are presented in Fig. 3.6. The *GMD*, $\sigma_{log\ d}$, and cut off diameter are given in Table 3.7. A clear difference exists between the samples of half-ripe and ripe aggregates. As expected, *GMD* and $\sigma_{log\ d}$ of half-ripe aggregates are larger than those of ripe aggregates. These observations are compatible with the observations reported by other researchers (Dexter 1988): in general, smaller aggregates have a higher density and a higher tensile strength compared to larger aggregates.

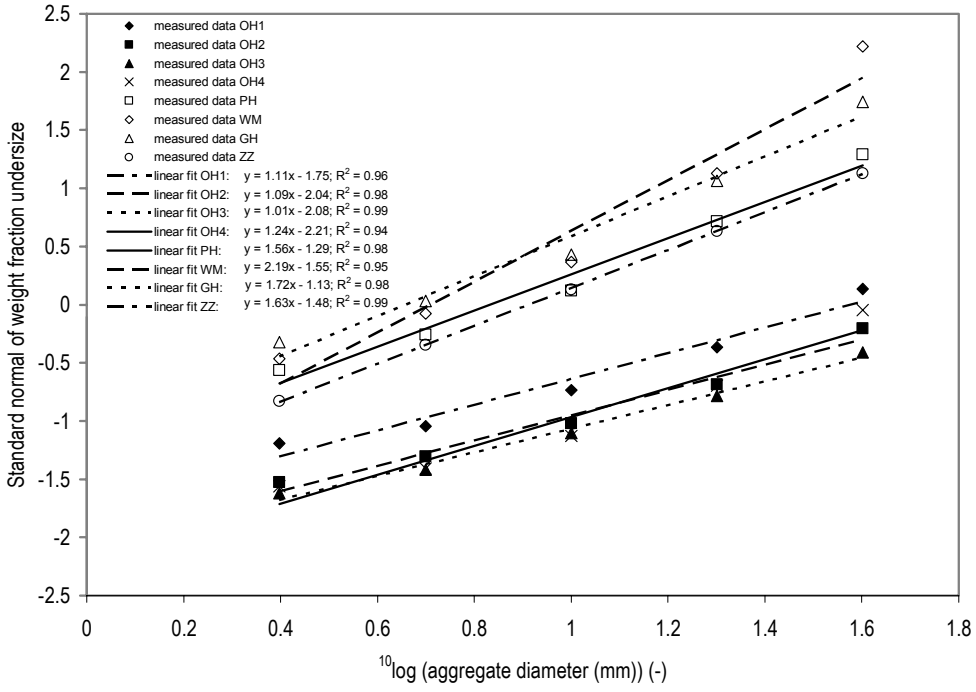

Fig. 3.6 Log-probability plot of aggregate diameter distributions of samples from half-ripe sediments (OH1 – OH4) and ripe soils (PH, WM, GH, and ZZ)

GMD and $\sigma_{log\ d}$ show the same pattern as the values found by Shiel et al. (1988) who reported that the *GMD* decreased from 44.7 mm after the second wet/dry cycle to

0.8 mm after the eighth cycle. In their study, $\sigma_{log\ d}$ decreased from 1.0 to 0.3. A value for $\sigma_{log\ d}$ close to 1 seems to be typical for sediments at an initial stage of structure development, whereas a $\sigma_{log\ d}$ lower than 0.6 indicates that an equilibrium aggregate size distribution is reached that is typical for a ripe soil. The largest aggregates in our samples of half-ripe sediments have a diameter > 100 mm. The first aggregates that are formed in a field disposal site are expected to be larger and are formed as a result of initial cracking. Their size is related to the distance between the initial cracks, which is > 250 mm (Chapter 2). The diameter of the pellets produced with the microdepots (section 3.2) compares well with the *GMD* of the field samples of half-ripe sediments.

Table 3.7 Aggregate-diameter distribution for half-ripe and ripe dredged sediments from different disposal sites. *GMD* = Geometric mean diameter, $\sigma_{log\ d}$ = log-standard deviation, Cut off diameter = maximum diameter found in the sample

	GMD (mm)	$\sigma_{log\ d}$ (-)	Cut off diameter (mm)
Half-ripe			
OH1	38	0.90	100
OH2	75	0.92	120
OH3	113	0.99	140
OH4	60	0.81	110
Ripe			
PH	6.8	0.64	55
WM	5.1	0.46	45
GH	4.5	0.58	50
ZZ	8.2	0.61	75

The cut off diameter ranges from 100 to 140 mm for the half-ripe aggregates and from 45 to 75 mm for ripe aggregates, and are only about 2 (half-ripe aggregates) to 9 (ripe aggregates) times larger than the *GMD*. Using a lognormal distribution without truncation would suggest the existence of aggregates that are 20 to 30 times larger than the *GMD* (Rappoldt and Crawford 1999), indicating that it is important to measure the cut off diameter.

As the ripening index n_{rip} only quantifies the degree of desiccation and gives no information about structure development, we propose to use the *GMD*, $\sigma_{log\ d}$, and cut off diameter in addition to n_{rip} to quantify the ripening stage.

3.5 Conclusions

The main objective of this study was to achieve input parameters for mathematical models describing the physical ripening processes in dredged sediments that have been disposed at an upland disposal site. We were able to artificially drain (ripen) three freshly dredged sediments to different, well defined extents in our specially designed pressure chambers (microdepots).

Techniques proposed in this study to measure the stage of ripening, shrinkage characteristics, swelling functions, hydraulic conductivity characteristics, moisture retention characteristics, and oxygen diffusion coefficients of the artificially ripened

sediment aggregates were verified. Our measurements resulted in a valuable data set of these physical properties for nearly water-saturated (unripe) sediments to air-dry (ripe) soils. Besides, we were able to use the aggregate diameter distribution to quantify the effect of physical ripening on structure development in samples from field disposal sites. This provides the essential extra information that is needed to translate our laboratory measurements to field situations.

In this study, we did not quantify the effects of wet/dry cycles or the effect of chemical and biological processes on physical properties of the pellets. These processes may play an important role in soil structure formation and stabilization processes (Dexter 1988, Horn and Dexter 1989, Shiel et al. 1988, Horn et al. 1994, Baumgartl and Horn 1999). However, we assume that the above processes affect the physical properties of ripening sediment aggregates far less than the desiccation process described in this study.

We measured most of the properties described in this study in artificially ripened aggregates that did not contain any (micro-)cracks. Therefore, the reported data can be used as input for so-called dual- or multi-domain models (Bronswijk 1988, Van Dam 2000, Smith 1980, Rappoldt 1990), in which water- and oxygen transport through cracks are calculated separately from transport through the soil matrix. Water and oxygen transport models that do not distinguish macro- from micro-pores require input data that are measured in a system that contains soil matrix as well as cracks (e.g. field measurements or measurements on undisturbed field samples).

With the data presented in this study, the coupled processes of water transport, consolidation, physical ripening, and oxygen diffusion can be modeled with a combination of models as described by Van Dam (2000), Kim et al. (1992a), and Smith (1980). Such a combination would be a helpful tool in predicting the course of physical ripening of dredged sediments at an upland disposal site.

In addition to the data presented in this study, quantitative data are also needed on the biodegradation kinetics of the present pollutants and the biochemical oxygen consumption kinetics of the sediments. The results of a study on these kinetics that we carried out in our laboratory, can be found in chapters 4 and 5 of this thesis.

Acknowledgements

We acknowledge Albert Boers (Soil Technology Group) for the assistance in his laboratory, Joop Harmsen (Alterra) for generously providing the samples from the field disposal sites, and Harry Bruning from our sub-department for the mathematical description of the shrinkage characteristic. We also acknowledge Katarzyna Kaziród and Magdalena Kromer (Technical University of Czestochowa, Poland) for their experimental work. Both of these students took part in the Socrates/Erasmus Programme of the European Union. Finally, we thank Jan Joziasse from the Dutch Organisation for Applied Scientific Research (TNO) and Ronald Sims from Utah State University for their helpful comments on the manuscript.

The research was supported by and performed within the Research Centre on Soil, Sediment and Groundwater Management and Remediation WUR/TNO.

4

BIOCHEMICAL RIPENING OF DREDGED SEDIMENTS

1. Kinetics of sulfur oxidation and soil organic matter mineralization

Vergeef het mij, maar 'k durf u niet genaken,
daar mijn gelaat nog glimt van 't laatst ontbijt,
en gij misschien reeds uren bezig zijt
uw duizendvierde slootje schoon te maken.

De baggerman – W. Elsschot

This chapter is based on a paper that was submitted for publication (Vermeulen et al. submitted a)

Abstract

After clayey dredged sediments have settled in a temporary upland disposal site, ripening starts which turns waterlogged sediment into aerated soil. Aerobic mineralization of Soil Organic Matter (SOM) and oxidation of reduced sulfur compounds are the major biochemical ripening processes. Quantitative data describing these processes are scarce. Therefore, we studied the aerobic oxidation and mineralization of five previously anaerobic dredged sediments during a 160 days incubation experiment at 30 °C in the laboratory. A double exponential model could adequately describe sulfur oxidation and SOM mineralization kinetics. A quantity of 7 to 34% of the total sulfur was oxidized during the first 7 days of incubation, after which no further sulfur oxidation was observed. Oxygen used for sulfur oxidation amounted up to 70% of the total oxygen uptake in the first 7 days and up to 30% of the oxygen uptake during the whole incubation period. Mineralization rates of the rapidly mineralizable SOM fractions that mineralized during the first 14 to 28 days of incubation were 100 to 1,000 times higher than the mineralization rates of the slowly mineralizable SOM during the remaining period. First order mineralization rates of the slowly mineralizable SOM were 0.00011 to 0.00026 d^{-1} and can be compared with those of terrestrial soils.. Yields of biomass on substrate ranged from 0.08 to 0.45 g $C_{biomass}$ / g C_{SOM} and appeared to be higher for rapidly mineralizing SOM than for slowly mineralizable SOM. The results of this study can be used to optimize conditions during temporary disposal of sediments, to estimate the potential decrease in SOM, and for future studies on the link between SOM mineralization and desorption of hydrophobic organic contaminants (HOC).

4.1 Introduction

Worldwide, enormous amounts of sediments have to be dredged for both maintenance and environmental reasons. For example, 400×10^6 m^3 of sediment have to be dredged annually in the United States (Linkov et al. 2002) and about 40×10^6 m^3 of sediment have to be dredged annually in the Netherlands. A large proportion of these sediments is heavily polluted with a 'cocktail' of pollutants (chapter 2). For different reasons a substantial proportion of the dredged sediments is disposed temporarily in an upland disposal facility. Upland disposal is an easy, cost-effective alternative for dredged material and is therefore a widely adopted technique.

Following the application of clayey dredged sediments to a temporary upland disposal site, the soil formation process ripening is initiated. Ripening is a soil formation process that irreversibly converts water-logged consolidated clayey sediments into aerated soil by desiccation and structure development (Pons and Van der Molen 1973). Ripening can be used as a bioremediation technique for contaminated sediments. If the quality of the ripened sediments meets the legal environmental and geotechnical standards (e.g. with respect to consistency), they can be beneficially used (chapter 2).

After structure development, oxygen can penetrate into the air-filled cracks of the disposed material and into the aggregates between these cracks. Chemical ripening starts in the part of the sediments in which oxygen has penetrated (the 'oxygenated' part). As a result of chemical ripening, the oxidation status expressed in the redox potential (Eh) increases from values as low as -300 to -250 mV when chemically unripe to +400 to +700 mV when chemically ripe. In general the most important chemical ripening process is the oxidation of reduced sulfur compounds like FeS and FeS_2 to $Fe(OH)_3$ and H_2SO_4 (De Glopper et al. 1992). At pH values above 4.5, FeS_2 (pyrite) is more stable than FeS. Therefore, only less stable sulfur compounds like FeS are susceptible to oxidation in sediments that are well buffered by $CaCO_3$ (chapter 2). Under poorly buffered conditions,

the drop in pH that is caused by sulfur oxidation may lead to an increased mobility of heavy metals that may subsequently leach from the disposal site (chapter 2).

Another effect of oxygenation is the development of aerobic micro-organisms. For this development and its effect on the dredged sediments the term biological ripening may be used. One of the results of biological ripening is the biological mineralization of easily mineralizable fractions of soil organic matter (SOM). After the mineralization of these easily degradable substrates, a new quasi-steady state will be achieved in which the amount of biomass is linearly related with the total amount of soil organic matter and organic micro-pollutants that are available as substrate (Anderson and Domsch 1989). In such situations, the amount of biomass will be at a level found in comparable oxygenated terrestrial soil (Van Schreven and Harmsen 1967, Del'Arco and De França 1999, chapter 2). The resulting soil may be characterized as biologically ripe.

SOM is the principal factor controlling sorption of hydrophobic organic contaminants (HOC) (Cornelissen et al. 2005). The slow release (and subsequent degradation) of HOC, which has been observed in many different studies, may be caused by sorption to carbonaceous SOM fractions (Cornelissen et al. 2005) and is possibly linked to the mineralization rates of SOM (Reemtsma et al. 2003, Harmsen 2004).

In this study, we define biochemical ripening as the combination of biological and chemical processes that consume oxygen. The high oxygen uptake rates (sediment reactivity) and water-logged conditions immediately after disposal limit the extent of oxygenation of the dredged sediment but will decrease over time as a result of exhaustion of FeS, easily degradable SOM, and bioavailable organic micro-pollutants. Thus, the ongoing physical ripening processes of desiccation and structure development and the biochemical ripening process (with its decreasing oxygen uptake rates) result in a higher degree of oxygenation.

It is known that, dependent on climate conditions, ripening can change a one-meter thick layer of dredgings into an oxygenated aggregated soil within 3 to 6 years (Harmsen 2001). However, it is currently not possible to predict the course of simultaneous ripening of dredged material during temporary disposal because quantitative data on biochemical ripening processes are missing and because of the complex relationships between the different ripening processes (chapter 2).

In this study, we quantified the kinetics of SOM mineralization and S oxidation during an incubation experiment with different types of dredged sediments. The results can be used to optimize conditions during temporary disposal, to make estimates about the potential decrease in SOM contents that can be achieved during temporary disposal, and for a better understanding of the link between SOM mineralization and the desorption of HOC. The kinetics of PAH and TPH degradation, which also may be considered as a form of biological ripening, were described in part 2 of this study (chapter 5).

4.2 Materials and methods

4.2.1 Sediments

To study the oxidation and mineralization processes in the laboratory five types of dredged freshwater sediment were collected at different places in the Netherlands: from a ditch in Rotterdam (ROSL), a canal in Woerden (WOGR), a river in Leeuwarden (LERI), a canal in Scharwoude (SCGR), and a ditch in Schagen (SCSL). All sediments were heavily polluted with Polycyclic Aromatic Hydrocarbons (PAH) and slightly to heavily polluted mineral oil (defined as Total Petroleum Hydrocarbons (TPH)). The collected dredgings were transported to the laboratory in airtight containers, sieved to pass a 2 mm-screen, and were stored under anaerobic conditions (under water) at 4 °C before use. Some properties of the dredgings are presented in Table 4.1.

Table 4.1 Sediment characterization (on dry matter basis with exception of dry matter)

	ROSL	WOGR	LERI	SCGR	SCSL
x-coordinate (km.m) [a]	96.300	120.300	183.170	115.940	115.350
y-coordinate (km.m) [a]	440.300	455.550	578.740	522.225	533.650
Dry matter (D.M.) (%, w/w)	26	25	29	20	27
Eh (mV)	+15	+45	+10	-15	+55
pH (-)	7.32	7.05	6.94	7.17	7.19
Clay (< 2 μm) (%, w/w)	13	22	22	21	21
$CaCO_3$ (%, w/w)	10	14	4	5	8
SOM [b] (%, w/w)	17.1	10.5	10.3	12.9	8.8
Total carbon (g kg^{-1})	118	71	66	72	53
Total carbon / SOM (g g^{-1})	0.69	0.67	0.64	0.56	0.61
Total nitrogen (g kg^{-1})	5.0	5.5	5.6	6.9	5.3
C/N-ratio (g g^{-1})	23.6	12.9	11.8	10.4	10.0
Total phosphorus (g kg^{-1})	1.2	2.5	1.5	1.1	0.9
C/P-ratio (g g^{-1})	98.3	28.4	44.0	65.5	58.9
Total sulfur [c] (g kg^{-1})	18	8	10	12	11
Total chloride (g kg^{-1})	0.30	0.20	0.76	0.46	0.86
Total potassium (g kg^{-1})	2.5	2.8	3.1	3.6	3.8
Total calcium (g kg^{-1})	54.8	58.9	16.7	24.4	31.2
Total magnesium (g kg^{-1})	5.37	5.39	4.53	4.44	5.92
Total sodium (g kg^{-1})	1.00	0.33	0.93	0.54	1.58
Total iron (g kg^{-1})	40	24	28	20	21
Total manganese (g kg^{-1})	0.63	0.71	0.26	0.31	0.35
TPH [d] (C_{10}-C_{40}) (mg kg^{-1})	9100	2300	2400	450	980
PAH [e] (Σ16EPA) (mg kg^{-1})	100	80	180	40	40
Total cadmium (mg kg^{-1})	5.34	8.82	1.85	n.a.[f]	1.21
Total nickel (mg kg^{-1})	50.7	36.9	31.5	n.a.[f]	19.2
Total lead (mg kg^{-1})	710	224	378	n.a.[f]	208
Total chromium (mg kg^{-1})	67.3	66.3	45.3	38.5	36.1
Total copper (mg kg^{-1})	260	80.1	151	66.3	57.5
Total zinc (mg kg^{-1})	1577	494	871	515	354

[a] position in Dutch Coordinate System

[b] Soil Organic Matter, loss on ignition at 550 °C (%) - (0.07 × clay (%))

[c] total of inorganic and organic sulfur

[d] total petroleum hydrocarbons, C_{10} – C_{40}

[e] polycyclic aromatic hydrocarbons, Σ16 EPA except Naphthalene, Acenaphtylene Benzo[*a*]anthracene and Chrysene

[f] n.a. = not analyzed

4.2.2 Incubation experiment

An incubation experiment was carried out following the method described by Bonten et al. (1999). Briefly, 14 to 20 g of wet anaerobic sediment samples (Table 4.1) were weighed into 100 ml glass serum bottles resulting in 4 g of dry matter per bottle. The bottles were closed with caps with rubber septa. The headspace was filled with air (78.09% N_2, 20.95% O_2, and 0.03% CO_2 (v/v)). Preliminary experiments revealed that addition of mineral medium and an enrichment culture had no significant effect on SOM mineralization and PAH and TPH degradation. Therefore, this addition was skipped from the original incubation procedure. The bottles were incubated for 160 days at 30 °C, whilst on a rotary tumbler (22 rev. min^{-1}).

An O_2 concentration > 10% (v/v) was maintained in the headspace of the bottles by flushing with compressed air. Continuous mixing in the bottles assured that the O_2 concentration in the slurry was not limiting biological activity.

4.2.3 Analytical methods

During incubation, headspace was sampled regularly with a Hamilton syringe. Gas samples (100 µl) were analyzed for O_2, CO_2, and N_2 on a gas chromatograph (Interscience 8340) equipped with a Teflon® column (2 mmID × 1.5 mL) packed with Chromosorb® 108 (60 – 80 mesh) parallel with a stainless steel column (2 mmID × 1.2 mL) packed with Molsieve 5A (60 – 80 mesh), with a 1:1 split and a Thermal Conductivity Detector. O_2 uptake and CO_2 evolution were calculated using gas concentration differences and head space volumes.

Bottles were sacrificed in triplicate at nine moments between 0 and 160 days after the start of incubation. pH and Eh in the sacrificed bottles were measured by inserting a WTW, SenTix® 21 electrode and a WTW, SenTix® ORP electrode, respectively. Both electrodes were inserted for 2 min. Subsequently, 1.5 ml slurry samples were collected and centrifuged for 5 minutes (16,000 g). The supernatant was diluted 25 times with Millipore water and a 25 µl sample was analyzed for SO_4^{2-}, NO_2^-, and NO_3^- on a DX-600 ion chromatograph system (Dionex) that was equipped with an IonPac® AS17 column (4 mmID × 250 mmL) and an electrochemical detector. Occasionally, the supernatant was analyzed for Dissolved Organic Carbon (TOC analyzer model 700, O.I.-Analytical) and NH_4^+ and PO_4^{3-} (segmented flow analyzer, Skalar Analytical). Finally, the sediments were analyzed for PAH and TPH (chapter 5).

4.2.4 Terminology and calculations

Oxidation and mineralization of FeS, SOM and organic micro-pollutants results in the production of $Fe(OH)_3$, SO_4^{2-}, CO_2, NH_4^+, NO_2^-, NO_3^-, PO_4^{3-}, H_2O, and H^+. Examples of oxidation and mineralization reactions of substances in dredged material are given in Table 4.2. In these reactions, the ratio of moles CO_2 evolution to moles O_2 uptake (CO_2/O_2) is called the respiratory quotient (RQ). Only when substrates equivalent to the composition of glucose are completely mineralized under steady state conditions the

RQ value equals 1 mol mol^{-1} (Dilly 2001). When aliphatic organic compounds, amino acids or refractory compounds having lower O content than glucose (e.g. humic acids) are predominantly mineralized, the RQ value is smaller than 1 mol mol^{-1}. The same is true under conditions of extensive nitrification.

Table 4.2 Stoichiometric relationships of oxidation and mineralization reactions with atom-C/O-ratio (C/O) of the substrate and corresponding respiratory quotient (RQ)

Conversion of:	Relationship	C/O mol mol^{-1}	RQ mol mol^{-1}
1 Carbohydrates [a]	$C_6H_{12}O_6 + 6O_2 \rightarrow 6CO_2 + 6H_2O$	1.00	1.00
2 Humic acids [b]	$C_{308}H_{328}O_{90}N_5 + 351.25O_2 \rightarrow 308CO_2 + 161.5H_2O + 5NO_3^- + 5H^+$	3.42	0.88
3 PAH [c]	$C_{10}H_8 + 12O2 \rightarrow 10CO_2 + 4H_2O$	∞	0.83
4 'average' SOM [d]	$(CH_2O)_{106}(NH_3)_{16}(H_3PO_4) + 138O_2 \rightarrow 106CO_2 + 122H_2O + 16NO_3^- + 16H^+ + H_3PO_4$	0.96	0.77
5 Straight alkanes	$2(CH_2)_n + 3nO_2 \rightarrow 2nCO_2 + 2nH_2O$	∞	0.67
6 Amino acids [e]	$2CH_2NH_2COOH + 7O_2 \rightarrow 4CO_2 + 4H_2O + 2NO_3^- + 2H^+$	1.50	0.57
7 Iron monosulfide	$4FeS + 9O_2 + 10H_2O \rightarrow 4Fe(OH)_3 + 4SO_4^{2-} + 8H^+$	-	-

[a] glucose is given as an example
[b] after Dilly 2001
[c] Polycyclic Aromatic Hydrocarbons, Naphthalene is given as an example
[d] Soil Organic Matter, after Park and Jaffé 1996
[e] glycine is given as an example

Growth of bacteria – with a cell composition that can be described with $CH_{1.8}O_{0.5}N_{0.2}$ (Roels 1983) – influences the RQ values that can be derived from stoichiometric relations. Under conditions of growth, RQ values are lower than the stoichiometrically derived values for RQ if mainly substrates like humic acids, mineral oil, and PAH having atom-C/O-ratios higher than 2 mol mol^{-1} (= C/O-ratio of biomass) are mineralized. On the other hand, RQ values are higher if substrates with atom-C/O-ratios lower than 2 mol mol^{-1} are mineralized under conditions of growth (e.g. growth on carbohydrates). Thus, the RQ value may vary depending on the composition of available substrate and the microbial growth phase.

In our study, we measured both CO_2 evolution and O_2 uptake and calculated RQ values based on linear regression analysis between the cumulative CO_2 evolution and cumulative O_2 uptake. Before regression was performed, O_2 uptake rates were corrected for O_2 uptake needed for the chemical sulfide oxidation (Table 4.2, relationship 7). Mineralized and oxidized fractions of C, N, and S at the different sampling moments were calculated using the measured CO_2, NH_4^+, NO_2^-, NO_3^-, and SO_4^{2-} production and initial C, N, and S contents (Table 4.1).

In literature about SOM mineralization in soils and sediments two approaches can be distinguished that describe their kinetics mathematically. In the first approach kinetics are described with one mineralization rate that decreases with time (Middelburg 1989, Janssen 1984, Feng and Li 2001). In general, this type of model is used to do long term predictions of carbon mineralization, which may be useful to study the impact of the global carbon cycle on global warming. In the second approach, SOM is divided into two or more mathematical components with different mineralization rates (Boudreau and Ruddick 1991, Burdige 1991, Murayama 1984, Kalbitz et al. 2003). This approach is more

suitable for predictions within a relatively short timeframe and may be compared with the two-compartment model that is used to describe the biphasic desorption and degradation of HOC in polluted soils and sediments (Cornelissen et al. 1997a).

It is expected that the residence time of dredged sediments that is needed for ripening in a temporary disposal site is limited to a relatively short period of 3 to 6 years (Harmsen 2001). Therefore, we applied the approach that SOM consists of two mathematical components representing rapidly mineralizable and slowly mineralizable fractions of SOM. The mathematical description of this double exponential model is given in Eq. (4.1).

$$\frac{X_t}{X_0} = (a_X)\,e^{(-k_{X,1}\,t)} + (1-a_X)\,e^{(-k_{X,2}\,t)} \qquad (4.1)$$

where:
X_t = amount of X at t = t, X = Carbon, Nitrogen or Sulfur (g)
X_0 = amount of X at t = 0, X = C, N or S (g)
t = time (d)
a_X = rapidly mineralizable/oxidizable fraction of X, X = C, N or S (-)
$k_{X,1}$ = mineralization rate constant of the rapidly mineralizable/oxidizable fraction, X = C, N, or S (d^{-1})
$k_{X,2}$ = mineralization rate constant of the slowly mineralizable/oxidizable fraction, X = C, N, or S (d^{-1})

Values of a_X, $k_{X,1}$ and $k_{X,2}$ were determined using the Levenberg-Marquardt least square optimization method of the statistical software package SPSS®. This resulted in mineralization and oxidation rates constants for C, N, and S ($k_{X,1}$ and $k_{X,2}$) and a rapidly mineralizable/oxidizable fraction (a_X) for the five different sediments. Oxidation of sulfur in contaminated sediments is mainly caused by an instantaneous chemical oxidation of the inorganic FeS (chapter 2). We assume that the remaining part of the S is present in different forms (organic S, FeS_2) that are not susceptible to oxidation. Therefore, we used a fixed value of 0 for $k_{S,2}$ in Eq. (4.1).

A linear relation exists between k_C and k_N of SOM (Van Veen et al. 1985, Voroney and Paul 1984). We expected such relations to exist for both the rapidly mineralizable fraction and the slowly mineralizable fraction. The relation between k_N and k_C for both fractions depends on the C/N ratio of the SOM and biomass and the dissimilation/assimilation factor (Hendriks 1991, McGechan and Wu 2001):

$$k_N = k_C \left(1 + \frac{1 - \frac{C/N_{SOM}}{C/N_{biomass}}}{diss/ass} \right) \qquad (4.2)$$

where:
C/N_{SOM} = C/N-ratio of the soil organic matter (g g^{-1})
$C/N_{biomass}$ = C/N-ratio of the mineralizing microorganisms (g g^{-1})
$diss/ass$ = dissimilation/assimilation ratio (-)
k_C = C-mineralization constant (d^{-1})
k_N = N-mineralization constant (d^{-1})

We assumed that the sediment have equal values for C/N_{SOM} for both the rapidly mineralizable fraction and the slowly mineralizable fraction.

The dissimilation/assimilation ratio is the ratio between the part of SOM that is converted to CO_2 to the part that is used for the building of new cell material. After rearranging Eq. (4.2), this factor can be calculated with Eq. (4.3).

$$diss/ass = \frac{1 - \frac{C/N_{SOM}}{C/N_{biomass}}}{\frac{k_N}{k_C} - 1} \quad (4.3)$$

In soil science, the ratio of assimilation to the sum of assimilation and dissimilation is called the biosynthesis efficiency (Rijtema et al. 1999). In biotechnology, this biosynthesis efficiency is better known as the yield of biomass on substrate (Roels 1983). Eq. (4.4) converts the dissimilation/assimilation ratio to the yield of biomass on substrate (*Y*).

$$Y = \frac{1}{diss/ass + 1} \quad (4.4)$$

where:
Y = yield of biomass on substrate (g $C_{biomass}$ / g C_{SOM})

4.3 Results and discussion

4.3.1 Composition of the soil solution

During the first week of incubation the pH of the samples decreased with 0.5 (WOGR) to 1.1 (ROSL) pH units. After this week the pH increased with about 0.2 units to stabilize at this value for the rest of the incubation period. The drop in pH is most likely related to the fast chemical oxidation of FeS to H_2SO_4 (relationship 7 of Table 4.2). The sediments we used for this study were well buffered against acidification because $CaCO_3$ contents were always higher than 4% (Table 4.1). This corroborates the data of Zevenbergen et al. (1999) who stated that most dredged sediments in the Netherlands contain an excess of $CaCO_3$ and are therefore not vulnerable to acidification.

Eh increased from about 0 to about +300 mV within a few days of incubation, which is normal for a system that undergoes oxidation by oxygen (chapter 2). Eh stabilized at about +450 mV after about 30 d of incubation. Before starting the incubation experiment we observed methane formation in the containers in which the sediments were stored. Therefore, we expected Eh values lower than about -200 mV at the start of the incubation (Stumm and Morgan 1996). Probably, the electrode was inserted a too short time to achieve complete equilibrium with the sediments (Patrick et al. 1996).

SO_4^{2-} concentrations increased from 120 – 360 mg l^{-1} to 1,570 – 2,760 mg l^{-1} during the first 7 days of incubation. Most probably, SO_4^{2-} formation was caused by the oxidation of inorganic sulfur compounds like FeS, which is a purely chemical process. After 7 to 14 days of incubation, no further increase of SO_4^{2-} concentrations was measured indicating that oxidation of inorganic sulfur compounds had ceased.

NH_4^+ concentrations ranged from < 0.5 to 21 mg l^{-1} at the start of the incubation and decreased to values < 0.5 mg l^{-1} in all samples during the first 20 days of incubation. The relatively high concentrations in some of the samples at the onset of the experiment were most probably a result of anaerobic mineralization of SOM. NH_4^+ formed under aerobic conditions is converted to NO_2^- and NO_3^- by nitrifying microorganisms. Consequently, NH_4^+ concentrations dropped below detection limits during the course of the experiment. NO_2^- concentrations were lower than the detection limit of 0.02 mg l^{-1} during the whole incubation time, because NO_2^- was instantaneously converted into NO_3^-. Contrary to the observed S-mineralization, N-mineralization is a biological process. Therefore, NO_3^- concentration steadily increased from values of < 0.02 – 27 mg l^{-1} at day 0 to 630 – 1,080 mg l^{-1} after 160 d of incubation.

PO_4^{3-} concentrations increased from concentrations below 0.6 to 0.6 – 1.8 mg l^{-1}. Although mineralization of SOM might have caused this increase, a more likely cause is the dissolution of inorganic P-fractions that were insoluble at the previously higher pH-values.

Concentrations of mineral N and P in the soil solution were never below detection limit (0.5 and 0.6 mg l^{-1} respectively) during the 160 days of incubation. Therefore, it is not likely that N or P limited microbial activity during the incubation experiment.

Concentrations of Dissolved Organic Carbon (DOC) were 60 to 120 mg l^{-1} at the start of incubation. No clear decrease or increase was observed during the 160 d of incubation.

4.3.2 Respiration

Oxygen uptake rates ranged from 0.06 (SCSL) to 0.19 mmol O_2 g^{-1} D.M. d^{-1} (ROSL) during the first day. After the first day, oxygen uptake rates sharply decreased, except for ROSL that showed an increase in rate up to 0.221 mmol O_2 g^{-1} D.M. d^{-1} until the third day. After ten days, oxygen uptake rates had further decreased to 0.009 (WOGR) to 0.018 (ROSL) mmol O_2 g^{-1} D.M. d^{-1}. After 21 days oxygen uptake rates were 0.005 (WOGR) to 0.013 (ROSL) mmol O_2 g^{-1} D.M. d^{-1}. During the remaining incubation time, oxygen uptake rates gradually leveled down to values of 0.001 (WOGR) to 0.003 mmol O_2 g^{-1} D.M. d^{-1} (SCSL) after 160 days.

As an example, ROSL oxygen uptake rate and carbon dioxide evolution during incubation are presented in Fig. 4.1. The figure shows relatively low CO_2/O_2 ratios (RQ) during the first days, after which this ratio stabilizes at values of about 0.8 mol mol^{-1}. During the first few days of incubation considerable amount of oxygen were needed for sulfur oxidation. This was confirmed by the increased SO_4^{2-} concentrations that were measured after 7 days (see section 4.3.1).

From the declining oxygen uptake rates, it may be assumed that the stages of exponential and stationary microbial growth were passed within one (WOGR, LERI, SCGR, SCSL) to three (ROSL) days and that the microbial population was in the phase of decline, characterized by negative growth rates (Monod 1949). In this phase the bioavailability

and/or degradability of the substrate (SOM) is limiting the mineralization rate and not the size of the microbial population.

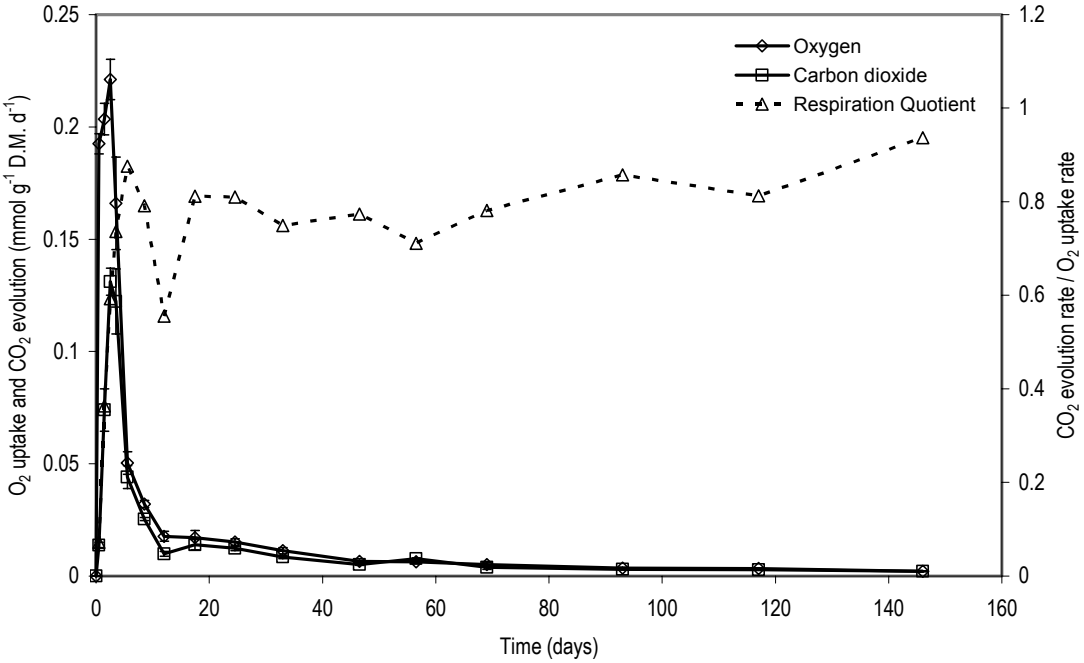

Fig. 4.1 Oxygen uptake rate, carbon dioxide evolution during incubation of ROSL sediment. Markers represent averages of triplicate measurements, ± standard deviation

Regressions between cumulative CO_2 evolution and O_2 uptake are given in Fig. 4.2. O_2 uptake by sulfur oxidation (relationship 7 of Table 4.2) was subtracted from cumulative O_2 uptake before regression was performed. Oxygen used for sulfur oxidation was 10 (ROSL) to 70% (WOGR) of the total oxygen uptake in the first 7 days and 4 to 30% of the oxygen uptake during the whole incubation period. All regression lines, except ROSL, have an intercept with the ordinate, which can be completely explained by CO_2 evolution originating from $CaCO_3$ that is dissolved during decreasing pH. The ROSL regression line has an intercept with the abscissa. This is probably caused by an explosive growth of microorganisms on relatively high amounts of well available and easily degradable substrates during the first few days, which is confirmed by the increasing O_2 uptake rates in ROSL during these days (see above). In the other sediments, this phase of exponential microbial growth was already finished within one day.

The value of the slope of the regression lines represents the average RQ value and amounted 0.82 (ROSL), 0.68 (WOGR), 0.78 (LERI), 0.69 (SCGR), and 0.79 mol mol^{-1} (SCSL), which is in line with values mentioned in the literature. After reviewing the literature, Sepers (1981) found RQ values between 0.69 and 0.83 mol mol^{-1} for aerobic mineralization of SOM in freshwater sediments. The RQ values that we measured are an indication that the major substrate that is mineralized is not TPH because mineralization of TPH leads to RQ values that are 0.40 (Dilly et al. 2001) to 0.67 mol mol^{-1} (Table 4.2). This is confirmed by calculations made on TPH (and PAH) degradation in part 2 of this study (chapter 5).

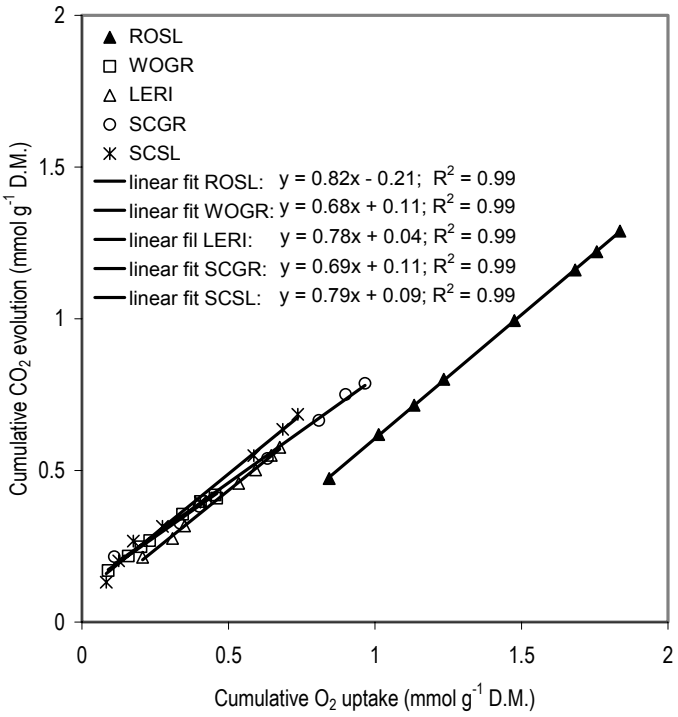

Fig. 4.2 Regressions between cumulative CO_2 evolution and O_2 uptake for ROSL, WOGR, LERI, SCGR, and SCSL dredged sediments

4.3.3 Kinetics of chemical S-oxidation

The S-oxidation kinetics of all studied dredged sediments could be described adequately with Eq. (4.1) with $k_{S,2} = 0$ (see Fig. 4.3). The oxidation rate constants of S ($k_{S,1}$) and the rapidly oxidizable fraction (a_S) of the five sediments are listed in Table 4.3. In addition, the *half-life* of the oxidizable fraction is given. Values for $k_{S,1}$ were higher than 3 d^{-1} for all sediments except SCSL, meaning that 95% of the rapidly oxidizable part of reduced sulfur was oxidized within 1 (ROSL, WOGR, LERI, and SCGR) to 15 (SCSL) days. The presence of relatively easily degradable organic sulfur might be an explanation for the lower value of $k_{S,1}$ for SCSL. The value of a_S ranges from 0.07 to 0.34, suggesting that 7 to 34% of the inorganic sulfur is present as FeS and 93 to 66% is present as the more stable FeS_2 and organic sulfur.

Table 4.3 Quantitative measures of oxidation of sulfur during 160 days of incubation at 30 °C for ROSL, WOGR, LERI, SCGR and SCSL dredged sediments

	a_S (-)	$k_{S,1}$ (d^{-1})	*Half-life 1* (d)	R^2
ROSL	0.069	3.54	0.20	0.98
WOGR	0.343	3.45	0.20	0.96
LERI	0.171	3.22	0.22	0.88
SCGR	0.229	3.18	0.22	0.90
SCSL	0.239	0.19	3.65	0.93

4.3.4 Kinetics of biological C-, N-, and P- mineralization

The mineralization rate constants of C ($k_{C,1}$ and $k_{C,2}$) and the rapidly mineralizable fraction (a_C) of the five sediments are listed in Table 4.4. In addition, the *half-lives* of the different fractions are given.

Table 4.4 Quantitative measures of mineralization of organic carbon during 160 days of incubation at 30 °C for ROSL, WOGR, LERI, SCGR and SCSL dredged sediments

	a_C (-)	$k_{C,1}$ (d^{-1})	$k_{C,2}$ (d^{-1})	*Half-life 1* (d)	*Half-life 2* (year)	R^2
ROSL	0.100	0.174	0.00047	3.98	4.05	0.99
WOGR	0.043	0.200	0.00022	3.47	8.64	0.99
LERI	0.063	0.183	0.00036	3.79	5.28	0.99
SCGR	0.068	0.067	0.00054	10.3	3.52	0.98
SCSL	0.094	0.050	0.00053	13.9	3.58	0.99

The double exponential model (Eq. 4.1) allowed to adequately describe the C-mineralization (Fig. 4.3).

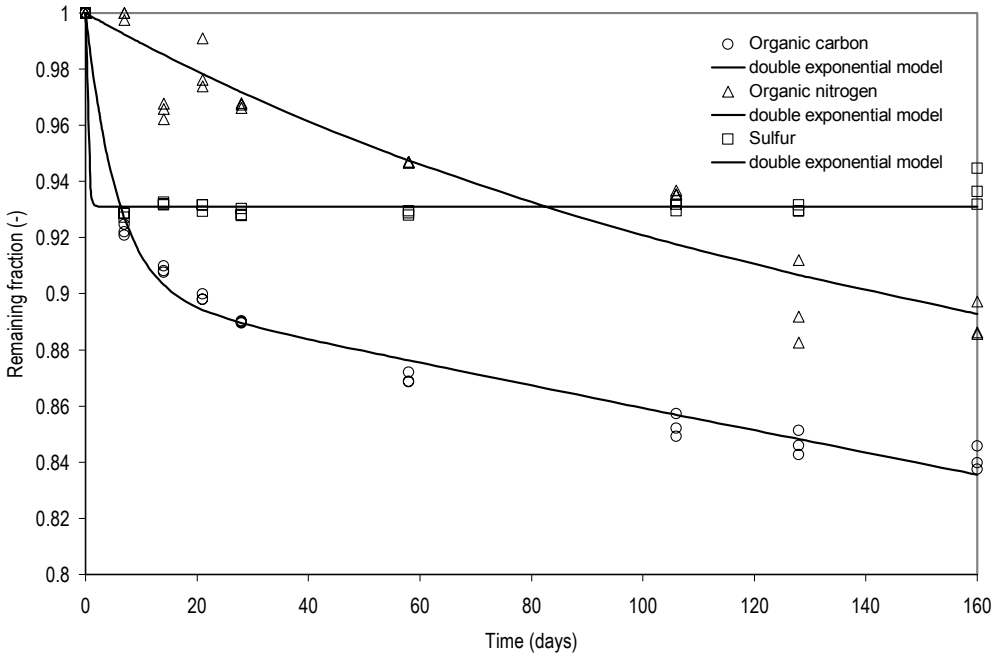

Fig. 4.3 Mineralization and oxidation kinetics of carbon, nitrogen and sulfur for ROSL dredged sediment

The rapidly mineralizable fraction SOM (a_C) varies between 0.04 and 0.10 (Table 4.4). 95% of the rapidly mineralizable fraction of SOM has been mineralized after about 20 (ROSL, WOGR, and LERI) to 50 (SCGR and SCSL) days. The size of this fraction is related to the mineralization history of the SOM. SOM that has a long history of mineralization, contains small fractions of rapidly mineralizable SOM and large fractions of slowly mineralizable SOM (Janssen 1984, Middelburg 1989). The small fraction rapidly mineralizable SOM (a_C) of our sediments points to SOM that already has a history of mineralization. This is an indication that the mineralization of 'fresh' organic matter (leaves and other plant residues) already begins at the bottom of the surface waters. ROSL has the largest rapidly mineralizable fraction, which correlates well with the high amounts of intact plant residues that were removed during sieving of this sediment sample. The

relatively high C/N ratio of ROSL (23.6 g g^{-1}) is also typical for relatively fresh SOM (chapter 2).

Mineralization rate constants of the rapid fraction ($k_{C,1}$) amount up to 0.05 to 0.20 d^{-1} (Table 4.4). These values are very similar to the values that were found in the literature. Summarizing different sources of data on mineralization of SOM, Hunt (1978) reported rate constants for rapid mineralization between 0.03 and 0.20 d^{-1}. Kalbitz et al. (2003) measured values of 0.11 to 0.31 d^{-1} for mineralization of dissolved organic matter at 20 °C.

Rate constants for the slowly mineralizable fractions SOM ($k_{C,2}$) vary between 0.00022 and 0.00054 d^{-1} (Table 4.4) and are therefore about 100 to 1,000 times lower than the rate constants for the rapidly mineralizable fractions. The values are lower than the values of Hunt (1978) who reported values of 0.00064 to 0.0067 d^{-1} but comparable to the values of 0.00022 to 0.00050 that were reported by Kalbitz et al. (2003) for dissolved organic matter with rapidly mineralizable fractions (a_C) of 0.03 to 0.06. Kalbitz et al. (2003) reported higher values for $k_{C,2}$ (0.0017 to 0.0085 d^{-1}) for dissolved organic matter with rapidly mineralizable fractions of 0.13 to 0.43. Assuming that every 10 °C increase in temperature increases the microbial activity with a factor 2 (Q_{10} = 2), the k-values in Table 4.4 that are measured at a temperature of 30 °C should be divided by a factor 4 to achieve values that are approximately valid for the Dutch yearly average temperature of 10 °C. This results in $k_{C,2}$-values ranging from 0.02 to 0.05 y^{-1}, which is exactly in the same range as the C-mineralization rate constants that are reported in literature for 'stable' SOM in terrestrial soils under moderate climatic conditions (Kortleven 1963, Saxena and Bartha 1983, Priesack et al. 2001).

The values of $k_{S,1}$, $k_{C,1}$, and $k_{C,2}$ are technologically interesting, because they can be used to optimize conditions for ripening during temporary disposal. If values of SOM content, (reduced) sulfur content, $k_{C,1}$, $k_{C,2}$ and $k_{S,1}$ are known, oxygen uptake rates and the maximum sediment layer thickness that can be oxygenated in a disposal site within the desired residence time can be calculated (chapter 6). Besides, the values of $k_{C,2}$ maybe interesting for long term environmental reasons since they may be correlated with the slow release and degradation of HOC (Reemtsma et al. 2003, Harmsen 2004). Mineralization rates based on slurry incubations may deviate from in situ rates. However, studies of the effects of slurrying on bacterial activity are not univocal (Dauwe et al. 2001). Our observation that $k_{C,2}$-values are in the same range as in situ C-mineralization rate contants suggests that the deviation from in situ rates are of minor importance only.

The mineralization rate constants of N ($k_{N,1}$ and $k_{N,2}$) and the rapidly mineralizable fraction ($a_N = a_C$) of the five sediments are listed in Table 4.5. In addition, the *half-lives* of the different fractions are given. As expected, N-mineralization rates were correlated well with C-mineralization rates. Consequently, also N-mineralization could be described well with the double exponential model (Table 4.5, Fig. 4.3). The values for $k_{N,1}$ are 4.9 – 18.7 times smaller than the values for $k_{C,1}$, whereas this ratio decreases to 1.2 – 2.2, for $k_{N,2}$ and $k_{C,2}$.

Table 4.5 Quantitative measures of mineralization of organic nitrogen during 160 days incubation at 30 °C for ROSL, WOGR, LERI, SCGR and SCSL dredged sediments

	a_N [a] (-)	$k_{N,1}$ (d^{-1})	$k_{N,2}$ (d^{-1})	*Half-life 1* (d)	*Half-life 2* (year)	R^2
ROSL	0.100	0.0093	0.00021	74.5	9.05	0.90
WOGR	0.043	0.019	0.00019	36.5	10.0	0.94
LERI	0.063	0.037	0.00011	18.7	17.3	0.93
SCGR	0.068	0.0091	0.00026	76.2	7.31	0.98
SCSL	0.094	0.0091 [b]	0.00020 [b]	76.2	9.51	0.69

[a] a_N was assumed to be equal to a_C (Table 4.4)

[b] the fit procedure did not converge, so the estimate of $k_{N,1}$ was found by assuming a value of 0.00020 d^{-1} for $k_{N,2}$

The ratio between k_N and k_C (Tables 4.4 and 4.5) was used to calculate the yield of biomass on substrate (Y) with Eqs. (4.3) and (4.4). For the C/N ratio of biomass ($C/N_{biomass}$) a value of 4.29 g g^{-1} (bacteria) was assumed according to Roels (1983). The C/N ratios of the SOM (C/N_{SOM}) were taken from Table 4.1 and assumed to be constant during the 160 days of incubation. Calculated yields are 0.17 to 0.38 g $C_{biomass}$ / g C_{SOM} for the rapidly mineralizing SOM and 0.06 to 0.31 g $C_{biomass}$ / g C_{SOM} for the slowly mineralizing SOM (Table 4.6). These values are comparable to yields reported in the literature that range from 0.05 to 0.60 g $C_{biomass}$ / g C_{SOM} for microbial growth on SOM or other organic substrates (Chapman and Gray 1986, Roels 1983). Holland and Coleman (1987) reported yields between 0.60 – 0.70 g $C_{biomass}$ / g C_{SOM} for aerobic bacteria in the exponential growth phase and 0.20 – 0.70 g $C_{biomass}$ / g C_{SOM} in the stationary growth phase. Natural substrates like SOM with a higher C/N ratio or molecular complexity generally result in a lower Y (Linley and Newell, according to Schwaerter et al. 1988). Similar relations between Y and substrate complexity were found for straight alkanes and the more complex branched alkanes (Geerdink et al. 1996). The relatively low Y_1 calculated for ROSL may therefore be related to the relatively high C/N ratio of the SOM. The most likely reason for the lower yield in the biochemically stabilized (ripe) sediment (Y_2) as compared with the yield in the freshly dredged (unripe) sediment (Y_1) lies in its higher average SOM complexity of the SOM. The extremely low $k_{C,2}$ of WOGR indicates that this sediment reached the highest average complexity (and therefore stability) of the studied sediments. This also explains its extremely low Y_2 of 0.06 g $C_{biomass}$ / g C_{SOM}.

Table 4.6 Calculated yields of biomass on labile (Y_1) and stable SOM (Y_2) (Eqs. (4.3) and (4.4))

	Y_1 (g $C_{biomass}$ / g C_{SOM})	Y_2 (g $C_{biomass}$ / g C_{SOM})
ROSL	0.17	0.11
WOGR	0.31	0.06
LERI	0.31	0.28
SCGR	0.38	0.27
SCSL	0.38	0.31

No correlation was observed between C-mineralization and P-concentrations in the soil solution. P-concentrations are most probably governed by the dissolution of non-organic P fractions caused by the decrease in pH and can therefore not be used to make estimates about P-mineralization rates.

4.4 Conclusions

Aerobic carbon, nitrogen, sulfur and phosphorus mineralization and oxidation of five previously anaerobic PAH and TPH polluted dredged sediments were monitored in the laboratory during a 160 days incubation experiment at 30 °C. During the experiment pH dropped 0.3 to 0.9 units as a result of (chemical) sulfur oxidation. Redox potentials increased from values of about 0 to +450 mV within the first 28 days and remained stable during the remaining incubation period.

O_2 uptake and CO_2 evolution were highly correlated and RQ values ranged from 0.68 to 0.82 mol mol^{-1} indicating that (biological) SOM mineralization is the major oxygen consuming process in ripening dredged sediments and not PAH or TPH. Chemical oxidation of reduced non-organic sulfur compounds (FeS) resulted in clearly higher oxygen uptake during the first few days only, after which no further sulfur oxidation was observed. During this short period 7 to 34% of the total sulfur content was oxidized. Oxygen used for sulfur oxidation amounted up to 70% of the total oxygen uptake in the first 7 days and up to 30% of the oxygen uptake during the whole incubation period.

Nutrients were not limiting the (biological) aerobic mineralization processes in the previously anaerobic dredged sediments because previously anaerobic dredged sediments are enriched with ample organic and inorganic nutrients while still on the bottom of the waterway.

A double exponential model could adequately describe carbon and nitrogen mineralization kinetics in dredged sediments. The rate constants of rapidly mineralizing SOM that mineralized for 95% during the first 20 to 50 days of incubation were 100 to 1,000 times higher than the rate constants of the slowly mineralizing SOM. First order rates of slowly mineralizing SOM were 0.00011 to 0.00026 d^{-1} and are similar to those of terrestrial soils. It can therefore be concluded that dredged sediments can be regarded biochemically ripened after an oxygenation period of 20 to 50 days (at 30 °C). The resulting 'soil' will have the same biochemical characteristics as a terrestrial soil with the same mineralogical composition. Differences between carbon and nitrogen mineralization rates were explained by yields of biomass on substrate between 0.20 and 0.45 g $C_{biomass}$ / g C_{SOM} for the rapidly mineralizable SOM and between 0.08 and 0.38 g $C_{biomass}$ / g C_{SOM} for the slowly mineralizable SOM.

The quantitative data presented in this paper can be used to estimate the maximum sediment layer thickness that can be oxygenated during temporary disposal of contaminated sediments. Besides, the data give insight into the potential reduction of SOM that can be achieved during disposal and the time needed to achieve a stabilized product that can be used as a building material. Finally, the data may be used to test the hypothesis that degradation kinetics of SOM are linked to the desorption and degradation of HOC.

Acknowledgements

Geert Meijer and Hillion Wegh from our sub-department are acknowledged for their invaluable assistance with the instrumental analyses. The research was supported by and performed within the Research Centre on Soil, Sediment and Groundwater Management and Remediation WUR/TNO.

5

BIOCHEMICAL RIPENING OF DREDGED SEDIMENTS

2. Degradation of PAH and TPH in slurried and consolidated sediments

Maar waar blijven het diepe inzicht
en de natuurlijke vertrouwdheid met de grote problemen,
als iemand zijn opleiding krijgt
in een laag landje van modder en klei,
zonder één berg?

Nooit meer slapen – W.F. Hermans

This chapter is based on a paper that was submitted for publication (Vermeulen et al. submitted b)

Abstract

Ripening of PAH and TPH polluted dredged sediment during upland disposal can be considered as a bioremediation technique. We studied the aerobic biodegradation of PAH and TPH in five previously anaerobic slurried sediments during a 360 days incubation experiment. Besides, we studied the oxygen penetration and degradation of PAH and TPH in three consolidated (physically ripened) sediments. All experiments were conducted in the laboratory at 30 °C. A double exponential model could adequately describe PAH and TPH degradation kinetics in the slurried sediments. First order degradation rate constants for the rapidly degradable fractions (12 to 58%) were about 0.13 and 0.058 d^{-1} for PAH and TPH, respectively, whereas the rate constants for the slowly degradable fractions were about 0.00044 (PAH) and 0.00067 d^{-1} (TPH). Rate constants for the rapidly and slowly degrading fractions are similar to the mineralization rate constants of the rapidly and slowly mineralizing SOM fractions in the sediments, indicating that degradation of PAH and TPH and SOM mineralization are linked processes. Oxygen uptake by degradation of PAH and TPH was negligible compared to the oxygen uptake by sulfur oxidation and soil organic matter mineralization. In consolidated sediments, PAH and TPH degradation was limited to the oxygenated part. Amounts of PAH and TPH that were degraded in the oxygenated parts of the consolidated sediments during 21 days of incubation were similar to the amounts that degraded during 21 days in the slurried sediments.

5.1 Introduction

Following the application of clayey dredged sediments to a temporary upland disposal site, the soil formation is initiated. This process is called ripening. Ripening irreversibly converts water-logged consolidated clayey sediments into soil by desiccation and structure development (Pons and Van der Molen 1973, chapter 2). After structure has been developed, oxygen can penetrate into the air-filled cracks of the disposed material and into the aggregates between these cracks. In the part of the sediments in which oxygen has penetrated (the 'oxygenated' part), biochemical ripening starts. In part 1 of this study on biochemical ripening (chapter 4), oxidation of reduced sulfur compounds and mineralization of soil organic matter (SOM) were described extensively.

Aerobic biodegradation of bioavailable organic micropollutants like Polycyclic Aromatic Hydrocarbons (PAH) and mineral oil, defined as Total Petroleum Hydrocarbons (TPH), is stimulated by oxygenation. This degradation can also be regarded as a biochemical ripening process. The toxicity of PAH and TPH polluted sediments is strongly reduced by active oxygenation of slurried sediments (Tabak et al. 2003) or ripening (passive oxygenation) of consolidated sediments (Harmsen 2004). Therefore, ripening can be considered as a bioremediation technique for sediments that are contaminated with these pollutants (chapter 2).

Hydrophobic organic carbons (HOC) like PAH and TPH strongly sorb to the soil organic matter (SOM) in sediments and can only be biodegradaded after they have been released (e.g. by desorption) into an aqueous phase containing microorganisms that are capable to degrade them (Reid et al. 2000, Johnsen et al. 2005). Desorption and subsequent biodegradation of micropollutants exhibits biphasic behavior. During the initial phase of biodegradation, desorption of pollutants is rapid and the rate of removal of organic pollutants like PAH and TPH is primarily limited by microbial degradation kinetics. Pollutants that are removed during this phase can be classified as 'bioavailable'. During the second phase, the rate of removal of pollutants is limited by desorption processes

(Cornelissen et al. 1998, Cuypers et al. 2000, Bonten 2001, Huesemann et al. 2003). Pollutants that are degraded during this phase can be classified as 'poorly available'. Different mechanisms to explain this poor availability are proposed in the literature (Gevao et al. 2000, Reid et al. 2000, Semple et al. 2003, Ehlers and Loibner 2006). However, regardless of the exact mechanisms, it may be hypothesized that degradation kinetics of hydrophobic pollutants are equal to the mineralization kinetics of the SOM (Reemtsma et al. 2003, Harmsen 2004).

To evaluate the hypothesis that biodegradation of PAH and TPH are linked to the mineralization of SOM, the kinetics of PAH and TPH degradation were quantified in this part of the study and were compared with the kinetics of SOM mineralization that were quantified in part 1 of this study (chapter 4). To investigate whether there is a bias in the measurements in slurries relative to in situ (upland disposal) degradation of PAH and TPH, the extent of PAH and TPH degradation in these slurries was compared with the degradation of PAH and TPH in consolidated sediments that had been physically ripened to different extents.

5.2 Materials and methods

5.2.1 Incubation experiment with slurried sediments

Five types of slurried clayey dredged sediments (ROSL, WOGR, LERI, SCGR, SCSL) were studied in an incubation experiment. The origin of the samples, sample preparation, sample characteristics, and the used incubation method were extensively described in part 1 of this study (chapter 4). Briefly, serum bottles containing 14 to 20 g of wet sediment and a headspace filled with air were incubated at 30 °C, whilst on a rotary tumbler. To get reliable measurements on slow PAH and TPH degradation, the incubation time was extended to 352 days. At ten moments between 0 and 307 to 352 days after the start of incubation, bottles were sacrificed in triplicate for PAH and TPH analyses (see section 5.2.3). Besides, bottles were sacrificed after 0, 21, and 160 days of incubation to monitor the bioavailability of PAH (see section 5.2.4). Table 5.1 presents the initial concentrations of low, medium and high molecular weight, as well as total PAH and TPH in the studied sediments.

Table 5.1 Initial PAH and TPH concentrations in ROSL, WOGR, LERI, SCGR, and SCSL dredged sediments

	PAH [a] (mg kg^{-1})				TPH (mg kg^{-1})		
	2 & 3 ring	4 ring	5 & 6 ring	Σ16 EPA	C10 – C20	C20 – C40	C10 – C40
ROSL	17	12	69	98	1,429	7,739	9,168
WOGR	36	37	30	82	451	1,871	2,322
LERI	117	26	32	175	566	1,820	2,386
SCGR	14	7	16	38	74	384	458
SCSL	17	9	16	42	171	828	999

[a] Σ16 EPA except Naphthalene, Acenaphtylene, Benzo[*a*]anthracene and Chrysene

5.2.2 Incubation experiment with consolidated sediments (pellets)

In addition to the incubation experiment with slurried sediments, an incubation experiment was carried out with consolidated sediments (artificial aggregates, hereafter referred to as pellets). Specially designed microdepots were used to physically ripen (consolidate) three different sediments (ROSL, WOGR, LERI) to different extents. This laboratory ripening of the sediments, that resulted into disc-shaped pellets with a diameter of about 45 mm and a height of about 20 mm, was extensively described in an earlier study of us (chapter 3). In this study, the matric potential (ψ_m) – a measure to quantify the moisture condition of sediments (appendix 3) – of the water in the pellets was adjusted to six different values: ψ_m = -100, -333, -1,000, -2,000, -16,000, and -1,000,000 hPa (all in triplicate).

To prevent ongoing desiccation due to evaporation during incubation, the pellets were stored over different NaCl solutions in desiccators. The osmotic potentials of the NaCl solutions, determining the vapor pressure of the air in the desiccators, were fixed at the same magnitude as the different matric potentials of the pellets. The desiccators were stored in the dark at 30 °C for 21 days. After 10 and 21 days of incubation, oxygen profiles were measured in the pellets. For a detailed description of the methods that we used to measure the oxygen profiles we refer to Vermeulen et al. (2002), Malina et al. (2004), and chapter 3. After 21 days, the pellets were separated into oxygenated and anoxic parts, based on the measured oxygen profiles. Both parts were analyzed for PAH and TPH (see section 5.2.3).

5.2.3 Analytical methods

5.2.3.1 Extractions

Both the slurried and the consolidated sediment samples were mixed with acetone and water up to an acetone/water ratio of 4:1 (v/v). The resulting slurry was sonicated for 15 min (Retsch UR 2) and shaken on a rotary tumbler at 20 °C (22 rev. min^{-1}) for one hour (after Noordkamp et al. 1997). After shaking, 1 ml of the slurry was centrifuged (5 min, 13,000 g), and the supernatant was analyzed for PAH by HPLC-UV as described in section 5.2.3.2.

The applied extraction procedure for TPH was a modified version of the method that was described in NEN 5733 (NEN 1997). Petroleum ether (30 ml) was added to the sediment slurry that remained after 1 ml of it had been centrifuged (see above) for PAH analysis. The slurry was mixed on the rotary tumbler at 20 °C for 30 min after which it was allowed to settle for 5 min and the liquid phase was decanted over a vacuum filter (glass filter, S&S GF 50). Petroleum ether (20 ml) was added to the (non-decanted) residue; the resulting slurry was mixed for 15 min and decanted over the glass filter. The filtrate was transferred to a separation funnel and shaken twice with 200 ml of acidified (1 ml H_2SO_4) tap water. The petroleum ether phase was transferred into a 100 ml bottle over a glass filter that was covered with 5 g of anhydrous Na_2SO_4. The filtrate was weighed for calculation of the exact petroleum ether volume. To remove extracted humic polar

compounds, 10 ml of the extract was transferred into a 30 ml bottle and cleaned up with 3 g of purified Florisil®. After shaking for 30 min (rotary tumbler at 20 °C) and settling of the Florosil®, the extract was analyzed by GC-FID as described in section 5.2.3.2. Between the different extraction steps, all glassware was rinsed with petroleum ether to include all TPH in the final extract.

5.2.3.2 Instrumental analyses

PAH in the acetone/water mixture (20 µl of extract) were separated on a reverse-phase C18 column (Vydac 201TP54, 5µm, 4.6mmID × 250mmL) with external guard column (Vydac 102GD54T, 5µm) using a mixture of acetonitrile and water. PAH were detected by UV absorbance (Gynkotec UVD340S). The following PAH were measured (used absorbance wavelengths as proposed in NEN 5771 (NEN 1999) are given between brackets): a) 2 – 3 rings: acenaphthene (227 nm), flurorene (261 nm), phenanthrene (251 nm), anthracene (252 nm), fluoranthene (236 nm); b) 4 rings: pyrene (240 nm), benzo[*b*]fluoranthene (256 nm), benzo[*k*]fluoranthene (307 nm); 5 – 6 rings: benzo[*a*]pyrene (296 nm), dibenzo[*a,h*]anthracene (297 nm), benzo[*g,h,i*]perylene (299 nm), indeno[*1,2,3-c,d*]pyrene (250 nm). Naphthalene and acenaphtylene were not analyzed because their concentration largely varied within the bulk samples. Benzo[*a*]anthracene and chrysene were not analyzed because they could not sufficiently be distinguished from each other.

Measurement of TPH in the petroleum ether (3 µl of extract) was performed on a gas chromatograph (Hewlett-Packard 5890 Series II) equipped with a WCOT fused silica column (Chrompack-Varian, 0.32 mmID × 10 mL) coated with CP SimDist (film thickness 0.1 mm). Helium was used as carrier gas. The GC was equipped with a Flame Ionization Detector. TPH concentrations were calculated by group integration (C10 – C20 and C20 – C40) of the unresolved peaks after subtraction of a blank (petroleum ether).

The oxygen profiles in the pellets were measured with a cathode-type microelectrode (Visscher et al. 1991) combined with an InLab® 302 Ag/AgCl reference electrode. An industrial precision height gauge was used to insert the microelectrode into the pellets with increments of 0.25 mm (± 0.01 mm).

5.2.4 Measurement of PAH bioavailability

To measure the bioavailability of PAH, the persulfate oxidation method was used that was developed at our laboratory (Cuypers et al. 2000). Briefly, the (wet) sediment was thoroughly mixed with $K_2S_2O_8$ and demineralized water to obtain a persulfate ($S_2O_8^{2-}$) to soil organic matter ratio of 12 g g^{-1} and an aqueous persulfate concentration of 0.0357 g ml^{-1}. The resulting slurry was placed in a water bath shaker at 70 °C and shaken end-to-end (120 rev. per min). After 3 hours, the slurry was filtered (glass filter, S&S GF 50) and solids were extracted for PAH analysis (see section 5.2.3).

The persulfate oxidation method is not suitable for the measurement of TPH bioavailability (Cuypers et al. 2001). Although other methods are currently available to measure TPH bioavailability, they have not been used in the current study.

5.2.5 Calculations

5.2.5.1 Slurried sediments

We used a double exponential model (Eq. 5.1) to describe the (biphasic) degradation kinetics of PAH and TPH during the incubation experiment with slurried sediments (after Cornelissen et al. 1997a). This equation was also used in part 1 of this study to describe the mineralization kinetics of soil organic matter (chapter 4).

$$\frac{X_t}{X_0} = (a_X)\,e^{(-k_{X,1}\,t)} + (1-a_X)\,e^{(-k_{X,2}\,t)} \qquad (5.1)$$

where:

X_t = amount of X at t = t, X = PAH or TPH (mg)
X_0 = amount of X at t = 0, X = PAH or TPH (mg)
t = time (d)
a_X = rapidly degradable fraction of X, X = PAH or TPH (-)
$k_{X,1}$ = degradation rate constant of the rapidly degradable fraction, X = PAH or TPH (d^{-1})
$k_{X,2}$ = degradation rate constant of the slowly degradable fraction, X = PAH or TPH (d^{-1})

Values of a_X, $k_{X,1}$ and $k_{X,2}$ were determined using the Levenberg-Marquardt least square optimization method of the statistical software package SPSS®. This resulted in degradation rates of PAH and TPH ($k_{X,1}$ and $k_{X,2}$) and an estimation of the rapidly degradable fraction (a_X) for the five different sediments.

5.2.5.2 Consolidated sediments (pellets)

To calculate average oxygen uptake rates (Q) of the pellets at day 10 and 21, we used Eq. 5.2. This equation describes the relation between Q and the oxygen penetration depth (z_{pen}) under steady state conditions (after Glinski and Stepniewski 1985).

$$Q = \frac{2D_{s,matrix}G_r}{(z_{pen})^2} \qquad (5.2)$$

$$\text{with} \quad G_r = (\phi_{a,matrix} + \alpha_B\,\theta)c_{atm} \qquad (5.3)$$

where:

Q = oxygen uptake rate per unit volume of oxygenated pellet ($cm^3\ O_2\ cm^{-3}$ matrix s^{-1})
$D_{s,matrix}$ = intra-pellet oxygen diffusion coefficient ($cm^2\ s^{-1}$)
G_r = apparent oxygen concentration at the surface of the pellet ($cm^3\ cm^{-3}$)
z_{pen} = oxygen penetration depth (cm)
$\phi_{a,matrix}$ = intra-pellet air-filled porosity ($cm^3\ cm^{-3}$)
α_B = Bunsen's coefficient, oxygen solubility in water / oxygen solubility in gas at P=101.3 kPa and T=303 K (0.0290) ($cm^3\ cm^{-3}$); after Glinski and Stepniewski 1985
θ = volumetric pellet moisture content ($cm^3\ cm^{-3}$)
c_{atm} = oxygen concentration in the atmosphere (0.21) ($cm^3\ cm^{-3}$)

In systems without oxygen consumption, the ratio between the passed time and the time needed to reach steady state can be expressed in a so called Fourier number (*Fo*). The Fourier number gives an indication whether it is legitimate to use Eq. (5.3) in our situation. For our pellets *Fo* is defined as:

$$Fo = \frac{D_{s,matrix}\, t}{\left(z_{pen}\right)^2} \tag{5.4}$$

where:
Fo = Fourier number (-)
t = time (s)

It can assumed that an equilibrium oxygen concentration profile has been achieved if *Fo* is larger than 1.

5.3 Results and discussion

5.3.1 Incubation experiment with slurried sediments

5.3.1.1 PAH and TPH degradation kinetics

The biodegradation of PAH and TPH generally showed a biophasic behaviour with concentrations dropping rapidly during the first period of incubation, after which degradation rates levelled off to low values. This behavior has been described by many researchers and can be explained by limitation of microbial degradation kinetics and desorption kinetics during the first and second phase, respectively (e.g. Cuypers et al. 2000).

Figs. 5.1 and 5.2 present the measured and fitted (Eq. (5.1)) degradation kinetics of PAH and TPH in ROSL slurried sediment. Similar curves were found for the other sediments studied. The PAH and TPH degradation kinetics could be described well with Eq. (5.1). The rapidly degradable fraction (a_{PAH} and a_{TPH}) and the rapid and slow degradation rate constants of PAH ($k_{PAH,1}$ and $k_{PAH,2}$) and TPH ($k_{TPH,1}$ and $k_{TPH,2}$) of the five sediments are listed in Table 5.2. The rate constants for rapid degradation of the low molecular weight PAH and TPH were higher (but had the same order of magnitude) than those of the high molecular weight PAH and TPH. No differences could be distinguished between the rate constants for slow degradation of PAH and TPH of different molecular weighs. This is in line with the observations of Harmsen (2004) and therefore, only average degradation rate constants are showed in Table 5.2.

The rapidly degradable fractions of PAH and TPH (*a*) varied between 0.24 and 0.58 and is obviously not related to the rapidly mineralizable fraction of SOM that were reported in part 1 of this study (chapter 4) and that were much lower (0.043 to 0.10). The size of the rapidly mineralizable fraction SOM is related to the length of the mineralization history of the SOM (chapter 4), whereas the sizes of the rapidly degradable fractions of PAH and TPH are related to length of the period between contamination and degradation (that is the sorption time). According to the values of Table 5.2, 95% of the rapidly degradable fraction of PAH was degraded after about 10 (LERI and SCGR) to 50 days (ROSL,

WOGR en SCSL), whereas 95% of the rapidly degradable fraction of TPH was degraded after about 25 (WOGR and LERI) to 100 days (ROSL and SCSL).

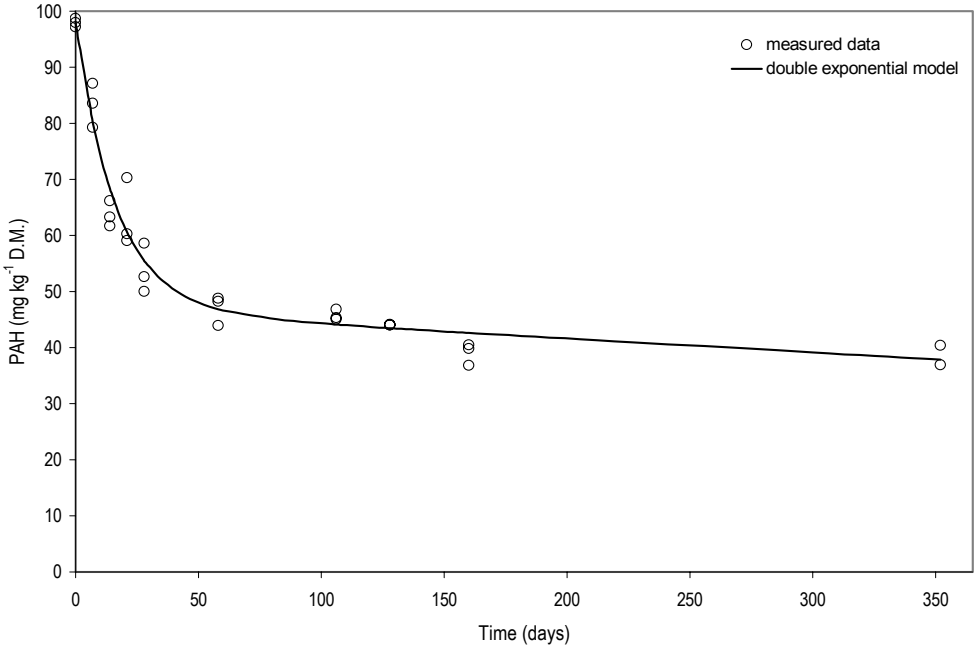

Fig. 5.1 Degradation kinetics of PAH (Σ16 EPA) in slurried ROSL dredged sediments during 352 days of incubation at 30 °C

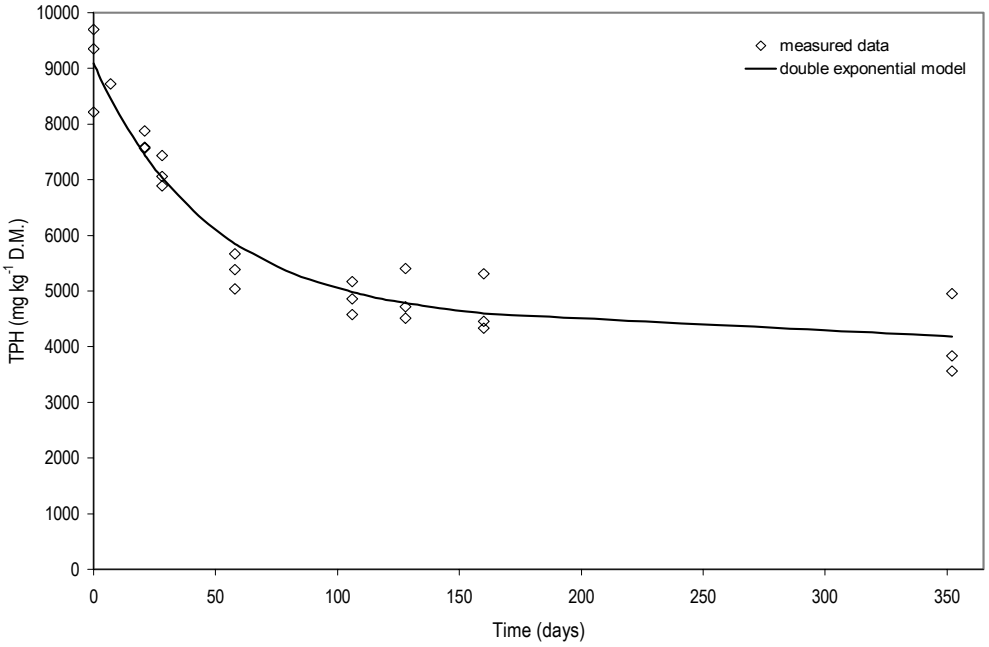

Fig. 5.2 Degradation kinetics of TPH (C10 – C40) in slurried ROSL dredged sediments during 352 days of incubation at 30 °C

Table 5.2 Quantitative measures of degradation of PAH and TPH during 307 – 352 days of incubation at 30 °C for ROSL, WOGR, LERI, SCGR and SCSL dredged sediments

	PAH (Σ16 EPA)				TPH (C10 – C40)			
	a_{PAH} (-)	$k_{PAH,1}$ (d^{-1})	$k_{PAH,2}$ (d^{-1})	R^2 (-)	a_{TPH} (-)	$k_{TPH,1}$ (d^{-1})	$k_{TPH,2}$ (d^{-1})	R^2 (-)
ROSL	0.52	0.061	0.00062	0.97	0.48	0.022	0.00035	0.92
WOGR	0.48	0.095	-0.00099 [a]	0.28	0.58	0.11	0.00036	0.95
LERI	0.33	0.26	0.00034	0.24	0.24	0.078	0.0017	0.90
SCGR	0.12	3.27 [b]	0.00066	0.75	- [c]	- [c]	- [c]	- [c]
SCSL	0.53	0.11	0.00015	0.77	0.40	0.021	0.00025	0.89

[a] negative value caused by an increase of PAH concentrations after 83 days of incubation

[b] probably unreliable because of low initial PAH concentrations (see also Table 5.1)

[c] no parameters could be estimated because all measured values scatter around a value of 450 mg kg^{-1}, which is close to the detection limit of the used method of analysis for sediments containing SOM (NEN 1997)

5.3.1.2 Rapid degradation of PAH and TPH

Neglecting the extremely high value for SCGR, values for $k_{PAH,1}$ vary between 0.061 and 0.26 d^{-1} and are similar to degradation constants that are reported in the literature. Based on a literature review, Cornelissen et al. (1998) reported degradation rate constants for rapid degradation varying from 0.02 to 0.2 d^{-1}.

Desorption of HOC is also quantified with a double (Cornelissen et al. 1997a), and sometimes triple (Cornelissen et al. 1997b), exponential model. Therefore, it is legitimate to make comparisons between rate constants for degradation and desorption. Literature rate constants for rapid desorption of PAH are 1 to 70 d^{-1} (Cornelissen et al. 1998, Bonten 2001) and are thus clearly larger, indicating that degradation kinetics were indeed limiting during this phase and not desorption kinetics.

Values for $k_{TPH,1}$ vary from 0.021 to 0.11 d^{-1} and are also comparable to literature degradation constants for TPH biodegradation that range from 0.01 to 0.04 d^{-1} (Nocentini et al. 2000, Salanitro et al. 1997). The k_1 values for TPH have the same order of magnitude as the values for PAH, indicating that the same release and degradation mechanisms might be at work during the first phase of degradation (Cuypers et al. 2001).

Sulfur oxidation, which consumed the largest proportion of oxygen during the rapid phase of degradation (chapter 4), might have limited SOM mineralization and PAH and TPH degradation through oxygen competition. However, oxidation rate constants for sulfur ($k_{S,1}$) are much higher than rapid mineralization and degradation constants of SOM and PAH and TPH (chapter 4), meaning that sulfur oxidation did not interfere with mineralization and degradation of SOM and PAH and TPH. Sulfur oxidation can also lead to severe acidification of oxygenated sediments with the result that bioremediation can be halted (Tabak et al. 2003). However, our sediments were well buffered (chapter 4) and the values measured for $k_{PAH,1}$ and $k_{TPH,1}$ are equal to the literature values that were measured under neutral conditions (Cornelissen et al. 1998, Nocentini et al. 2000, Salanitro et al. 1997). We therefore conclude that biodegradation of PAH and TPH was not negatively impacted by sulfur oxidation.

5.3.1.3 Slow degradation of PAH and TPH

Values for $k_{PAH,2}$ vary between 0.00015 and 0.00066 d^{-1} and are similar to the values found in the literature. Harmsen (2004) found an average value of 0.0004 d^{-1} during long term experiments with ripening sediments in the field. The values are about a factor 10 to 100 smaller than the desorption rate constants of 0.008 to 0.09 d^{-1} that were found in the literature for slow desorption (Cornelissen et al. 1997a, Bonten 2001), but are similar to the desorption rate constants of 0.0002 to 0.002 d^{-1} that were classified as very slow (Cornelissen et al. 1997b). The unexpected negative value for $k_{PAH,2}$ of WOGR was completely caused by an increase in the measured concentrations of 5 and 6 ring PAH after 83 days, which was probably caused by heterogeneity of the initial sediment or by an increase in analytical availability (see also section 5.3.1.5).

Values for $k_{TPH,2}$ are 0.00025 to 0.0017 d^{-1} and are also comparable to values of 0.0003 to 0.0005 d^{-1} that Harmsen (2004) measured during field experiments. No desorption rate constants for slowly desorbing TPH were found in the literature, but it may be assumed they are similar to slow desorption rate constants of PAH (Cuypers et al. 2001).

5.3.1.4 PAH and TPH degradation versus SOM mineralization

In part 1 of this study (chapter 4) we measured an average value of 0.13 d^{-1} for the rapid mineralization rate constant of SOM ($k_{C,1}$). On the average, values for $k_{PAH,1}$ are equal to the this value. Values for $k_{TPH,1}$ are about half of the rapid mineralization constants for SOM. Generally, also the found slow degradation rate constants for both PAH and TPH are similar to the average slow SOM mineralization rate constant of 0.00042 d^{-1} ($k_{C,2}$) that we measured in part 1 of this study (chapter 4).

We conclude that our hypothesis that PAH and TPH degradation are strongly linked to SOM mineralization is true. Different mechanisms have been described in the literature that can explain the observed similar kinetics of PAH and TPH degradation and SOM mineralization. Sorbed PAH and TPH might be released by mineralization of the SOM matrix (Reemtsma et al. 2003) and subsequently degraded (Harmsen 2004). However, our observations can also be explained by slow desorption of both HOC and SOM fractions from non-degrading SOM fractions (e.g. black carbon or other carbonaceous material (Nam and Alexander 1998, Cornelissen et al. 2005)) and subsequent degradation and mineralization. Our experiments show that PAH and TPH degradation rates have indeed equal orders of magnitude as very slow desorption rates that have been reported by Cornelissen et al. (1997b). Although we can not prove this, we assume that the similarity between PAH and TPH degradation and SOM mineralization can be explained by their similar desorption characteristics. SOM mineralization kinetics that often has been explained by the formation of stable (slowly mineralizable) SOM compounds (Janssen 1984 and Middelburg 1989), can thus (also) be explained in terms of 'bioavailability' like this is commonly done for HOC degradation.

The reduced sulfur contents, the parameters describing the oxidation kinetics of sulfur (a_S and $k_{S,1}$), the SOM contents, and the kinetics of SOM mineralization (a_C, $k_{C,1}$, and $k_{C,2}$) that are reported in part 1 of this study (chapter 4) can be used to make estimates about

the oxygen uptake rates during the different stages of biochemical ripening. Using the initial PAH and TPH contents of the sediments and the parameters on PAH and TPH degradation kinetics (a_{PAH}, $k_{PAH,1}$, $k_{PAH,2}$, a_{TPH}, $k_{TPH,1}$, $k_{TPH,2}$), similar estimates can be made for the oxygen uptake rates that are caused by PAH and TPH degradation. In part 1 of this study (chapter 4) it was already shown that oxygen uptake by sulfur oxidation may account for more than 70% of the total oxygen uptake during the first 7 days of incubation and up to 30% of the total oxygen uptake during the whole incubation period. Indicative calculations for the studied sediments show that oxygen uptake rates by PAH and TPH degradation were, respectively, less than 1 and 5% of the oxygen uptake rate by SOM mineralization.

5.3.1.5 Biodegradation versus bioavailability of PAH

Rapid degradation of PAH within 21 days has often been described in the literature. Residual PAH concentrations after persulfate oxidation are strongly correlated with this biodegradation after 21 days (Cuypers et al. 2000). Therefore, we used a persulfate oxidation to predict the bioavailability of PAH.

In Figs. 5.3 and 5.4 the initial PAH and TPH concentrations are compared with the concentrations after persulfate oxidation and 21 days of biodegradation. Residual PAH concentrations after persulfate oxidation are equal to PAH concentrations after 21 days of incubation for LERI, SCGR, and SCSL, but not for ROSL and WOGR. Even after 160 days of degradation, PAH concentrations of these sediments are larger than the residual concentrations after persulfate oxidation. The differences between the biodegraded fraction and the measured bioavailable fraction of ROSL can be explained by the relatively large fractions of PAH with 5 and 6 rings in this sediment (Table 5.1). This fraction was slower degraded compared to the fractions of PAH with 2, 3, and 4 rings (data not shown). So, these high molecular weight PAH are bioavailable, but not easily biodegradable. Their delayed biodegradation is probably the result of cometabolic processes by microorganisms growing on smaller PAH (Bonten 2001) or SOM compounds. Probably, a similar explanation is valid for PAH in WOGR and the high molecular weight TPH fractions. The observed increasing PAH concentration after 83 days of incubation (Table 5.2 and Fig. 5.3) could be explained by heterogeneity of the sediment which might have caused differences in initial PAH concentrations between the different incubated bottles. Another explanation could be an increase of PAH extractability as a result of mineralization of SOM to which PAH were previously bound (Quantin et al. 2005).

No significant differences were found between residual PAH concentrations after persulfate oxidation that were measured after 0, 21, and 160 days. This is in line with the observations of Cuypers et al. (2000).

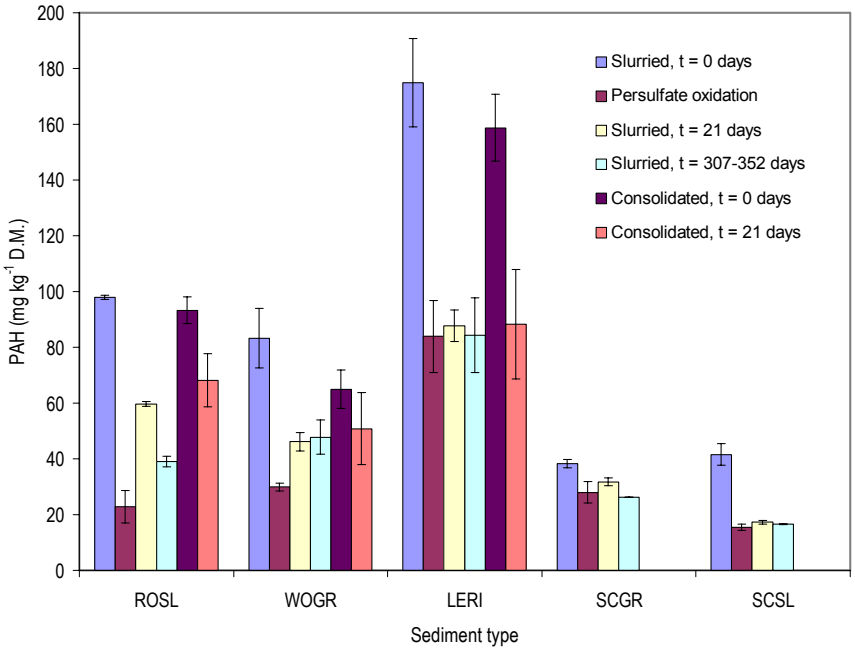

Fig. 5.3. PAH concentrations at t = 0, 21, and 307 – 352 days (slurried sediments), after persulfate oxidation, and at t = 0 and 21 days (consolidated sediments). Bar heights represent averages of triplicate measurements, ± standard deviation

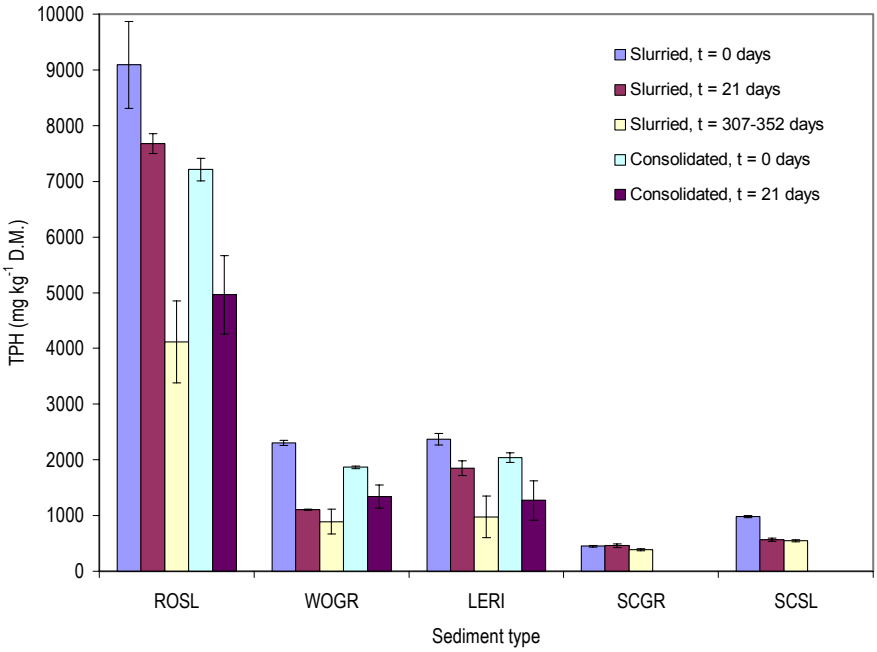

Fig. 5.4 TPH concentrations at t = 0, 21, and 307 – 352 days (slurried sediments), and at t = 0 and 21 days (consolidated sediments). Bar heights represent averages of triplicate measurements, ± standard deviation

5.3.2 Incubation experiment with consolidated sediments (pellets)

5.3.2.1 Oxygen penetration

Oxygen penetration depths into the sediment pellets (z_{pen}) are presented in Table 5.3. Oxygen penetration depths are 1.1 to 5.0 mm after 10 days of incubation, whereas they are 1.3 to 6.9 mm after 21 days of incubation. In general, penetration depths are smaller

than those found in the literature (Sextone et al. 1985, Zausig et al. 1993), which can be explained by high initial oxygen uptake rates (Q) that were caused by the relatively high amounts of oxidizable reduced sulfur and labile SOM in biochemically unripe sediments (chapter 4).

Table 5.3 Oxygen penetration depth (z_{pen}) in sediment pellets of ROSL, WOGR and LERI at different matric potentials (ψ_m) after 10 and 21 days of incubation at 30 °C

	ψ_m (hPa)	z_{pen} (mm)	
		10 days	21 days
ROSL	-100	1.1 (0.4)	1.3 (0.3)
	-333	1.3 (0.4)	1.5 (1.0)
	-1,000	- [b]	2.0 (0.7)
	-2,000	1.9 (1.2)	4.3 (1.1)
	-16,000 [a]	- [c]	- [d]
	-1,000,000 [a]	- [d]	- [d]
WOGR	-100	2.2 (0.1)	2.5 (0.3)
	-333	2.1 (0.1)	2.3 (0.3)
	-1,000	2.8 (1.1)	4.3 (1.9)
	-2,000	5.0 (1.4)	6.9 (0.3)
	-16,000 [a]	- [c]	- [d]
	-1,000,000 [a]	- [d]	- [d]
LERI	-100	1.5 (0.5)	1.5 (0.0)
	-333	1.3 (0.6)	1.7 (0.5
	-1,000	2.1 (0.6)	3.1 (1.2)
	-2,000	2.9 (0.8)	6.3 (2.2)
	-16,000 [a]	- [c]	- [d]
	-1,000,000 [a]	- [d]	- [d]

Values are averages of triplicate measurements (± standard deviation)

[a] No reliable values for ψ_m = -16,000 and -1,000,000 hPa could be measured with the microelectrodes because the used microelectrodes did not perform well at ψ_m < -2,000 hPa

[b] microelectrode malfunction

[c] partly oxygenated, based on visual observations of redoximorphic features (after Patrick et al. 1996)

[d] completely oxygenated, based on visual observations of redoximorphic features (after Patrick et al. 1996)

Because low matric potentials (ψ_m) cause high intra-pellet air-filled porosities ($\phi_{a,matrix}$) and therefore are responsible for high oxygen diffusion coefficients ($D_{s,matrix}$) (chapter 3), higher oxygen penetration depths generally correspond with lower matric potentials. By far the smallest penetration depths were found in ROSL pellets, which can be explained by the relatively high oxygen uptake rates (Q) of this sediment caused by sulfur and soil organic matter oxidation (chapter 4). Oxygen penetration depths in WOGR pellets are slightly larger than in LERI sediments, which can be explained by its slightly lower oxygen uptake rates (chapter 4).

Fourier numbers that we calculated with Eq. (5.4) for day 10 and 21 (t), using oxygen diffusion coefficients that were measured in the same pellets during another experiment (chapter 3), were much larger than 1 for all pellets, at all matric potentials. These high Fourier numbers indicate that the incubation time of the pellets was sufficiently long to reach a steady state in which the penetration depths are solely dependent on the average oxygen uptake rates (Q). Therefore, Eq. (5.2) may be used to calculate these rates. Based on their observations in soil aggregates, Zausig et al. (1993) concluded the same. Using

Eq. (5.2) and values for $D_{s,matrix}$, θ, $\phi_{a,matrix}$, and ${}^{b}\rho_{d}$ (aggregate dry bulk density) of pellets at the different matric potentials (ψ_m) from chapter 3* we calculated average oxygen uptake rates of 0.09 (WOGR and LERI) to 0.22 mmol O_2 g^{-1} D.M. d^{-1} (ROSL) after 10 days and 0.04 (WOGR and LERI) to 0.10 mmol O_2 g^{-1} D.M. d^{-1} (ROSL) after 21 days.

The increased penetration depths after 21 days and therefore the decreased calculated oxygen uptake rates can be explained by a decrease in reactivity of the sediments with time as a result of biochemical ripening (see also chapter 4). The average oxygen uptake rates of the pellets are larger than the average uptake rates that we measured after 10 and 21 days of incubation in the continuously mixed slurry experiment with the same sediments, which amounted up to 0.03 (after 10 days) and 0.008 mmol O_2 g^{-1} D.M. d^{-1} (after 21 days) (chapter 4). This difference is caused by the character of the pellets in which the sediments are not mixed. The oxygen uptake rates of the oxygenated part of a pellet at a certain moment in time increases with depth in the pellet because material at small depths has been biochemically ripened for a longer period – and therefore has a smaller reactivity – than material at larger depths.

From our observations, no conclusions can be drawn about the possible dependency between oxygen uptake rates and oxygen concentrations. At the time scales of our observations, Eq. (5.2) seems to describe the oxygenation process of the pellets adequately. This is in line with the assumption of Smith (1980) that oxygen uptake by microorganisms may be considered as a zero-order process.

5.3.2.2 PAH and TPH degradation

Initial PAH concentrations in consolidated sediment (pellets) were equal to the initial concentrations in the slurried sediments (Fig. 5.3). After 21 days of incubation, PAH concentrations in the oxygenated parts of the pellets were similar to the concentrations measured in the slurries after 21 days. No decrease in PAH concentrations was measured in the parts that remained anoxic during the whole period of 21 days, confirming that PAH and TPH are only substantially degraded under oxygenated (aerobic) conditions.

Surprisingly, initial TPH concentrations in the consolidated sediments, but also concentrations after 21 days of incubation, seem to be substantially smaller than the corresponding concentrations in the slurries (Fig. 5.4). Probably, these apparently lower concentrations were caused by a lower analytical availability of TPH in the desiccated pellets as compared to the wet slurries. Such decreased availability was earlier described for desiccating soils by White et al. (1997). Notwithstanding these odd observations, it is clear that TPH concentrations after 21 days are substantially lower than the concentrations at the start of the incubation, whereas TPH concentrations did not decrease in the part that remained anoxic.

Our observations that PAH degradation (and probably also TPH degradation) was limited to the oxygenated part of our pellets, confirm the study of Nocentini and Pinelli (2001)

* Values for ${}^{b}\varrho_{d}$ are needed to make the conversion from cm^3 O_2 cm^{-3} matrix s^{-1} to mmol O_2 g^{-1} D.M. d^{-1}

who measured PAH concentration profiles in spiked, hand formed soil aggregates during incubation of 160 days. It may be concluded that degradation rates in slurries were equal to degradation rates in consolidated sediments, like it was the case for SOM mineralization (chapter 4).

From our observations, no conclusions can be drawn about the possible dependency between degradation rates and oxygen concentrations. This is in line with the findings of Hurst et al. (1996) and Heerenklage et al. (1998) who reported that a decrease in oxygen concentration from 0.21 down to 0.01 to 0.02 $cm^3\ cm^{-3}$ has no influence on the biodegradation of PAH and diesel fuel, respectively. The thickness of the layer in which oxygen concentrations dropped below these values is negligible compared to the total oxygen penetration depths (Vermeulen et al. 2002, Malina et al. 2004) and had therefore no measurable effect on the extent of PAH en TPH degradation.

At matric potentials lower than -250 hPa (chapter 2) or a water-filled pore space ($WFP = \theta / (\theta + \phi_{a,matrix})$) lower than 60% (Linn and Doran 1984), microbial activity is likely to be limited by a lack of moisture. In our experiments no clear differences could be observed between the degradation of PAH and TPH in pellets at matric potentials between -100 to -2,000 hPa ($WFP \approx$ 99% and 87%, respectively (chapter 3)). Degradation in most of the pellets at ψ_m = -16,000 and -1,000,000 hPa ($WFP \approx$ 71% and 11%, respectively (chapter 3)) was slightly less than in the pellets at higher matric potentials.

5.4 Conclusions

Slurried sediments

A double exponential model could adequately describe PAH and TPH degradation kinetics in slurries that were incubated for one year at 30 ºC in the laboratory.

First order degradation rate constants for the rapidly degradable fractions (12 to 58%) were about 0.13 and 0.058 d^{-1} for PAH and TPH, respectively. Rapid desorption of HOC as reported in the literature was clearly larger than the rapid PAH and TPH degradation rates that we measured, confirming that degradation is not limited by desorption during this phase. Our average slow degradation rate constants were 0.00044 (PAH) to 0.00067 d^{-1} (TPH) and are similar to very slow desorption rate constants as reported in the literature.

Both slow and rapid degradation rate constants were very similar to the mineralization rate constants of SOM that were reported in part 1 of this study (chapter 4). This forms a strong confirmation of the hypothesis that SOM mineralization and PAH and TPH degradation are linked processes. We assume that the background of this link lies in their similar desorption characteristics. Based on our measurements on sulfur oxidation, SOM mineralization and PAH and TPH degradation that are all part of biochemical ripening, it can be concluded that oxygen uptake by degradation of PAH and TPH is negligible compared to the oxygen uptake by sulfur oxidation and SOM mineralization.

The validity of the persulfate oxidation for the measurement of the bioavailable PAH fraction in sediments was confirmed by this study. Our study showed that high molecular weight PAH and TPH might be bioavailable but not degradable at the short term. Cometabolic processes probably played a role in the long term degradation of these fractions.

Consolidated sediments

Oxygen penetrations depths in consolidated sediments were strongly correlated with the extent of intra-pellet air filled porosity and reactivity resulting from physical and biochemical ripening, respectively. The penetration depths were limited to 1 to 2 mm in wet, unripe pellets (ψ_m = -100 hPa) but reached values that are larger than 20 mm in dry, completely physically ripe sediments (ψ_m < -16,000 hPa).

The amounts of PAH and TPH degradation in the oxygenated parts of consolidated sediments were equal to the extent of PAH degradation in optimally oxygenated slurried sediments. No oxygen or moisture limitation could be observed in our experimental set up for PAH degradation at -2,000 < ψ_m < -100 hPa. This means that the amounts of PAH that could be degraded during ripening of dredged sediments are comparable to the amounts that are degraded in slurry bioreactors. Probably, PAH and TPH degradation were limited at $\psi_m \leq$ -16,000 hPa.

Acknowledgements

We thank Katarzyna Kaziród and Magdalena Kromer (Technical University of Czestochowa, Poland) for the experimental work they conducted with the consolidated sediments. Both of these students took part in the Socrates/Erasmus programme of the European Union. Geert Meijer and Ilse Gerrits from our sub-department are acknowledged for their invaluable assistance with the instrumental analyses. The research was supported by and performed within the Research Centre on Soil, Sediment and Groundwater Management and Remediation WUR/TNO.

6

OXYGENATION OF DREDGED SEDIMENTS

Modeling of oxygen diffusion

Bagger is een min of meer dunne, waterige substantie
met een droge-stofgehalte van 8 à 15%,
die bestaat uit een mengsel van mineraal
en gedeeltelijk omgezet organisch materiaal,
en op de bodem van sloten, vaarten, e.d. wordt aangetroffen.

Het baggeren in relatie tot het toemaken – Th. van Egmond

This chapter is based on a paper that was originally published in the Proceedings of the seventh In Situ and On-Site Bioremediation symposium (Vermeulen et al. 2004)

Abstract

A dual porosity oxygen diffusion model was used to predict the extent of oxygenation in a 150 cm thick layer of ripening clayey dredged sediments (clay, soil organic carbon, and reduced sulfur content of 22, 7.6, and 1.2%, respectively) in an upland disposal site. The model input consists of values for the sediment layer thickness, aggregate size distribution, inter- and intra-aggregate oxygen diffusion coefficients, and sediment reactivity. The model results show that the combination of physical and biochemical ripening of a layer of dredged sediments increases the oxygenated depth from a few millimeters up to 110 cm. Therefore, ripening is a feasible bioremediation technique. Depending on the degree of ripening, either intra-aggregate aeration or inter-aggregate aeration is limiting aerobic biodegradation of PAH and TPH in ripening sediments. The presented model can be used to determine the maximum permissible sediment layer thickness for optimal aerobic biodegradation of PAH and TPH contaminated sediments during ripening.

6.1 Introduction

Ripening of clayey dredged sediments at an upland disposal site consists of physical, chemical, and biological processes that lead to an increase in air-filled porosity, a decrease in average aggregate size, and in a decrease in oxygen uptake rate. After these changes, conditions are more favorable for aerobic biodegradation of organic pollutants like mineral oil (Total Petroleum Hydrocarbons, TPH) and Polycyclic Aromatic Hydrocarbons (PAH) than conditions before ripening. Therefore, ripening can be seen as a bioremediation technique for polluted sediments (chapter 2).

Oxygen penetration in ripening sediments is restricted to a few millimeters (chapter 5, Vermeulen et al. 2002 and Malina et al. 2004). Complete oxygenation of a layer of sediments can only be established by crack- and aggregate formation (physical ripening) that results in (fast) oxygen diffusion through the air-filled cracks and (slow) oxygen diffusion into the aggregates (chapter 2). In this way, physical ripening, which is considered to be the driving force of the whole ripening process, can change a 90-cm-thick layer of clayey dredgings into an oxygenated aggregated soil within 3 to 6 years (Harmsen 2001).

Currently, it is not possible to predict the course of ripening of dredged material during temporary disposal. Therefore, development of a mathematical model that describes these processes and their interactions would be useful. Such a model could consist of a combination of existing models, including an oxygen diffusion model (chapter 3). Huesemann and Truex (1996) derived several equations based on Fick's Law (Fick 1855) to describe oxygen diffusion during bioremediation of petroleum contaminated soils. The equations demonstrate the dependency between the diffusion coefficient for oxygen in soil (D_s) and the depth of oxygen penetration and the required bioremediation time by passive oxygenation of petroleum contaminated soils. The study of Huesemann and Truex is useful for sandy soils without any soil structure, but their equations are not able to describe oxygen diffusion in a dual porosity system of cracks and pores in aggregates (matrix) that results from physical ripening. For such situations, mathematical models have been developed by soil scientists that simultaneously consider oxygen diffusion through the inter-aggregate pores (cracks) and the diffusion into the aggregates (e.g. Leffelaar 1979, Smith 1980, Rappoldt 1990, Arah and Vinten 1995, Sierra et al. 1995). The concepts for these models have been developed to calculate denitrification rates in

aggregated terrestrial soil profiles, but we used the same concept to evaluate the extent of oxygenation in ripening sediments that are characterized by dynamic aggregate size distributions, oxygen diffusion coefficients, and oxygen uptake rates.

Physical ripening, biochemical ripening, and biodegradation of PAH and TPH were quantified in independent laboratory studies in chapters 3, 4, and 5 of this thesis. The aim of this chapter is to show the usefulness of an oxygen diffusion model as proposed by Smith (1980) and Arah and Smith (1989) to describe ripening processes at an upland disposal site. After a brief description of the model and the values that we used for the different input parameters, we present the results of some model scenario calculations. With the calculations, we quantified the effect of physical and biochemical ripening on the overall oxygenation of sediments at an upland disposal site. Besides, we present a sensitivity analysis in which we show the relative influence of the different input parameters. Finally, we show some possibilities to combine the oxygen diffusion model with existing water transport and ripening models.

6.2 Model description

The equations that we used in the oxygen diffusion model are only discussed briefly below. Smith (1980) and Arah and Smith (1989) reported similar equations. The presented dual porosity model describes oxygen diffusion through inter-aggregate cracks (= downward diffusion into a layer of sediment) and intra-aggregate pores (= radial diffusion into the aggregates).

6.2.1 Inter-aggregate oxygen diffusion (cracks)

The relationship between the oxygen concentration (c) and depth from the surface (z) in a layer of sediment containing matrix zones in which no oxygen uptake takes place (ϕ_{an}) and zones in which place and time independent oxygen uptake takes place ($1-\phi_{an}$) can be given by equation (6.1*) describing linear steady state diffusion (Smith 1980).

$$\frac{d^2 c}{dz^2} = \frac{Q}{D_{s,layer}}\left(1-\phi_{a,layer}\right)\left(1-\phi_{an}\right) \qquad (6.1)$$

where:

c	= oxygen concentration in the air of the air-filled cracks ($cm^3\ cm^{-3}$)
z	= depth into layer of dredged sediments, positive downwards (cm)
Q	= oxygen uptake rate per unit volume of oxygenated matrix ($cm^3\ O_2\ cm^{-3}\ s^{-1}$)
$D_{s,layer}$	= inter-aggregate oxygen diffusion coefficient ($cm^2\ s^{-1}$)
$\phi_{a,layer}$	= inter-aggregate air-filled porosity ($cm^3\ cm^{-3}$)
ϕ_{an}	= oxygenated volume fraction of matrix ($cm^3\ cm^{-3}$)

Solving Eq. (6.1) with boundary conditions $c = c_{atm}$ at $z = 0$ and $c = 0$ and $dc/dz = 0$ at $z = z_{pen}$, results in Eq. (6.2) (after Radford and Greenwood 1970 or Huesemann and Truex 1996):

* The diffusion coefficient $D_{s,layer}$ is missing in the analogous equation in the original paper (Vermeulen et al. 2004)

$$c = c_{atm}\left(1-\frac{z}{z_{pen}}\right)^2 ;0 \le z \le z_{pen} \tag{6.2}$$

$$\text{with} \quad z_{pen} = \sqrt{\frac{2D_{s,layer}c_{atm}}{Q(1-\phi_{a,layer})(1-\phi_{an})}} \tag{6.3}$$

where:
c_{atm} = oxygen concentration in the atmosphere (0.21) (cm^3 cm^{-3})
z_{pen} = vertical oxygen penetration depth into layer of sediment (cm)

For a layer of dredged material that has been disposed on an impermeable liner at a depth that is smaller than z_{pen}, Eq. (6.1) has to be solved with boundary conditions c = c_{atm} at $z = 0$ and $dc/dz = 0$ at $z = z_{imp}$, resulting in (after Huesemann and Truex 1996):

$$c = c_{imp} + (c_{atm} - c_{imp})\left(1-\frac{z}{z_{imp}}\right)^2 ;0 \le z \le z_{imp} \tag{6.4}$$

$$c_{imp} = c_{atm}\left[1-\left(\frac{z_{imp}}{z_{pen}}\right)^2\right] \tag{6.5}$$

where:
c_{imp} = oxygen concentration at the depth of impermeable layer (cm^3 cm^{-3})
z_{imp} = depth of impermeable layer (cm)

The presented analytical solutions (Eqs. (6.2) and (6.4)) are only valid if $D_{s,layer}$, $\phi_{a,layer}$, and ϕ_{an} are constant with depth. For many other situations, Eq. (6.1) can only be solved numerically.

6.2.2 Intra-aggregate oxygen diffusion (micro-pores)

In reality, sediment aggregates are irregular and can consist of prismatic, blocky, platy, or angular structures, depending on the degree of physical ripening. A schematic representation of the effect of physical ripening on structure development is given in chapter 2. However, during the determination of the aggregate size distribution no information was obtained about the exact shape of the aggregates (chapter 3) and we therefore assumed in this study that all aggregates formed by physical ripening are spherical. If information about aggregate shapes would be available, the use of so-called 'equivalent radii' (Greenwood and Berry 1962) or 'equivalent aggregates' (Rappoldt 1990, Rappoldt and Verhagen 1999) could be considered.

The extent of structure development by physical ripening can be quantified with a truncated log-normal aggregate distribution using the geometric mean radius (μ), the log-standard deviation ($\sigma_{log\ r}$), and the radius of the largest aggregate in the distribution (r_{max}) (chapter 3). For spherical aggregates, the volumetric cumulative probability function for a truncated log-normal distribution C(r) can be given by:

$$C(r) = \frac{\operatorname{erfc}\left[\dfrac{^{10}\log(\mu/r)}{\sigma_{\log r}\sqrt{2}}\right]}{\operatorname{erfc}\left[\dfrac{^{10}\log(\mu/r_{max})}{\sigma_{\log r}\sqrt{2}}\right]} \tag{6.6}$$

The derivative D(r) of Eq. (6.6) is given by:

$$D(r) = \frac{2\exp\left\{-\tfrac{1}{2}\left[\dfrac{^{10}\log(\mu/r)}{\sigma_{\log r}}\right]^2\right\}}{\sqrt{2\pi}\; r\; \sigma_{\log r}\ln(10)\operatorname{erfc}\left[\dfrac{^{10}\log(\mu/r_{max})}{\sigma_{\log r}\sqrt{2}}\right]} \tag{6.7}$$

where:

r = aggregate radius (cm)
μ = geometric mean radius (cm)
$\sigma_{\log r}$ = standard deviation of log-normal r-distribution, base 10 (-)
r_{max} = radius of the largest aggregate in the distribution (cm)

Oxygen diffusion in a place and time independently oxygen consuming spherical aggregate (steady state radial diffusion), can be described by (after Greenwood and Berry 1962):

$$\frac{d^2(xc)}{dx^2} = \frac{Qx}{D_{s,matrix}} \tag{6.8}$$

where:

x = distance from the center of a spherical aggregate (cm)
$D_{s,matrix}$ = intra-aggregate oxygen diffusion coefficient (cm^2 s^{-1})

For an aggregate with radius r and boundary conditions $c = G_r$ at $x = r$; $c = 0$ and $dc/dx = 0$ at $x = r_{an}$, Eq. (6.8) has the following solution (after Smith 1980):

$$c = \frac{Q}{6D_{s,matrix}}\left(x^2 - 3r_{an}^2 + 2\frac{r_{an}^3}{x}\right);\; r_{an} \le x \le r \tag{6.9}$$

in which r_{an} is implicitly given by:

$$r^2 - 3r_{an}^2 + 2\frac{r_{an}^3}{r} = r_c^2 \tag{6.10}$$

$$\text{with} \quad r_c = \sqrt{\frac{6D_{s,matrix}G_r}{Q}} \tag{6.11}$$

$$\text{with} \quad G_r = (\phi_{a,matrix} + \alpha_B\,\theta)c \quad \text{(after Arah and Smith 1989)} \tag{6.12}$$

where (see next page):

r_{an} = radius of the anoxic interior of a spherical aggregate (cm)
G_r = apparent oxygen concentration on the aggregate surface ($cm^3\ cm^{-3}$)
$\phi_{a,matrix}$ = intra-aggregate air-filled porosity ($cm^3\ cm^{-3}$)
α_B = Bunsen's coefficient, oxygen solubility in water / oxygen solubility in gas at P=101.3 kPa and T=283 K (0.0394) ($cm^3\ cm^{-3}$); after Glinski and Stepniewski (1985)
θ = volumetric aggregate moisture content ($cm^3\ cm^{-3}$)
r_c = critical radius of largest aggregate that can be wholly oxygenated (cm)

The fraction of the total aggregate volume that is anoxic (ϕ_{an}) can now be given by:

$$\phi_{an} = \int_{r_c}^{\max(r_c, r_{max})} D(r)\left(\frac{r_{an}}{r}\right)^3 dr \tag{6.13}$$

The ratio between r_{an} and r varies with r as follows (after Smith 1980 and Arah and Smith 1989)†

$$\frac{r_{an}}{r} = \frac{1}{2} - \sin\left\{\frac{1}{3}\arcsin\left[2\left(\frac{r_c}{r}\right)^2 - 1\right]\right\} \tag{6.14}$$

It should be emphasized that the coefficient $D_{s,layer}$ and $D_{s,matrix}$ in Eqs. (6.1) and (6.8) represent the *effective* diffusion coefficients that are related to the sediment layer aggregates as a whole (and not to the cracks and pores only). G_r is the *apparent* concentration of oxygen within the aggregate at radius r; it is not the external concentration c in the air-filled cracks surrounding the aggregate (Arah and Smith 1989).

In this study, we assumed that Q is not affected by the oxygen concentration (neither c nor G). This assumption is supported by the publication of Smith (1980) who refers to the publications of Longmuir (1954) and Greenwood and Berry (1962) who measured a Michaelis-Menten oxygen half saturation constant (K_M) of about 5×10^{-6} M ($\approx 0.002\ cm^3\ O_2\ cm^{-3}$ air) for the biodegradation of glucose and organic acids, respectively. Hurst et al. (1996) and Heerenklage et al. (1998) report that a decrease in oxygen concentration down to 0.01 to 0.02 $cm^3\ cm^{-3}$ has no influence on the biodegradation of PAH and diesel fuel, respectively. Most probably, biodegradation rates are not inhibited at even lower oxygen concentrations. Although other researchers (e.g. Sierra and Renault (1995)) suggest that rates are already inhibited below much higher oxygen concentrations, we here copied the assumptions of Smith (1980) and treat oxygen uptake as a zero-order process. Compared to a model in which the effect of a concentration dependent oxygen uptake rate (Q) is incorporated, our model will underestimate oxygen penetration depth (z_{pen}) and overestimate the anoxic matrix fraction ϕ_{an} (Sierra et al. 1995).

† The analogous equations published by Smith (1980) and Arah and Smith (1989) contain errors. Therefore we rederived the equation by solving the cubic equation (Eq. 6.10) using the software package Derive™, resulting in Eq. (6.14)

6.3 Materials and methods

We derived the input data for the oxygen diffusion model (Eqs. (6.1) through (6.11)) from experimental data that we reported in chapters 3 and 4. Data for the different types of dredged sediments that were described in these chapters were averaged and interpolated, resulting in values for the different input parameters of the model that are typical for clayey dredged sediments at different degrees of physical and biochemical ripening (Tables 6.1, 6.2, 6.3, and 6.5).

6.3.1 Degree of physical ripening (n_{rip})

An empirical measure of the degree of physical ripening of dredged sediments is the often used n-value (see also chapters 2 and 3 and Pons and Van der Molen (1973)):

$$n_{rip} = \frac{w_{sat} - 0.2R}{L + 3H} \tag{6.15}$$

where:
n_{rip} = n-value (g moisture g^{-1} clay)
w_{sat} = saturated moisture ratio (g moisture per 100 g dry matter (D.M.))
R = sand + silt content (g sand + silt per 100 g D.M.)
L = clay content (g clay per 100 g D.M.)
H = organic matter content (g organic matter per 100 g D.M.)

n_{rip} ranges from > 2.0 (unripe, recently deposited sediment) via 2.0 – 1.4 (consolidated, but practically unripe), 1.4 – 1.0 (half-ripe), and 1.0 – 0.7 (nearly ripe) to < 0.7 $g.g^{-1}$ (ripe, normal soil). n_{rip} is determined by past minimum matric potential ($\psi_{m,min}$) of the sediment. Therefore, the degree of physical ripening can also be expressed in this more physically based parameter (see also chapter 3).

Volumetric aggregate moisture contents (θ) of clayey dredged sediments having a clay content of 22% at different stages of desiccation range between 0.83 and 0.37 $cm^3\ cm^{-3}$ for n-values of 3.31 (unripe) and 0.70 $g.g^{-1}$ (ripe), respectively (Table 6.1). The presented moisture contents are the moisture contents that were reached after controlled desiccation from ψ_m = 0 hPa to ψ_m = -100, -333, -1,000, -2,000, and -16,000 hPa (chapter 3). Under field conditions, it is likely that the sediments are exposed to rewetting caused by rainfall, resulting in higher (actual) values of ψ_m and θ at the same values of n_{rip}. Maximum values for θ after rewetting can be calculated using the concept of the 'swelling function' (chapter 3).

Table 6.1 n_{rip} and volumetric aggregate moisture content (θ) of clayey dredged sediment at different stages of physical ripening (ψ_m); after chapter 3

ψ_m (hPa)	n_{rip} ($g\ g^{-1}$)	θ ($cm^3\ cm^{-3}$)
0	3.31 (unripe, recently deposited)	0.83
-100	1.73 (consolidated)	0.71
-333	1.44 (practically unripe)	0.67
-1,000	1.01 (half-ripe)	0.56
-2,000	0.86 (nearly ripe)	0.48
-16,000	0.70 (ripe)	0.37

6.3.2 Structure development: aggregate size distribution (μ, $\sigma_{log\ r}$, r_{max})

Strictly speaking, n_{rip} only quantifies the degree of desiccation and provides no information on the structure development part of physical ripening (chapter 3). Structure development can better be characterized by the structure parameters μ, $\sigma_{log\ r}$, and r_{max} (Eq. (6.3)). During physical ripening or through the action of tillage, these parameters decrease (chapter 2 and 3). We derived values for the structure parameters (μ, $\sigma_{log\ r}$, r_{max}) that are valid for the whole range of physical ripening from unripe to ripe (Table 6.2). The volumetric cumulative probability functions that can be constructed with these parameters are presented in Fig. 6.1.

Table 6.2 Aggregate size distribution (μ, $\sigma_{log\ r}$, and r_{max}) of clayey dredged sediment at different stages of physical ripening (ψ_m); after chapter 3

ψ_m (hPa)	μ [a] (cm)	$\sigma_{log\ r}$ [a] (-)	r_{max} [b] (cm)
0	∞	-	∞
-100	∞	-	∞
-333	3.58	0.91	5.88
-1,000	2.65	0.81	5.01
-2,000	2.06	0.75	4.46
-16,000	0.31	0.57	2.81

[a] values at ψ_m = -333 and -16,000 hPa originate from chapter 3, intermediate values were calculated assuming linear relationships between μ and $log\ \psi_m$ and $\sigma_{log\ r}$ and $\log \psi_m$

[b] values at ψ_m = -333 and -16,000 hPa originate from chapter 3, intermediate values were calculated assuming linear relationships between r_{max}/μ and $\log \psi_m$

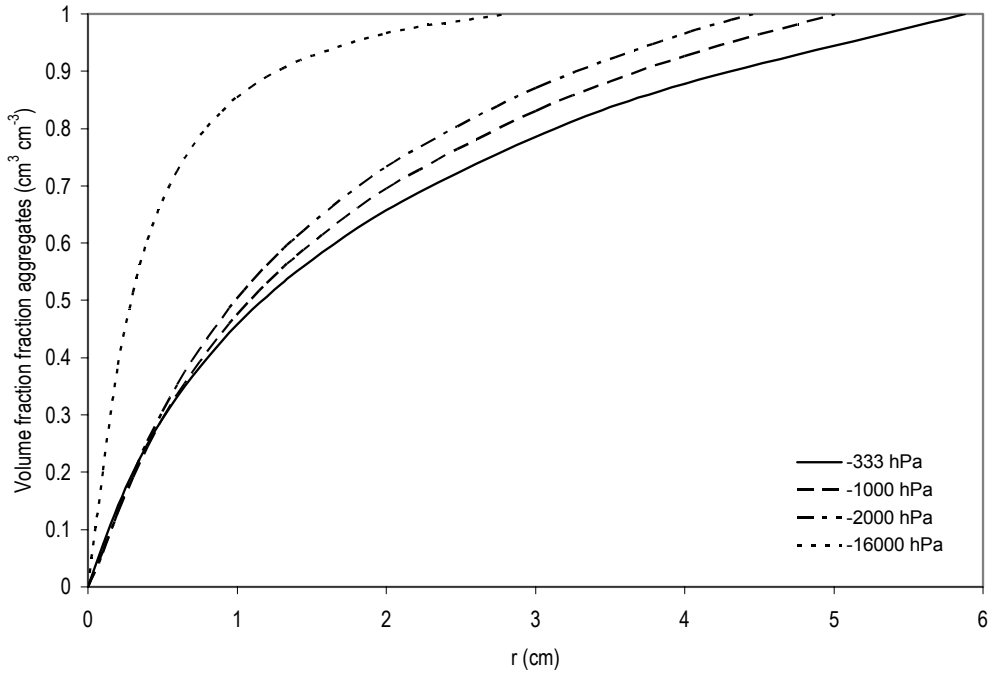

Fig. 6.1 Volumetric cumulative probability function (D(r)) for sediment aggregates at different stages of physical ripening (ψ_m)

PAH can be considered as immobile in aggregates with radii larger than 1 mm (Harmsen 2004). Under these conditions, degradation of PAH is limited by oxygen diffusion alone. Therefore, an oxygen diffusion model as described in this chapter can be

used to make predictions about the course of PAH degradation (and most probably also of TPH).

6.3.3 Aeration: oxygen diffusion coefficients ($D_{s,layer}$ and $D_{s,matrix}$)

Separate diffusion coefficients were used for oxygen diffusion through the profile (intra-aggregate diffusion) and for radial diffusion through the aggregates (intra-aggregate diffusion).

Inter-aggregate diffusion coefficients depend on the degree of (air-filled) crack formation, the degree of structure development, and the temperature. Therefore, we related inter-aggregate diffusion coefficients ($D_{s,layer}$) with the fraction inter-aggregate porosity ($\phi_{a,layer}$) and a tortuosity factor (F) (after Bronswijk 1991):

$$D_{s,layer} = F \phi_{a,layer} D_0 \tag{6.16}$$

$$\text{with} \quad \phi_{a,layer} = 1 - \left(1 - \phi_{a,cracks}\right)^{1-\frac{1}{r_s}} \tag{6.17}$$

$$\text{and} \quad D_0 = 0.178\left(\frac{T}{273}\right)^2 \text{ (Penman 1940)} \tag{6.18}$$

where:

F	= inter-aggregate tortuosity factor (-)
$\phi_{a,layer}$	= inter-aggregate air-filled porosity ($cm^3\ cm^{-3}$)
$\phi_{a,cracks}$	= fraction air-filled cracks, including the 'volume' of subsidence ($cm^3\ cm^{-3}$)
r_s	= geometry factor (-)
D_0	= oxygen diffusion coefficient in the atmosphere ($cm^2\ s^{-1}$)
T	= temperature (K)

For three-dimensional isotropic shrinkage, $r_s = 3$. When cracking dominates subsidence, $r_s > 3$. In case of subsidence only, $r_s = 1$, meaning that no cracks are formed (consolidation). Shrinkage geometry is affected by soil material, depth in soil profile, soil strength and n-value (see also chapter 3).

$D_{s,layer}$ was calculated with Eq. (6.17), using different values for r_s for different stages of physical ripening. During physical ripening, r_s gradually changes from 1 to 3 (Kim et al. 1992). Therefore, Rijniersce (1984) related r_s to n_{rip} and the 'load' (as defined in appendix 3). His relation suggests that cracking in a ripening soil can only occur if loads are smaller than about 240 hPa (≈ layer of 170 cm sediment). However, because no exact data on the relation between r_s, n_{rip}, and load are available, for this study, we assumed one-dimensional shrinkage ($r_s = 1$) for matric potentials from 0 to -100 hPa, whereas we assumed three-dimensional isotropic shrinkage ($r_s = 3$) for the lower matric potentials. We used a value of 1 for the inter-aggregate tortuosity factor (F) for sediments at initial crack formation -333 hPa < ψ_m < -100 hPa and $F = 0.3$ for completely 'ripe', well structured sediment (Table 6.3) (after Bronswijk 1991).

Intra-aggregate diffusion coefficients depend on the degree of (air-filled) micro-pores within the aggregates, the tortuosity and connectivity of these pores, and the temperature.

Therefore, we related intra-aggregate diffusion coefficients ($D_{s,matrix}$) to the air-filled porosity within the aggregates ($\phi_{a,matrix}$) and a tortuosity factor (f) (Penman (1940)):

$$D_{s,matrix} = f\,\phi_{a,matrix} D_0 \qquad (6.19)$$

where:
$D_{s,matrix}$ = intra-aggregate oxygen diffusion coefficient ($cm^2\ s^{-1}$)
f = intra-aggregate tortuosity factor (-)
$\phi_{a,matrix}$ = air-filled porosity ($cm^3\ cm^{-3}$)

Table 6.3 Air-filled porosities ($\phi_{a,layer}$ and $\phi_{a,matrix}$), oxygen diffusion coefficients at T=10 °C ($D_{s,layer}$ and $D_{s,matrix}$) and tortuosity factors (F and f) of clayey dredged sediments at different stages of physical ripening (ψ_m); after chapter 3

ψ_m (hPa)	$\phi_{a,layer}$ ($cm^3\ cm^{-3}$)	F [a] (-)	$D_{s,layer}$ ($cm^2\ s^{-1}$)	$\phi_{a,matrix}$ ($cm^3\ cm^{-3}$)	f (-)	$D_{s,matrix}$ ($cm^2\ s^{-1}$)
0	0	-	-	0	-	3.2×10^{-7}
-100	0	-	-	0.01	0.009	1.4×10^{-5}
-333	0.07	1.0	1.3×10^{-2}	0.01	0.009	2.4×10^{-5}
-1,000	0.22	0.8	3.4×10^{-2}	0.03	0.011	6.3×10^{-5}
-2,000	0.27	0.7	3.6×10^{-2}	0.07	0.007	1.0×10^{-4}
-16,000	0.30	0.3	1.7×10^{-2}	0.15	0.033	9.7×10^{-4}

[a] values at ψ_m = -333 and -16,000 hPa were assumed to be 1.0 and 0.3, respectively (after Bronswijk 1991), intermediate values were calculated assuming a linear relationship between F and $\log \psi_m$

Both the intra- and inter-aggregate diffusion coefficients reported in chapter 3 and used in this study are 'effective diffusion coefficients', as defined above (Eqs. (6.1) and (6.8)). The diffusion coefficients of chapter 3 were measured during a laboratory experiment at a constant temperature of 30 °C and were corrected with Eq. (6.18) to achieve values that are valid for the average Dutch temperature of 10 °C at field conditions. The resulting values for $D_{s,layer}$ and $D_{s,matrix}$ range from 1.3×10^{-2} (practically unripe) to 3.4×10^{-2} $cm^2\ s^{-1}$ (ripe) and 3.2×10^{-7} (unripe) to 9.7×10^{-4} $cm^2\ s^{-1}$ (ripe), respectively. All presented values represent diffusion coefficients that are valid for the air-filled porosities ($\phi_{a,layer}$ and $\phi_{a,matrix}$) mentioned in Table 6.2. Due to rewetting, actual values might be lower (see also section 6.3.1). During desiccation, $\phi_{a,matrix}$ increases. The tortuosity factor f is about 0.01 for the complete measured range of desiccation (Table 6.3).

6.3.4 Biochemical ripening: oxygen uptake rates (Q)

Oxygen uptake in ripening dredged sediments is a result of chemical oxidation of reduced sulfur and biological oxidation of soil organic carbon. Besides, oxygen is used to oxidize organic pollutants like TPH and PAH. However, the contribution of these pollutants to the total oxygen uptake is negligible (chapter 4). Therefore, oxygen uptake rates depend only on the reduced sulfur (S) and soil organic carbon (C) content, and the reactivity of these sediment constituents.

Oxygen uptake rates (Q) of disposed dredged sediments are high during initial contact with oxygen. These high values are caused by chemical oxidation of rapidly mineralizable reduced sulfur and rapidly degradable soil organic carbon (biochemical ripening). After approximately 30 days of incubation at 30 °C, these components have been oxidized and the oxygen uptake rates stabilize at a value that is in the same order of magnitude as rates reported in the literature for ripe terrestrial soils (see also chapter 4). It can be assumed

that the 'bioavailable' fraction of organic pollutants like TPH and PAH are also degraded during this period of biochemical ripening (chapter 5).

From the equations on sulfur and carbon oxidation kinetics (chapter 4), we derived the following equation to calculate oxygen uptake kinetics of biochemically ripening dredged sediments:

$$Q_m = \left\{ \begin{matrix} \left[k_{S,1} a_{S,1} \exp\left(-k_{S,1} t\right)\right]\left[Q_S S\right] + \\ \left[k_{C,1} a_{C,1} \exp\left(-k_{C,1} t\right) + k_{C,2} a_{C,2} \exp\left(-k_{C,2} t\right)\right]\left[RQ\ C\right] \end{matrix} \right\} \times \frac{1000}{M_{O_2}} \qquad (6.20)$$

where:

Q_m = oxygen uptake rate (mmol O_2 g^{-1} D.M. d^{-1})
S = reduced sulfur content (g g^{-1} D.M.)
$k_{S,1}$ = mineralization rate constant of the rapidly mineralizable fraction S (d^{-1})
$a_{S,1}$ = rapidly mineralizable fraction of S (g g^{-1})
t = time (d)
Q_S = quotient between SO_4^{2-} and O_2 in relationship 7 Table 4.2 (mol mol^{-1})
C = organic carbon content (g g^{-1} D.M.)
$k_{C,1}$ = mineralization rate constant of the rapidly mineralizable fraction C (d^{-1})
$a_{C,1}$ = rapidly mineralizable fraction of organic C (g g^{-1})
$k_{C,2}$ = mineralization rate constant of the slowly mineralizable fraction C (d^{-1})
$a_{C,2}$ = 1-$a_{C,1}$, slowly mineralizable fraction of organic C (g g^{-1})
RQ = respiratory quotient carbon (mol mol^{-1})
M_{02} = molar mass of oxygen (g mol^{-1})

Table 6.4 summarizes the oxygen uptake kinetics parameters that were measured in chapter 4 and presents parameters for 'average' dredged sediments that we used to perform calculations with the oxygen diffusion model.

Table 6.4 Oxygen uptake kinetics parameters [a] for ROSL, WOGR, LERI, SCGR, SCSL, and 'average dredged sediments' at 30 °C; after chapter 4

	ROSL	WOGR	LERI	SCGR	SCSL	'average sediment'
$k_{S,1}$ (d^{-1})	3.54	3.45	3.22	3.18	0.19	2.72
$a_{S,1}$ (-)	0.069	0.343	0.171	0.229	0.239	0.210
S (g g^{-1} D.M.)	0.018	0.008	0.010	0.012	0.011	0.012
Q_S (mol mol^{-1})	0.44	0.44	0.44	0.44	0.44	0.44
$k_{C,1}$ (d^{-1})	0.174	0.200	0.183	0.067	0.050	0.135
$a_{C,1}$ (-)	0.100	0.043	0.063	0.068	0.094	0.074
$k_{C,2}$ (d^{-1})	0.00047	0.00022	0.00036	0.00054	0.00053	0.00042
$a_{C,2}$ (-)	0.900	0.957	0.937	0.932	0.906	0.926
C (g g^{-1} D.M.)	0.118	0.071	0.066	0.072	0.053	0.076
RQ (mol mol^{1})	0.82	0.68	0.78	0.69	0.79	0.75

[a] all values presented in this table originate from measurements in optimally oxygenated slurries (chapter 4)

With the values of table 6.4, average initial 'high' (t = 1 d), average stabilized 'low' (t = 30 d) and average 'intermediate' oxygen uptake rates were calculated with Eq. (6.20) that are valued for 'typical' dredged sediments (C, and S contents of 7.6 and 1.2%, respectively (chapter 4 and Table 6.4)). The average initial (t = 1 d) 'high' uptake rate is 0.108 mmol O_2 g^{-1} D.M. d^{-1}, whereas the average stabilized (t = 30 d) 'low' uptake rate is 0.00478 mmol O_2 g^{-1} D.M. d^{-1}.

The oxygen uptake rates were derived from an experiment with slurried sediments (chapter 4). Probably, microbial activity is inhibited at ψ_m values lower than -250 hPa

(chapter 2). Nevertheless, we assumed that the oxygen uptake rates for slurried sediments are equal to the rates for consolidated and ripened sediments and can therefore be used in this study for all stages of ripening and values of ψ_m. The oxygen uptake rates depend on temperature. Because the values of table 6.4 were measured during a laboratory experiment at a constant temperature of 30 °C, they were corrected with Eq. (6.21) to achieve values that are valid for the average Dutch temperature at field conditions of 10 °C (Table 6.5 and Fig. 6.2) and can be used in the oxygen diffusion model (Eqs. (6.1) and (6.8)). We used a value of 0.25 for f_T, assuming that oxygen uptake rates double with every increase of 10 °C‡.

$$Q = \frac{V_m \, {}^{b}\rho_d f_T}{24 \times 3{,}600} Q_m \qquad (6.21)$$

where:

Q	= oxygen uptake rate per unit volume of oxygenated matrix ($cm^3\ O_2\ cm^{-3}\ s^{-1}$)
V_m	= volume of 1 mmol O_2 at T=283 K (23.22) (cm^3)
${}^{b}\rho_d$	= dry aggregate bulk density ($g\ cm^{-3}$)
f_T	= correction to account for the temperature difference between laboratory (30 °C) and field (10 °C) (0.25) (-)
24	= # hours per day
3,600	= # seconds per hour

Table 6.5 High, intermediate and low oxygen uptake rates (Q) of 'average' clayey dredged sediments with C and S contents of 7.6, and 1.2%, respectively, at T = 10 °C [a] (calculated with Eq. (6.21))

ψ_m (hPa)	${}^{b}\rho_d$ [b] ($g\ cm^{-3}$)	Q_{high}[c] $cm^3\ O_2\ cm^{-3}\ s^{-1}$	$Q_{intermediate}$[d] $cm^3\ O_2\ cm^{-3}\ s^{-1}$	Q_{low}[e] $cm^3\ O_2\ cm^{-3}\ s^{-1}$
0	0.42	3.1×10^{-6}	1.6×10^{-6}	1.4×10^{-7}
-100	0.70	5.1×10^{-6}	2.6×10^{-6}	2.2×10^{-7}
-333	0.78	5.7×10^{-6}	3.0×10^{-6}	2.5×10^{-7}
-1,000	1.02	7.4×10^{-6}	3.9×10^{-6}	3.3×10^{-7}
-2,000	1.11	8.1×10^{-6}	4.2×10^{-6}	3.6×10^{-7}
-16,000	1.17	8.5×10^{-6}	4.5×10^{-6}	3.8×10^{-7}

[a] Values that originate from measurements in slurried sediments (unit mmol $O_2\ g^{-1}$ D.M. d^{-1}) were converted with Eq. (6.21) to values that can be used in the model (unit $cm^3\ O_2\ cm^{-3}\ s^{-1}$) and are valid for different dry aggregate bulk densities (${}^{b}\rho_d$) belonging to different stages of physical ripening (ψ_m). All values are slightly higher than the values presented in Vermeulen et al. (2004)

[b] Average of values presented in chapter 3

[c] $Q_{high} \sim Q_m$ at t = 1 d

[d] $Q_{intermediate} = (Q_{high} + Q_{low}) / 2$

[e] $Q_{low} \sim Q_m$ at t = 30 d

Q_{high} is representative for the phase during which reduced sulfur is oxidized (chemical ripening), $Q_{intermediate}$ for the phase during which rapidly degradable (bioavailable) soil organic carbon and TPH and PAH are degraded (biological ripening), and Q_{low} for the phase during which slowly degradable soil organic carbon is mineralized in biochemically ripe sediments (chapter 4).

‡ Probably, it is more correct to adjust values for k to account for temperatures changes. However, to keep in line with Vermeulen et al. (2004) we made the correction with f_T. Adjusting of values for k would result in slightly different values for Q

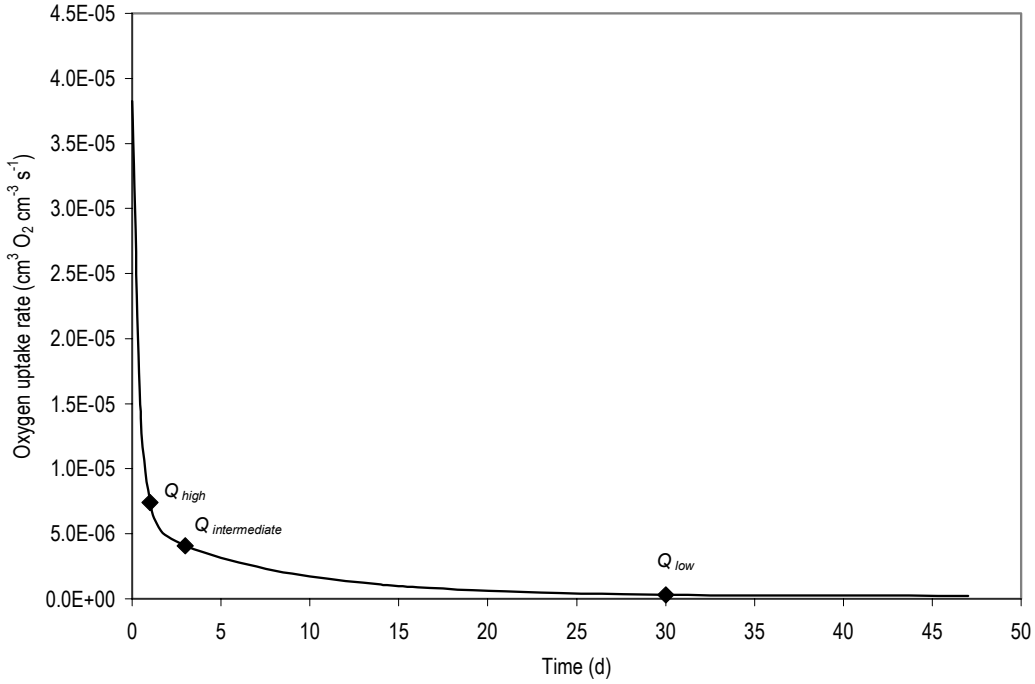

Fig 6.2 Oxygen uptake rate of 'average' dredged sediments with C and S contents of 7.6, and 1.2%, respectively, during 30 days of optimal oxygenation at T=10 °C

6.3.5 Scenario calculations and sensitivity analysis

A model based on Eqs. (6.1) and (6.10) was evaluated numerically by a FORTRAN code. To integrate Eq. (6.1) the Bulirsch-Stoer method, with shooting based on Brent's method to meet the boundary conditions, was applied. Eq. (6.10) was integrated by Gauss-Legendre quadrature (Press et al. 1992).

With this model, we made calculations for a 150-cm-thick layer (Δz) of dredged sediments at matric potentials (ψ_m) of -333, -1,000, -2,000 and -16,000 hPa and for 'low', 'intermediate' and 'high' values of Q, resulting in relationships between c and z and ϕ_{an} and z. Besides, we estimated the effect of independent variation of the parameters z, μ, $\sigma_{log\ r}$, r_{max}, $\phi_{a,layer}$, $\phi_{a,matrix}$, and Q on the model's output.

6.4 Results and discussion

6.4.1 Scenario calculations

The data presented in Tables 6.1, 6.2, 6.3, and 6.5 were used to evaluate the effect of physical ripening – expressed in actual matric potential (ψ_m) – on the oxygen concentration in air-filled cracks (Fig. 6.3) and on the fraction of the total aggregate volume that is oxygenated (Fig. 6.4) in a 150 cm thick layer of sediments. The presence of an impermeable liner (zero flux of oxygen) was assumed at the bottom of the layer of sediment.

6.4.1.1 Inter-aggregate aeration (cracks)

Fig. 6.3 shows the penetration depth of oxygen in a layer of sediments. Notice that the curve for unripe sediments (ψ_m = 0 hPa) almost descends vertically from 0.21 to 0 $cm^3\ O_2\ cm^{-3}$. For ψ_m = 0 hPa, the penetration depth is limited to less than 2 mm for all values of Q (see also Table 6.7). At other stages of physical ripening, the penetration depth is 36 to 83 cm for high Q values, 49 to 105 cm for intermediate Q values, and 130 ((ψ_m = -16,000 hPa and low Q) to 150 cm ((ψ_m = -333, -1,000, -2,000 hPa and low Q) for low Q values.

The oxygen penetration depth does not increase monotonically with decreasing values of ψ_m. This phenomenon can be explained by the lower values for ϕ_{an} (and therefore higher overall oxygen uptake rates) and the lower values for $D_{s,layer}$ that are caused by the lower tortuosity factors (F) at lower values of ψ_m.

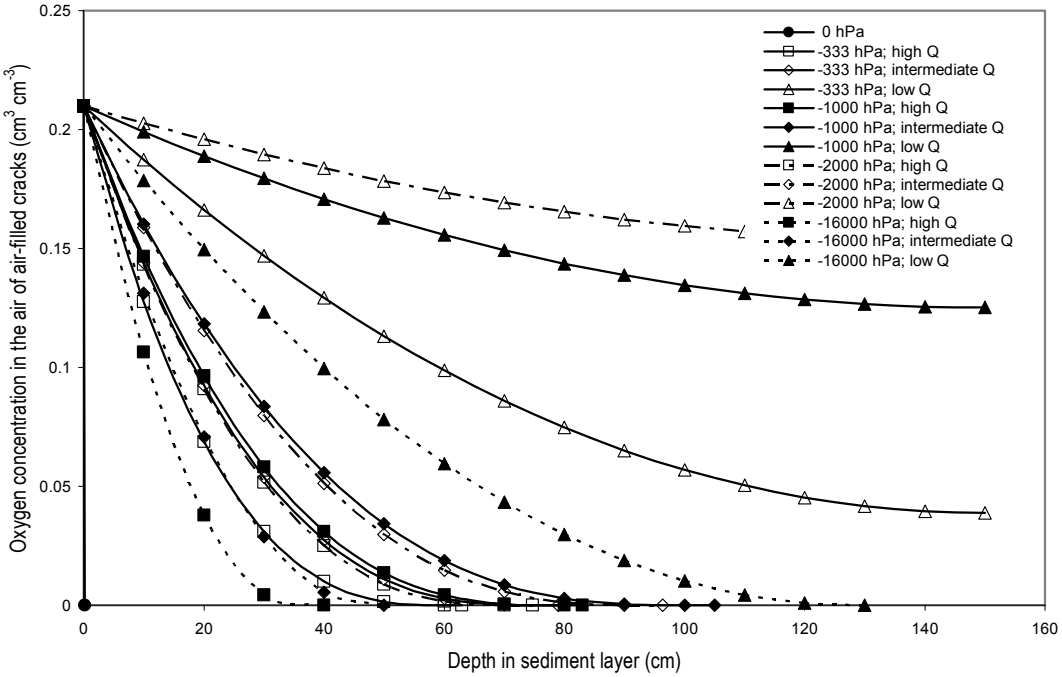

Fig. 6.3 Relationship between oxygen concentration in air-filled cracks (inter-aggregate aeration, $\phi_{a,layer}$) and depth in the layer of clayey dredged sediments (z) for different matric potentials (ψ_m) and oxygen uptake rates (Q)

6.4.1.2 Intra-aggregate aeration (sediment matrix)

Fig. 6.4 shows that only extensive physical ripening (ψ_m = -2,000 and -16,000 hPa) can cause full oxygenation in 25 (ψ_m = -16,000 hPa, high Q), 35 (ψ_m = -16,000 hPa, intermediate Q), 110 cm (ψ_m = -16,000 hPa, low Q), and 150 cm (ψ_m = -2,000 hPa, low Q) of the layer of dredged sediments. Oxygenation of the layer at ψ_m = -1,000 hPa and low Q is slightly less than 100% in the whole layer. At ψ_m = 0 hPa only a negligible fraction is completely oxygenated. Under other conditions, between 64 and 96% (at the surface) and between 0 and 81% (at 150 cm depth) of the aggregate volume is oxygenated. The model results show that, theoretically, the largest layer of sediments can be completely oxygenated under conditions of "ψ_m = -2,000 hPa and low Q". However, in Fig. 6.4 it can also be seen that sediments at ψ_m = -2,000 hPa that have been less extensively

biochemically ripened (intermediate and low Q), are never completely oxygenated. Therefore it is unlikely that the combination "ψ_m = -2,000 hPa and low Q" will ever occur in practice.

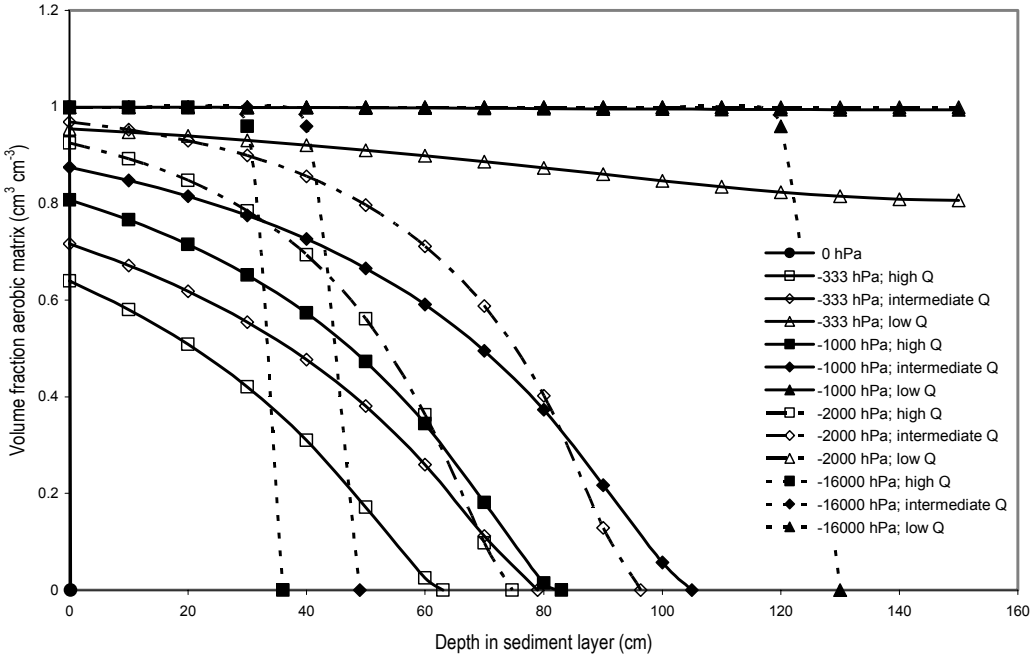

Fig. 6.4 Relationship between the oxygenated volume fraction of the sediment matrix (intra-aggregate aeration, 1-ϕ_{an}) and depth in the layer of clayey dredged sediments (z) for different matric potentials (ψ_m) and oxygen uptake rates (Q). Notice that curves for "-1,000 hPa; low Q", "-2,000 hPa; low Q", and "-16,000 hPa; low Q" are almost similar

Fig. 6.3 and 6.4 clearly show that the requirements for inter- and intra-aggregate aeration are in conflict. For instance, the high penetration depth into the layer of dredged sediments at "ψ_m = -333 hPa, low Q" (Fig. 6.3) does not result in 100% oxygenation (Fig. 6.4). Vice versa, the low penetration depths at "ψ_m = -16,000 hPa, high and intermediate Q" result in 100% oxygenation of the top 25 and 35 cm of the layer of dredged sediments. So, physical or biochemical ripening alone, will never lead to complete oxygenation of a substantial fraction of a 150 cm thick sediment layer. Physical ripening alone can not oxygenate more than about 25 cm. Also substantial biochemical ripening (decrease of Q) is needed before a larger layer can be oxygenated. Therefore, sediment layer thicknesses at a disposal site should be smaller during the first stage of ripening (that is approximately 25 cm) and can be larger (that is approximately 110 cm) during the last stage of ripening.

The maximum layer thickness is mainly caused by the reactivity (Q) of the sediment. Q completely depends on the reduced sulfur and soil organic carbon content of the sediment. In this study, calculations were made for an 'average' sediment containing 7.6% soil organic carbon and 1.2% reduced sulfur. Eqs. (6.3) and (6.9) show that any doubling of Q – which can be caused by a doubling of the soil organic carbon content - results into a decrease of z_{pen} or r_c with a factor 1.4 ($\sqrt{2}$). A doubling of Q can also be caused by an increase in temperature of about 10 °C. Such an increase would not only reduce z_{pen} and r_c, and therefore the maximum allowed *layer thickness* (Δz), but also the *time* needed for biochemical ripening (see also Harmsen (2001)).

In this study, values of Q were assumed to be independent of the location in the sediment aggregates. However, in reality these values will be relatively high in the interiors of the aggregates and relatively low in the exteriors due to heterogeneous biochemical ripening. This phenomenon should probably be included in the model if a more detailed description of course of ripening during temporary disposal is needed.

Using redoximorphic features (as defined in Patrick et al. (1996) of the sediment profile, Harmsen (2001) observed similar patterns in ripening sediments during a long-term field study in The Netherlands. During the first year, a 90-cm-thick layer of disposed sediments remained completely anoxic. Between the first year and the sixth year, the sediments were partly oxygenated down to a depth of 90 cm meaning that oxygen has penetrated down to this level (compare with Fig. 6.3). After the sixth year, the whole layer of 90 cm sediments was completely oxygenated (compare with Fig. 6.4). In a later study, Harmsen and Sims (2004) also reported an increasing oxygen penetration as a result of ongoing ripening and suggested to use this property by applying one or more additional surface layers after the first layer of sediment has been ripened.

6.4.2 Sensitivity analysis

For the sensitivity analysis, we varied the input parameters Δz, $\phi_{a,layer}$, $\phi_{a,matrix}$, μ, $\sigma_{log\ r}$, r_{max}, and Q among 'standard values' and estimated the effect of this variation on the oxygenated fraction. Using the 'standard values' as input in the model, results in an aerobic fraction of 0.39 $cm^3\ cm^{-3}$. For the 'standard values', we used the values for 'half ripe' sediments (Tables 6.1, 6.2, and 6.3) and 'intermediate' oxygen uptake rates (Table 6.5). We varied all values between 0.05 and 2 times the 'standard values' (Table 6.6).

Table 6.6 Standard values used for sensitivity analysis (1) and 0.01 and 2 times the standard values

Parameter	Meaning	Standard value times:		
		1	0.01	2
Δz (cm)	layer thickness	150	1.5	300
$\phi_{a,layer}$ ($cm^3\ cm^{-3}$)	air-filled cracks	0.22	0.0022	0.44
$\phi_{a,matrix}$ ($cm^3\ cm^{-3}$)	air-filled matrix	0.03	0.0003	0.06
μ (cm)	geometric mean radius	2.65	0.0265	5.30
$\sigma_{log\ r}$ (-)	standard deviation r	0.81	0.0081	1.62
r_{max} (cm)	r of largest aggregate	5.01	0.0501	10.02
Q ($cm^3\ O_2\ cm^{-3}\ s^{-1}$)	Oxygen uptake rate	3.90×10^{-6}	3.90×10^{-8}	7.80×10^{-6}

Fig. 6.5 presents the results of the sensitivity analysis of the model. Different groups of parameters can be distinguished. The parameters $\phi_{a,layer}$ and $\phi_{a,matrix}$ show a steep slope at 0.01 to 0.1 times the standard value. This indicates the importance of initial crack formation ($\phi_{a,layer}$) and desiccation ($\phi_{a,matrix}$). Both parameters increase as a result of physical ripening. Between 0.1 and 2 times the standard value, the effect of an increase in crack volume is clearly greater than that of an increase in air-filled pores in the aggregates. The curves for the parameters Δz and Q, indicating that the importance of application practice and biochemical ripening, respectively, are also equivalent. The effect of both parameters

is negligible at 0.01 to 0.1 times the standard value, relatively large at 0.1 to 1 times the standard value and relatively low at 1 to 2 times the standard value.

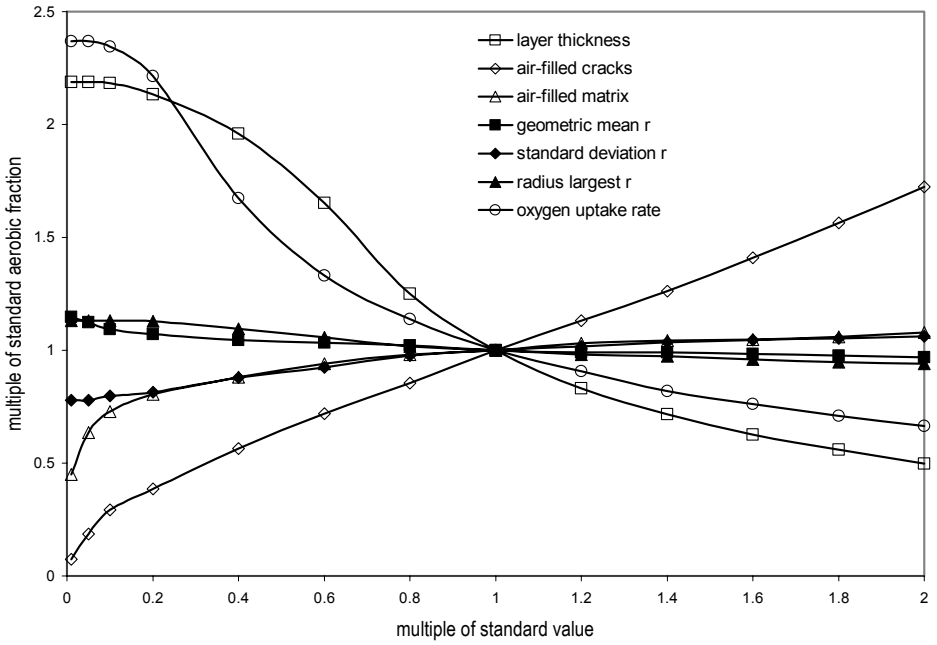

Fig. 6.5 Sensitivity analysis of the oxygen model for independent variation of Δz (layer thickness), $\phi_{a,layer}$ (air-filled cracks), $\phi_{a,matrix}$ (air-filled matrix), μ (geometric mean radius), $\sigma_{log\ r}$ (standard deviation radius), r_{max} (radius largest aggregate), and Q (oxygen uptake rate)

Compared to the parameters $\phi_{a,layer}$, $\phi_{a,matrix}$, Δz, and Q, the effect of the structure parameters μ, $\sigma_{log\ r}$, r_{max} is relatively small in the whole range of values that we used in the sensitivity analysis. However, it should be emphasized that full oxygenation of a layer of sediments is only possible if actual radii (r) are smaller than the critical radii (r_c). Table 6.7 presents values of r_c that we calculated with Eq. (6.9) for spherical aggregates of dredged sediments at matric potentials (ψ_m) of -333, -1,000, and -16,000 hPa. The table clearly shows the effects of both physical (within table columns) and biochemical ripening (within table rows) on the magnitude of r_c. Comparing r_c with the actual radii (table 6.3), we conclude that only complete physical ripening (ψ_m = -16,000 hPa) can lead to complete oxygenation of the aggregates at high values of Q. At low values of Q, complete oxygenation can already be reached at higher values of ψ_m.

Table 6.7 Critical radius[a] (r_c) of spherical aggregates at different stages of physical ripening (ψ_m) and oxygen uptake rates (Q) for external oxygen concentrations (c) of 0.21 and 0.10 cm^3 cm^{-3}

ψ_m (hPa)	r_c, Q_{high} (cm)		r_c, $Q_{intermediate}$ (cm)		r_c, Q_{low} (cm)	
	c=0.21	c=0.10	c=0.21	c=0.10	c=0.21	c=0.10
0[b]	0.04	-	0.05	-	0.2	-
-100[b]	0.4	-	0.5	-	1.7	-
-333	0.4	0.3	0.6	0.4	2.1	1.5
-1,000	0.7	0.5	1.0	0.7	3.5	2.4
-2,000	1.2	0.8	1.6	1.1	5.6	3.8
-16,000	4.9	3.4	6.7	4.6	23.0	15.9

[a] assuming radial diffusion, calculated with Eq. (6.9) using values from Tables 6.1, 6.2, 6.3, and 6.5

[b] no aggregates exist at this stage of physical ripening, meaning downward linear diffusion into the layer of sediment, calculated with $z_{pen}=\sqrt{((2D_{s,matrix}G_r)/Q)}$, Eq. (5.2) of chapter 5

Reduction of the aggregate size will also have an indirect effect on the level of oxygenation. Overall desiccation of the sediments will be increased, resulting in higher values for $\phi_{a,matrix}$ (and therefore $D_{s,matrix}$), leading to lower values for r_c, and thus higher levels of oxygenation.

6.5 Conclusions and outlook

Model concepts, which were developed in the past by soil scientists to calculate denitrification rates in aggregated soils, were successfully applied to predict the fraction of the total aggregate volume that is oxygenated in a ripening layer of clayey dredged sediments. With the model we were able to integrate the available laboratory data on physical (chapter 3) and biochemical ripening (chapters 4 and 5) and to upscale these data to a field scale.

For this study, we made model calculations for 'average' clayey sediment with clay, soil organic carbon, and reduced sulfur contents of 22, 7.6, and 1.2%, respectively. The model results show that ripening can change a layer of anoxic sediments into a layer of oxygenated soil. This transformation is initiated by crack and aggregate formation, an increase in air-filled aggregate porosity, and an ongoing aggregate size reduction (physical ripening). Complete physical ripening (ψ_m = -16,000 hPa) can lead to complete oxygenation of the aggregates. However, to reach full oxygenation, also substantial biochemical ripening is necessary. Disposal of sediments with a bioremediation intention should be restricted to layer thicknesses smaller than about 25 for biochemically unripe sediments. For biochemically ripe sediments, layer thicknesses up to about 110 cm are feasible. The model results confirm field observations on ripening sediments made by other researchers.

Because oxygen uptake kinetics are of the same magnitude as PAH and TPH degradation kinetics (chapter 5), the approach that we present here forms a sound basis to model oxygen diffusion processes that occur during physical ripening. To achieve this goal, the presented model should be combined with a water transport model that also describes water movement and physical ripening in disposed sediments. Bronswijk et al. (1992) already presented a combination of a water transport, an oxygen transport, and an organic matter and pyrite oxidation model. Many other models exist that describe different coupling effects (Vulliet et al. 2002). However, currently no models exist that describe all coupled processes that determine ripening (including PAH and TPH degradation) of sediments. Probably, ingredients for such a model can be found in existing computer models for water transport and crack formation (e.g. Bronswijk 1988, Jarvis et al. 1991, Hendriks et al. 1999, Van Dam 2000, Perrier et al. 2002), physical ripening (e.g. Rijniersce 1983, Kim et al. 1992), and oxygen diffusion (e.g. Smith 1980, Rappoldt 1990, Bronswijk et al. 1992, Arah and Vinten 1995, Sierra et al. 1995). To construct an integrated model from these ingredients, efforts have to be made to rebuild and combine existing models into a single model that is able to simulate water transport in irreversibly shrinking (ripening) sediments. Besides, model components that describe structure development during physical ripening have to be developed. Efforts have to be put into describing the water transport and ripening in a Lagrangian coordinate frame and

in defining correct top (infiltration and evapo(transpi)ration from surface and cracks) and bottom boundary conditions (drainage) in a three dimensionally shrinking dual porosity system. Finally, this physical ripening model has to be coupled to a model describing dynamic oxygen diffusion, sulfur oxidation, SOM mineralization, and PAH and TPH degradation.

With a combination of the different ingredients, all coupling effects between hydraulics, mechanics, chemistry, and biology (HMCB coupling) that occur during ripening could be described in a single computer tool. With such a tool, it would be possible to determine the residence time that is required for ripening of PAH and TPH contaminated sediments at an upland disposal site.

Acknowledgements

The research was supported by and performed within the Research Centre on Soil, Sediment and Groundwater Management and Remediation WUR/TNO.

7

SUMMARY AND GENERAL CONCLUSIONS

overal zanikt bagger
zwachtelend rond de reuzenlaarzen
waarin ik mijn tijd beklim haast verzadigd ja
maar het is nog steeds de mij bemestende tijd
mijn voertuig vore en trog

Uit het heerlijkste hout blaft het land – Lucebert

7.1 Summary

Introduction

In chapter 1 of this thesis, a short introduction is given on the nature and history of the problem of polluted dredged sediments in The Netherlands. An overview is given of the recent developments in the research on remediation of dredged sediments that are polluted with Polycyclic Aromatic Hydrocarbons (PAH) and Total Petroleum Hydrocarbons (TPH). A promising bioremediation technique that can be applied during temporary upland (above ground) disposal of these sediments is ripening.

Literature review

Chapter 2 is a literature review on the various aspects of sediment ripening. Ripening is an initial soil formation process that results from drainage of disposed water-logged sediments. Ripening can be subdivided into physical, chemical and biological ripening. Physical ripening irreversibly converts water-saturated clayey sediment (clay content > 15%) into aerated (unsaturated), structured clayey soil by desiccation. Chemical ripening changes the chemical composition of sediments by oxidation processes like the conversion of reduced sulfur into sulfate. Biological ripening consists of the development of aerobic (micro)organisms and their effect on for instance soil organic matter (SOM) mineralization.

Conditions for aerobic biological PAH and TPH degradation are improved by the combination of the different ripening processes. Therefore, ripening can be deployed as a bioremediation technique for dredged sediments that are polluted with PAH and TPH. It is concluded in chapter 2 that the available knowledge on ripening is not sufficient to distinguish critical process steps during ripening of polluted sediments. More fundamental research is needed in which the effects of the different ripening processes – including PAH and TPH degradation – can be studied independently. Therefore, the different sub-processes of physical ripening, chemical ripening, biological ripening were studied in several independent laboratory experiments that are described in chapters 3, 4, and 5 of this thesis. Chapter 6 describes a study in which the measured parameters of the preceding chapters are integrated in a mathematical model.

Quantification of physical properties

In chapter 3, physical properties of ripening sediments are described and quantified. In the laboratory, three dredged sediments were artificially ripened in specially designed pressure chambers (microdepots). With the microdepots, aggregates were formed and desiccated to different levels of physical ripening. The level of physical ripening, ranging from unripe to ripe, was quantified by the matric potential (ψ_m) of the water in the aggregates. This mechanistic measure was compared with the empirical n-value (n_{rip}) that is often used to quantify physical ripening. Shrinkage characteristics, swelling functions, moisture retention characteristics, and hydraulic conductivity characteristics were measured in the aggregates. Besides, intra-aggregate oxygen diffusion coefficients were

measured using oxygen microelectrodes and diffusion chambers. Inter-aggregate oxygen diffusion coefficients were calculated using information derived from the measured shrinkage characteristics. Finally, four samples of half-ripe aggregates and four samples of ripe aggregates that had been formed by natural ripening were collected from field locations and their aggregate size distributions were characterized with truncated log-normal distributions.

Major conclusions of the chapter are:
- the data that are presented in chapter 3, quantify all physical ripening parameters that are relevant for biodegradation of PAH and TPH in disposed dredged sediments;
- for complete physical ripening of dredged sediments ($n_{rip} < 0.7$ g g^{-1}), matric potentials (ψ_m) lower than -16,000 hPa are needed;
- for a good description of physical ripening, not only information is needed on the lowest past matric potential ($\psi_{m,min}$), but also on the aggregate size distribution;
- using the information and data developed in this chapter, the course of physical ripening at upland disposal sites can be predicted with a combination of existing water- and oxygen transport and ripening models.

Sulfur oxidation and soil organic matter mineralization

In chapter 4, biochemical ripening – in this thesis defined as the combination of biological and chemical ripening processes that consume oxygen – in the sediment matrix is discussed and quantified. Five series of slurried dredged sediments were incubated in the laboratory during an aerobic slurry experiment of 160 days. During incubation, oxygen consumption, carbon dioxide production, Eh, and pH were measured in the incubated bottles. Besides, bottles were sacrificed at nine moments to measure SO_4^{2-}, Dissolved Organic Carbon, NH_4^+, NO_3^-, NO_2^-, and PO_4^{3-} concentrations. Based on these measurements, kinetics of sulfur oxidation and SOM mineralization were characterized using a double exponential model. With this model, labile and stable sulfur fractions and rapidly and slowly mineralizing SOM fractions could be distinguished. Sulfur oxidation and SOM mineralization rates could be quantified with first order rate constants.

Most important conclusions of chapter 4 are:
- oxygen uptake rates of biochemically ripening sediments can completely be explained by oxidation of reduced sulfur and mineralization of SOM;
- the fraction labile sulfur is 5 to 35% of the total amount of initially reduced sulfur;
- oxygen uptake by sulfur oxidation may account for more than 30% of the total oxygen uptake during biochemical ripening;
- no measurable amounts of the stable sulfur fractions (e.g. pyrite) are oxidized during the incubation time;
- the fraction rapidly mineralizing SOM is 5 to 10% of the total amount of SOM;
- rates of rapidly mineralizing SOM are 100 to 1000 times greater than rates of slowly mineralizing SOM;
- nutrients are available in sufficient quantities to prevent nutrient limitation during ripening.

PAH and TPH degradation

In chapter 5, the effects of chemical, biological, and physical ripening on the degradation of PAH and TPH are quantified during the same incubation experiment that is described in chapter 4. To get reliable measurements on slow PAH and TPH degradation, the incubation time was extended to 352 days. Besides, degradation of PAH and TPH was studied in the artificial sediment aggregates of three dredged sediments (consolidated sediments) that were physically characterized in the study that is described in chapter 3.

Bottles with slurried sediments were sacrificed at ten moments to measure PAH and TPH concentrations. Based on the measurements, PAH and TPH degradation kinetics were characterized using the double exponential model that was also used to characterize sulfur oxidation and SOM mineralization. Rapidly and slowly degradable PAH and TPH fractions could be distinguished and their degradation rates were quantified with first order rate constants. PAH bioavailability tests were performed using a persulfate oxidation.

The consolidated sediments were incubated for 21 days. After 10 and 21 days, oxygen concentration profiles were measured with oxygen microelectrodes and oxygen uptake rates were calculated. Finally, the aggregates were sacrificed and PAH and TPH removal was measured in their oxic and anoxic parts.

The conclusions of chapter 5 can be summarized as:
- rapidly degradable (bioavailable) PAH and TPH fractions amount up to 10 to 60% of the total amounts of PAH and TPH;
- Relative PAH and TPH degradation rates are in the same order of magnitude as relative SOM mineralization rates;
- oxygen uptake by degradation of PAH and TPH plays only a negligible role in the total oxygen uptake;
- amounts of PAH and TPH that are degraded in the oxygenated fractions of partly physically ripened sediments are equal to amounts that are degraded in oxygenated slurries. Most probably, degradation rates in the oxygenated fractions are also equal and therefore, bioremediation by ripening can be as successful as bioremediation in slurry reactors.

Modeling of oxygen diffusion

In chapter 6, a study is described with an oxygen diffusion model for aggregated soils. The input of the model consists of the sediment layer thickness, the geometric mean aggregate radius, the largest occurring aggregate radius, the standard deviation of the aggregate size distribution, the fraction air-filled cracks, the fraction air-filled matrix, and the oxygen uptake rate of the matrix.

The model was used to calculate the oxygen penetration depth and the oxygenated fraction in a layer of disposed dredged sediments at a field scale. Data on physical and biochemical ripening that were collected in the studies that are described in chapters 3 and 4 were used as input for the model. Scenario calculations were made for 'average'

dredged sediment (clay, soil organic carbon, and reduced sulfur content of 22, 7.6, and 1.2%, respectively) at different stages of physical and biochemical ripening. Finally, a sensitivity analysis was performed of the model output (oxygenated layer fraction) for all input parameters.

Conclusions that can be drawn from the modeling work are:
- the maximum layer thickness of 'average' clayey dredged sediments that can be completely oxygenated increases from a few millimeters to 1.10 meter as a result of the combination of physical and biochemical ripening. during the combination of physical and biochemical ripening;
- each doubling of oxygen uptake rates decreases the layer thickness that can be completely oxygenated with a factor 1.4.

7.2 General conclusions

The research described in this thesis has increased our insight into the individual processes of physical ripening and biochemical ripening – including PAH and TPH degradation – that result from drainage of disposed water-logged sediments. This increased insight can be used to optimize conditions at sediment disposal sites that are favorable for ripening and aerobic biodegradation of pollutants such as PAH and TPH.

This thesis shows that physical ripening is the most important and driving process step in the whole ripening process. The matric potential (ψ_m) is the key parameter to describe the physical ripening process. A layer of disposed dredged sediments can only be completely ripened if ψ_m reaches a value of about -16,000 hPa. Monitoring of matric potentials during disposal of sediments would provide direct information on the course and extent of physical ripening and indirect information on inter- and intra-aggregate oxygen diffusion characteristics. Besides, measurements of ψ_m can be used as an indicator for optimal conditions for tillage operations like turning, mixing, and aggregate size reduction. Low values of ψ_m result in low hydraulic conductivities and therefore reduction of evaporation rates from sediment surfaces. Especially in the top few centimeters of ripening sediments, this reduction can be substantial. Therefore, growth of plants on the ripening sediments is advantageous because of their ability to create low values of ψ_m throughout the whole root zone.

No detailed calculations on the maximal sediment layer thickness that can be (physically) ripened within one summer season are presented in this thesis. However, historical figures on the annual summer evaporation excess in The Netherlands (chapter 2), combined with the physical properties of 'average' unripe ($\psi_{m,min}$ = -100 hPa) and ripe ($\psi_{m,min}$ = -16,000 hPa) clayey sediments that are presented in chapter 3 of this thesis, indicate that sediment layers can only be completely physically ripened within one summer if their thickness is less than 0.10 to 0.25 m. In chapter 6, it was shown that the maximally permissible final layer thickness is 1.10 m for 'average' dredged sediments that already have been subjected to physical ripening. Based on the degradation kinetics provided in chapter 5, it can be reasoned that the required residence time to degrade bioavailable fractions of PAH and TPH in physically ripe sediments, is about 1 year in The Netherlands (assuming an

average sediment temperature of 10 °C). Altogether, it can be concluded that 1 year of disposal is required to physically ripen sediment layers of 0.25 m, after which another year is needed to biodegrade pollutants like PAH and TPH. During this second year, several layers that have been physically ripened during the first year can be applied up to thicknesses of about 1 meter. This knowledge on optimal initial layer thicknesses, final layer thicknesses, and required residence times can be useful for optimal management of temporary disposal sites.

The data that are provided in this thesis (chapters 3, 4, and 5) can be used as input in a model that describes all coupled processes that are at work during ripening of PAH and TPH polluted sediments at upland disposal sites. Several ingredients that are needed to build such a model are mentioned in this thesis (chapter 6). With the model, exact predictions could be made on the required residence time for ripening of PAH and TPH polluted sediments during temporary disposal. Furthermore, it would be possible to quantify the effects of management operations like for instance a layer by layer application instead of the application of one thick layer, weather conditions, active ventilation systems, constructions that prevent rainfall, vegetation, heating, trenches, tile drainage, and tillage.

7'

SAMENVATTING EN ALGEMENE CONCLUSIES

7.1' Samenvatting

Inleiding

In hoofdstuk 1 van dit proefschrift wordt een korte inleiding gegeven over de aard en geschiedenis van het probleem van verontreinigde baggerspecie in Nederland. Er wordt een overzicht gegeven van de recente ontwikkelingen in het onderzoek naar reiniging van baggerspecie die is verontreinigd met Polycyclische Aromatische Koolwaterstoffen (PAK) en minerale olie. Minerale olie is in dit proefschrift gekarakteriseerd als de totale hoeveelheid petroleumkoolwaterstoffen (TPH). Een veelbelovende reinigingstechniek die kan worden toegepast tijdens de tijdelijke bovengrondse opslag van deze baggerspecie, is rijping.

Literatuuronderzoek

Hoofdstuk 2 is het resultaat van een literatuuronderzoek naar de verschillende aspecten van rijping van baggerspecie. Rijping is een proces van initiële bodemvorming, dat optreedt als gevolg van ontwatering van waterverzadigde baggerspecie. Rijping kan worden onderverdeeld in fysische, chemische en biologische rijping. Fysische rijping verandert waterverzadigde kleiige baggerspecie (lutumgehalte > 15%) irreversibel in ge-aereerde (onverzadigde) kleiige bodem door uitdroging. Chemische rijping verandert de chemische samenstelling van baggerspecie door oxidatieprocessen zoals de omzetting van gereduceerd zwavel in sulfaat. Biologische rijping bestaat uit de ontwikkeling van aerobe (micro)organismen en hun effect op bijvoorbeeld de mineralisatie van organische stof (SOM).

De omstandigheden voor aerobe biologische afbraak van PAK en TPH worden verbeterd door de combinatie van de verschillende rijpingsprocessen. Daarom kan rijping worden aangewend als een reinigingstechniek voor baggerspecie die is verontreinigd met PAK en TPH. In hoofdstuk 2 wordt geconcludeerd dat de beschikbare kennis over rijping niet voldoende is om de kritische processtappen van elkaar te onderscheiden. Meer fundamenteel onderzoek is nodig, waarin de effecten van de verschillende rijpingsprocessen – inclusief PAK en TPH afbraak – onafhankelijk van elkaar kunnen worden bestudeerd. Daarom zijn de deelprocessen fysische, chemische en biologische rijping bestudeerd in verschillende onafhankelijke laboratoriumexperimenten die zijn beschreven in hoofdstuk 3, 4 en 5 van dit proefschrift. Hoofdstuk 6 beschrijft een studie waarin de gemeten parameters uit de voorgaande hoofdstukken zijn geïntegreerd in een mathematisch model.

Kwantificering van fysische eigenschappen

In hoofdstuk 3 worden de fysische eigenschappen van rijpende baggerspecies beschreven en gekwantificeerd. In het laboratorium werden drie kleiige baggerspecies kunstmatig gerijpt in speciaal daarvoor ontworpen drukcellen (microdepots). Met de microdepots werden aggregaten gevormd en uitgedroogd tot verschillende niveaus van fysische rijping. Het niveau van fysische rijping werd gekwantificeerd met de matrixpotentiaal (ψ_m) van het

water in de aggregaten. Deze mechanistische maat werd vergeleken met de empirische n-waarde (n_{rip}) die in de praktijk vaak wordt gebruikt om fysische rijping te kwantificeren. In de aggregaten werden krimpkarakteristieken, zwelfuncties, vochtkarakteristieken en doorlaatkarakteristieken gemeten. Hiernaast werden intra-aggregaat zuurstof-diffusiecoëfficiënten gemeten gebruik makend van micro-elektroden en diffusiekamers. Inter-aggregaat zuurstofdiffusiecoëfficiënten werden berekend met de informatie die was afgeleid van de gemeten krimpkarakteristieken. Ten slotte werden vier monsters verzameld met half rijpe en vier monsters met rijpe aggregaten die door natuurlijke rijping in baggerdepots waren gevormd. Hun aggregaatgrootteverdelingen werden gekarakteriseerd met afgeknotte lognormaalverdelingen.

De belangrijkste conclusies uit dit hoofdstuk zijn:
- de gepresenteerde gegevens kwantificeren alle fysische rijpingsparameters die relevant zijn voor de biologische afbraak van PAK en TPH in gestorte baggerspecie;
- voor de volledige rijping van baggerspecie ($n_{rip} < 0.7$ g g^{-1}) zijn matrixpotentialen (ψ_m) nodig die lager zijn dan -16.000 hPa;
- voor een goede beschrijving van fysische rijping is niet alleen informatie nodig over de laagste in het verleden opgetreden matrixpotentiaal ($\psi_{m,min}$), maar ook over de aggregaatgrootteverdeling;
- met de informatie die is ontwikkeld in dit hoofdstuk, kan het verloop van fysische rijping in bovengrondse baggerdepots worden voorspeld met een combinatie van bestaande water- en zuurstoftransport en rijpingsmodellen.

Oxidatie van zwavel en mineralisatie van organische stof

In hoofdstuk 4 wordt de biochemische rijping – in dit proefschrift gedefinieerd als de combinatie van zuurstofconsumerende chemische en biologische rijpingsprocessen – van baggerspecie beschreven en gekwantificeerd. Vijf series met baggerslurry's werden tijdens een laboratoriumexperiment van 160 dagen onder aerobe omstandigheden geïncubeerd in flesjes. Tijdens het experiment werden zuurstofopname, kooldioxideproductie, redoxpotentiaal en zuurgraad gemeten. Op negen momenten werden flesjes opgeofferd om de concentraties sulfaat, opgeloste organische stof, ammonium, nitraat, nitriet en fosfaat te meten. Gebaseerd op deze metingen werd de kinetiek van oxidatie van zwavel en mineralisatie van organische stof gekarakteriseerd, gebruik makend van een dubbelexponentieel model. Met dit model konden labiele en stabiele zwavel en snel en langzaam mineraliserende fracties organische stof worden onderscheiden. Relatieve oxidatiesnelheden van zwavel en mineralisatiesnelheden van organische stof konden worden gekwantificeerd met eerste-ordesnelheidsconstanten.

De belangrijkste conclusies van hoofdstuk 4 zijn:
- de zuurstofconsumptie van biochemisch rijpende baggerspecie kan volledig worden verklaard door de oxidatie van gereduceerd zwavel en mineralisatie van organische stof;
- de fractie labiele zwavel bedraagt 5 tot 35% van de totale hoeveelheid initieel aanwezige zwavel;

- de zuurstofconsumptie door zwaveloxidatie kan meer dan 30% bedragen van de totale zuurstofconsumptie als gevolg van biochemische rijping;
- van de stabiele zwavelfracties (bijvoorbeeld pyriet) worden geen meetbare hoeveelheden geoxideerd tijdens de incubatieperiode;
- de snel mineraliseerbare fractie organische stof bedraagt 5 tot 10% van de totale hoeveelheid organische stof;
- de relatieve mineralisatiesnelheden van de snel mineraliseerbare fracties organische stof zijn 100 tot 1.000 maal groter dan de relatieve mineralisatiesnelheden van de langzaam mineraliseerbare fracties;
- tijdens biochemische rijping zijn de gehalten aan beschikbare voedingsstoffen voldoende hoog om te voorkomen dat limitatie van de micro-organismen optreedt.

PAK en TPH afbraak

In hoofdstuk 5 zijn de effecten van chemische, biologische en fysische rijping op de afbraak van PAK en TPH gekwantificeerd tijdens het incubatie-experiment dat al uitgebreid is beschreven in hoofdstuk 4. Om betrouwbare metingen te krijgen van de langzame PAK- en TPH-afbraak, werd de incubatietijd verlengd tot 352 dagen. Hiernaast werden afbraak van PAK en TPH bestudeerd in kunstmatige aggregaten gevormd uit drie kleiige baggerspecies (geconsolideerde baggerspecie). De fysische karakterisering van de aggregaten werd al eerder beschreven in hoofdstuk 3.

De flesjes met de baggerslurry's werden opgeofferd op tien momenten om PAK- en TPH-concentraties te meten. Gebaseerd op de metingen werd de afbraakkinetiek van PAH en TPH gekarakteriseerd met het dubbelexponentieel model dat ook werd gebruikt voor de beschrijving van zwaveloxidatie en organischestofmineralisatie (hoofdstuk 4). Snel en langzaam afbrekende PAK- en TPH-fracties konden worden onderscheiden en hun relatieve afbraaksnelheden werden gekwantificeerd met eerste-ordesnelheidsconstanten. Verder werd de biobeschikbaarheid van PAK gemeten met een persulfaatoxidatie.

De geconsolideerde baggerspecies werden geïncubeerd gedurende 21 dagen. Na 10 en 21 dagen werden zuurstofconcentratieprofielen gemeten met zuurstofmicro-electroden. Uit deze metingen werden zuurstofconsumptiesnelheden afgeleid. Tenslotte werden de aggregaten opgeofferd en werden de PAK- en TPH-afname gemeten in de ge-aereerde en onge-aereerde delen.

De conclusies van hoofdstuk 5 kunnen worden samengevat als:
- de snel afbreekbare fracties PAK en minerale olie bedragen 10 tot 60% van de totale hoeveelheden PAK en minerale olie;
- de relatieve PAK- en TPH-afbraaksnelheden zijn van een zelfde ordegrootte als de relatieve mineralisatiesnelheden van organische stof;
- zuurstofconsumptie door de afbraak van PAK en TPH speelt slechts een verwaarloosbare rol in de totale zuurstofconsumptie;
- de hoeveelheden PAK en TPH die worden afgebroken in ge-aereerde delen van gedeeltelijk fysisch gerijpte baggerspecie zijn gelijk aan de hoeveelheden die worden

afgebroken in beluchte slurry's. Waarschijnlijk zijn de afbraaksnelheden ook gelijk. Daarom kan worden geconcludeerd dat baggerreiniging door rijping even effectief is als reiniging in slurryreactoren.

Modellering van zuurstofdiffusie

In hoofdstuk 6 wordt een studie beschreven met een zuurstofdiffusiemodel dat oorspronkelijk is ontwikkeld voor geaggregeerde bodems. De invoer van het model bestaat uit de baggerlaagdikte, de geometrische gemiddelde aggregaatstraal, de straal van het grootste aggregaat in het depot, de standaardafwijking van de aggregaatgrootteverdeling, de fractie luchtgevulde scheuren, de fractie luchtgevulde matrix en de zuurstofopnamesnelheid van de baggermatrix.

Het model is gebruikt om de zuurstof-indringingsdiepte en de geaereerde fractie in een laag gestorte baggerspecie voor een veldsituatie te berekenen. Gegevens over fysische en biochemische rijping die werden verzameld in de onderzoeken beschreven in hoofdstuk 3 en 4, zijn gebruikt als invoer voor het model. Scenarioberekeningen werden uitgevoerd voor 'gemiddelde' baggerspecie (met gehalten aan lutum, organische koolstof en gereduceerd zwavel van respectievelijk 22, 7,6 en 1,2%) in verschillende stadia van fysische en biochemische rijping. Tenslotte is voor alle invoerparameters een gevoeligheidsanalyse van het model uitgevoerd.

Conclusies die kunnen worden getrokken uit het modelleerwerk zijn:
- de grootste laagdikte van 'gemiddelde' kleiige baggerspecie die volledig kan worden ge-aereerd neemt toe van een paar millimeters tot 1,10 meter als resultaat van de combinatie van fysische en biochemische rijping;
- elke verdubbeling van de zuurstofopnamesnelheid (bijvoorbeeld door een verdubbeling van het organischestofgehalte) resulteert in een afname met een factor 1.4 in de laagdikte die maximaal kan worden ge-aereerd.

7.2' Algemene conclusies

Het onderzoek dat wordt beschreven in dit proefschrift heeft het inzicht vergroot in de individuele processen fysische rijping en biochemische rijping – inclusief PAK en TPH-afbraak – die optreden na het storten en ontwateren van baggerspecie in een bovengronds baggerdepot. Dit vergrote inzicht kan worden gebruikt om de omstandigheden voor rijping te optimaliseren.

Dit proefschrift laat zien dat fysische rijping de meest belangrijke en drijvende processtap is van het hele rijpingsproces. De matrixpotentiaal (ψ_m) kan worden gezien als de sleutelparameter voor de beschrijving van het volledige rijpingsproces. Een laag gestorte baggerspecie kan alleen volledig worden gerijpt wanneer ψ_m een waarde bereikt van ongeveer -16.000 hPa. Wanneer de matrixpotentiaal tijdens de opslag van baggerspecie in depot zou worden gemonitord, zou dit directe informatie verschaffen over het verloop van de fysische rijping en indirecte informatie of de inter- en intra-aggregaatzuurstofdiffusiekarakteristieken. Bovendien kunnen metingen van ψ_m worden

gebruikt om het tijdstip te bepalen waarop de omstandigheden voor het uitvoeren van grondbewerkingen als keren, mengen en aggregaatverkleining optimaal zijn. Lage matrixpotentialen leiden tot een lage waterdoorlatendheid en daardoor tot een verlaging van de verdampingssnelheden uit de baggerspecie. Deze verlaging treedt vooral op in de bovenste centimeters van rijpende baggerspecie. Het laten groeien van planten op baggerspecie is daarom gunstig vanwege hun capaciteit vocht op te nemen tot lage matrixpotentialen in de hele wortelzone.

In dit proefschrift zijn geen gedetailleerde berekeningen gepresenteerd over de grootste laagdikte die (fysisch) kan worden gerijpt binnen het tijdsbestek van één zomerseizoen. Echter, historische cijfers van het jaarlijkse zomerverdampingsoverschot in Nederland (hoofdstuk 2), gecombineerd met de fysische eigenschappen van 'gemiddelde' onrijpe (ψ_m = -100 hPa) en rijpe (ψ_m = -16.000 hPa) kleiige baggerspecie die worden gepresenteerd in hoofdstuk 3 van dit proefschrift, geven aan dat baggerlagen alleen volledig fysisch kunnen worden gerijpt in één zomer als de dikte ervan wordt beperkt tot 0,10 tot 0,25 m. Hoofdstuk 6 laat zien dat de grootst toelaatbare uiteindelijke laagdikte 1,10 m is voor 'gemiddelde' baggerspecie die al is onderworpen aan fysische rijping. Gebaseerd op de afbraakkinetiek beschreven in hoofdstuk 4 en 5, kan worden beredeneerd dat de benodigde verblijftijd om de biobeschikbare fracties PAK en TPH in fysisch rijpe baggerspecie af te breken, ongeveer één jaar is onder Nederlandse weersomstandigheden (aangenomen dat de gemiddelde baggertemperatuur 10 °C bedraagt). Alles bij elkaar kan worden geconcludeerd dat een verblijftijd van één jaar in depot nodig is om baggerlagen van circa 0,25 m fysisch te rijpen, waarna nog een jaar nodig is om verontreinigingen als PAK en TPH af te breken (biochemische rijping). Tijdens dit tweede jaar kunnen meerdere lagen die al één jaar fysische rijping achter de rug hebben worden opgebracht tot een totale laagdikte van ongeveer één meter. Deze kennis over optimale initiële laagdikten, uiteindelijke laagdikten en benodigde verblijftijden kan nuttig zijn voor een optimaal beheer van tijdelijke baggerdepots.

De gegevens die zijn gepresenteerd in dit proefschrift (hoofdstukken 3, 4 en 5) kunnen worden gebruikt als invoer in een model dat alle gekoppelde processen beschrijft die een rol spelen tijdens de rijping van verontreinigde baggerspecie in bovengrondse depots. Verschillende ingrediënten die nodig zijn om zo'n model te bouwen zijn genoemd in dit proefschrift (hoofdstuk 6). Met dit model zouden exacte voorspellingen kunnen worden gemaakt over de benodigde verblijftijd in depot voor rijping van PAK- en TPH-verontreinigde baggerspecie. Verder zou het mogelijk zijn om de effecten van beheersmaatregelen, zoals een laagsgewijs aanbrengen in plaats van stort van één dikke laag, weersomstandigheden, actief ventileren, constructies tegen regen, plantgroei, opwarmen, begreppeling, buisdrainage en grondbewerking, te voorspellen.

APPENDICES

APPENDIX 1: Water contents

In Soil Science, the water content is often expressed as a gravimetric ratio between water and solids in the wetness (*w*). The often used dry matter content (*D.M.*) is related to the wetness as follows:

$$D.M. = \frac{100}{w + 100} \tag{A1.1}$$

where:
D.M. = dry matter content, in percent (g water (100 g)$^{-1}$ wet sediment)
w = wetness, in percent (g water (100 g)$^{-1}$ solids)

For modeling purposes, it can be more convenient to express the water content as the volumetric moisture content (cm^3 water per cm^3 sediment or soil). If the dry bulk density of a sediment ($^b\rho_d$) is known, the volumetric moisture content can be calculated with:

$$\theta = \frac{w}{100}{}^b\rho_d \tag{A1.2}$$

where:
θ = aggregate volumetric water content (cm^3 water cm^{-3} wet matrix)
$^b\rho_d$ = aggregate dry bulk density (g cm^{-3})

In shrinking/swelling sediments, it is more convenient to express the water content as a volumetric moisture ratio (after Bronswijk 1991), hereafter referred to as moisture ratio:

$$\vartheta = \frac{V_w}{V_s} \tag{A1.3}$$

where:
ϑ = moisture ratio (cm^3 cm^{-3})
V_w = water volume (cm^3)
V_s = solid volume (cm^3)

The relationship between ϑ and θ is given by:

$$\vartheta = (1 + e)\theta \tag{A1.4}$$

where:
e = void ratio (cm^3 cm^{-3})

It should be emphasized that θ in Eqs. (A1.2) and (A1.4) represents the aggregate volumetric moisture content. The volumetric moisture content of a layer of sediment (θ_{layer}) consisting of aggregates (sediment matrix) and air-filled intra-aggregate pores ($\phi_{a,layer}$) can be calculated with:

$$\theta_{layer} = (1 - \phi_{a,layer})\theta \tag{A1.5}$$

where:
θ_{layer} = volumetric moisture content (cm^3 cm^{-3})
$\phi_{a,layer}$ = inter-aggregate air-filled porosity (cm^3 cm^{-3})

APPENDIX 2: Consistency

If the water content of a clayey soil is gradually reduced by slow desiccation, the clay passes from a liquid state through a plastic state, and finally into a solid state. In soil mechanics, the boundaries between different these different states of consistency are often quantified with the so called Atterberg limits (Terzaghi and Peck 1967): liquid limit (w_l), plastic limit (w_p), sticky limit (w_s), and shrinkage limit (w_{sh}). The different limits are defined as follows.

Liquid limit

The liquid limit is defined as the wetness, in percent of the dry weight, of a soil at the boundary between the semi-liquid and plastic states.

Plastic limit

The plastic limit is defined as the wetness, in percent of the dry weight, of a soil at the boundary between the plastic and semi-solid (brittle, friable) states.

Sticky limit

The sticky limit is defined as the wetness, in percent of the dry weight, of a soil that loses its ability to adhere to a metal blade.

Shrinkage limit

The shrinkage limit is defined as the wetness, in percent of the dry weight, below which further loss of water by evaporation does not result in reduction of volume (shrinkage).

Standardized laboratory devices are used to measure the different limits (Sowers 1965).

The plastic limit quantifies the wettest condition at which agricultural tillage can cause a decrease of aggregate sizes. The sticky limit quantifies the wettest condition at which (agricultural) tillage is possible. In most soils, the sticky limit has a slightly larger value than the plastic limit. Tillage is possible between the plastic limit and the sticky limit, but does not result in aggregate size reduction. In the literature, attempts are described to relate the optimal range for tillage also to the moisture retention characteristic (Dexter and Bird 2001). For many engineering purposes, clay is at its best desired packing density for working with when the wetness lies close to the plastic limit, which is between the plastic and liquid limit (TAW 1996).

Plasticity index

The range of wetness within which a soil possesses plasticity is known as the plastic range, and the numerical difference between w_l and w_p is called the plasticity index (I_p):

$$I_p = w_l - w_p \tag{A2.1}$$

where:
I_p = plasticity index (mass-%)
w_l = liquid limit (mass-%)
w_p = plastic limit (mass-%)

Soils with a high I_p tend to contain predominantly clay, those with a lower I_p tend to contain predominantly silt, and those with a I_p of 0 tend to contain little or no silt or clay. The value gives insight into the sensitivity of a clay to differences in wetness.

Consistency index

The following ratio:

$$I_c = \frac{w_l - w}{w_l - w_p} = \frac{w_l - w}{I_p} \tag{A2.2}$$

where:
I_c = consistency index (-)
w = wetness (g water g^{-1} solids)×100%)

is called the consistency index (I_c). In soil engineering, the consistency index is the most common way of expressing the consistency of cohesive soils and it is used to indicate the workability of a soil. Depending on its value, the different states (consistencies) can be distinguished (Table A2.1)

Table A2.1 Classification of sediment material according to the degree of consistency (after DWW 1999)

Consistency index (I_c)	state description
< 0.00	semi-liquid
0 – 0.25	mushy
0.25 – 0.50	very soft
0.50 – 0.75	soft
0.75 – 1.00	stiff
> 1.00	semi-solid (brittle, friable)

If the consistency index has a value of 0.6 to 0.7, a clay is usually able to bear earth-moving and compaction equipment and does not stick to it. Besides, compaction of the clay under these conditions gives good results. Clays with a lower consistency index (e.g. caused by higher values of w) are not able to bear heavy machinery. Moreover, such clays are sensitive to future cracking. At a higher consistency index, compaction will require relatively high loads (TAW 1996).

Ripening index

The consistency index (I_c) is related to the ripening index (n_{rip}), which is defined as (Pons and Van der Molen 1973):

$$n_{rip} = \frac{w_{sat} - 0.2R}{L + bH} \tag{A2.3}$$

where:

n_{rip} = n-value (g water g^{-1} clay)
w_{sat} = saturated moisture ratio in (g moisture (100 g)$^{-1}$ dry matter (D.M.))
R = sand + silt content (g sand + silt (100 g)$^{-1}$ D.M.)
L = clay content (g illite clay (100 g)$^{-1}$ D.M.)
b = ratio between water adsorption of 1 g organic matter compared to that of 1 g clay (-)
H = organic matter content (g organic matter (100 g)$^{-1}$ D.M.)

For sediments/soil containing other clay minerals than illite, Pons and Zonneveld (1965) proposed to convert the measured value for n_{rip} into that for illite with Eq. (A2.4).

$$n_{rip} = \frac{w_{sat} - 0.2R}{b_1 L + bH} \tag{A2.4}$$

$$with:: \; b_1 = \frac{CEC}{CEC_i} \tag{A2.5}$$

where:

b_1 = ratio between the water-binding capacity of illite and that of the clay in question (-)
CEC = cation exchange capacity of the clay in question (mmol (+) (100 g)$^{-1}$ clay
CEC_i = cation exchange capacity of illite (mmol (+) (100 g)$^{-1}$ illite-clay)

Pons and Zonneveld (1965) suggested to use a value of 60 mmol (+) (100 g)$^{-1}$ for CEC_i.

Different classes of physical ripening can be distinguished. These classes and their state description are given in Table A2.2.

Table A2.2 Classification of sediment/soil material according to physical ripening (after Pons and Zonneveld 1965)

n_{rip}	ripening class	state description
> 2.0	unripe, recently deposited sediment	liquid slurry, non kneadable
2.0 – 1.4	consolidated, but practically unripe	soft, sticks fast to the hands and can be easily squeezed through the fingers
1.4 – 1.0	half ripe	fairly soft, sticks to the hands and can be easily squeezed through the fingers
1.0 – 0.7	nearly ripe	fairly firm, tends to stick to the hands and cannot be easily squeezed through the fingers
< 0.7	ripe, normal soil	firm, does not stick to the hands, and cannot be squeezed through the fingers

Relation between ripening and consistency

Most probably, the liquid limit (and, to a lesser extent the also the plastic limit) of a sediment decreases as a result of drying (Sowers 1965), and therefore also as a result of physical ripening. The result of this decrease is that an unripe sediment has a higher consistency index (is 'stiffer') than a ripe soil having the same wetness (after Rijniersce 1983).

APPENDIX 3: Water potentials

In soil physics, the total water potential at any point in a sediment/soil profile is defined as the work done per unit of moving water in a reference state from a datum position to the point of question (Koorevaar et al. 1983).

Total potential

Neglecting thermal potentials, the total water potential (ψ) at any depth (z, positive downwards in this thesis) in a layer of sediments can be calculated by the sum of constituent potentials (Young and Sisson 2002):

$$\psi = \psi_g + \psi_p + \psi_m + \psi_\Omega + \psi_\Pi \qquad \text{(A3.1)}$$

where:

ψ	= total water potential (hPa)
ψ_g	= gravitational potential (hPa)
ψ_p	= pneumatic potential (hPa)
ψ_m	= matric potential (hPa)
ψ_Ω	= overburden potential (hPa)
ψ_Π	= osmotic potential (hPa)

Gravitational potential

The gravitational potential (ψ_g) needs no special discussion and is simply related to the depth from the surface into the sediment layer (assuming a density of water of 1,000 kg m^{-3}):

$$\psi_g = -z \qquad \text{(A3.2)}$$

where:

z	= depth into sediment profile, positive downwards (cm)

Pneumatic potential

Water potentials are expressed relative to atmospheric pressure. Under most conditions, it can be assumed that the pneumatic potential is equal to the atmospheric pressure. Only in deep, layered sediment profiles, or in (anaerobic) sediments with gas generation, pneumatic potentials could be significant.

Matric potential

The matric potential (ψ_m) consists of the work performed, per unit of water against the forces arising from interaction with the sediment/soil particles (e.g. capillary and adsorptive forces). As we define it, $\psi_m \leq 0$, and is a function (the so called moisture retention characteristic, see also chapter 3 of this thesis) of the moisture ratio (ϑ). The quantity $-\psi_m$ is often called 'suction' and sometimes, in swelling systems, 'swelling pressure'.

In soil physics, ψ_m is frequently used as a quantitative measure to express the moisture condition of sediment/soil (Koorevaar et al. 1983). The matric potential is directly related to the relative vapor pressure (p/p_0):

$$\psi_m = -\rho_w \frac{R_g T}{100M} \ln\left(\frac{p}{p_0}\right) \qquad \text{(A3.3)}$$

where:

ρ_w = density of water (≈ 1,000 kg m^{-3})
R_g = molar gas constant (= 8.314 J mol^{-1} K^{-1})
T = absolute temperature (K)
M = molar mass of water (18×10^{-3} kg mol^{-1})
p = vapor pressure (hPa)
p_0 = vapor pressure at a free surface of water under atmospheric pressure (hPa)
p/p_0 = relative vapor pressure (-)

Eq. (A3.3) can be used to calculate the relative vapor pressure that is needed to dewater a sediment sample down to a specific matric potential (Klute 1986). This method was also used in chapter 3 of this thesis.

Furthermore, the maximum diameter of water-filled pores (d_{eff}) of a mineral sediment/soil depends on the matric potential:

$$d_{eff} = -\frac{4\sigma_w}{100\psi_m} \qquad \text{(A3.4)}$$

where:

d_{eff} = effective pore diameter (m)
σ_w = surface tension at T = 293 K (73×10^{-3}) (N m^{-1})

Biologists use the term water activity for the relative vapor pressure (Parr et al. 1981).The water activity is used as a measure of water content that is related to microbial activity. At matric potentials higher than -250 hPa, moisture conditions are optimal microbial activity, whereas activity is inhibited for 80% at matric potentials lower than -16,000 hPa (Rijtema et al. 1999).

Table A3.1 gives the relation between ψ_m, p/p_0, and d_{eff} and the corresponding verbal terms.

Table A3.1 Relationships between matric potential (ψ_m), *pF*, relative vapor pressure (p/p_0), effective pore diameter (d_{eff}) at T=293K, and its verbal state description (after Parr et al. 1981 and Koorevaar et al. 1983)

ψ_m (hPa)	*pF* (log(-ψ_m)) (-)	p/p_0 (-)	d_{eff} (µm)	state description [c]
0	-	1	-[a]	water-saturated
-1	0	1	2908	very wet
-10	1	1	291	Wet
-100	2	1	29.1	moist ('field capacity')
-1,000	3	0.999	2.91	dry
-16,000	4.2	0.988	0.182	very dry ('wilting point')
-1,000,000	6	0.478	-[b]	air-dry
-10,000,000	7	0.0006	-[b]	oven-dry (105 °C)

[a] no capillary forces exist at $\psi_m = 0$
[b] capillary theory is not valid because the matric potential is lower than the so called hygroscopic point
[c] after Werkgroep Herziening Cultuurtechnisch Vademecum 1988

The matric potential can be measured with so called tensiometers. In the tensiometric measurement of soil water matric potential, the overburden potential (see below) is manifested (Young and Sisson 2002). Therefore, the 'true' matric potential needs to be corrected for this potential (Smiles 2000), when significant (e.g. in ripening sediments). The lower limit for tensiometer measurements is approximately -800 hPa (Young and Sisson 2002). Several indirect techniques have been developed to measure matric potentials down to much lower values (Andraski and Scanlon 2002 and Scanlon et al. 2002). Recently, a new polymer tensiometer has been developed that is capable to measure matric potentials down to -16,000 hPa (Bakker et al. accepted). For monitoring of potentials in ripening dredged sediments, a device should be used that gives accurate measurements in the whole range of physical ripening (i.e. 0 to -16,000 hPa according to chapter 3 of this thesis) in a shrinking matrix in which cracks develop.

Overburden potential

The overburden potential (ψ_Ω) is the work performed, per unit of water extracted to realize the required movement of particles against gravity and external load. Therefore, it is only used in the context of shrinking and swelling sediments/soils. For a one-dimensionally vertically shrinking (consolidating) layer of sediments ψ_Ω is defined by:

$$\psi_\Omega = \frac{\mathrm{d}e}{\mathrm{d}\vartheta}\mathrm{P}(z) \tag{A3.5}$$

$$\text{with } \mathrm{P}(z) = \mathrm{P}(0) + \int_{z_0}^{z} {}^{b}\rho_w \, \mathrm{d}z \tag{A3.6}$$

$$\text{with } {}^{b}\rho_w = \frac{\vartheta + \rho_p}{1+e} \tag{A3.7}$$

where:

e	= void ratio ($cm^3\ cm^{-3}$)
ϑ	= volumetric moisture ratio ($cm^3\ cm^{-3}$)
z_0	= surface of sediment profile (0 cm)
$P(z)$	= total vertical load (hPa)
$P(0)$	= external load on the surface at z = 0 (hPa)
${}^{b}\rho_w$	= wet bulk density ($g\ cm^{-3}$)
ρ_p	= particle density ($g\ cm^{-3}$)

In soil mechanics (and also in chapter 2), P is called the total stress or overburden pressure. The analogue term for the matric potential (ψ_m) is called the effective or interparticle stress (Smiles 2000).

To make calculations for situations with more-dimensional shrinkage (e.g. physical ripening), researchers like Kim et al. (1992a) and Garnier et al. (1997) attempted to generalize Eq. (A3.5) using a geometry factor (r_s) that accounts for the relative magnitude of vertical shrinkage caused by the changes in total volume shrinkage (see also chapters 3 and 6).

Osmotic potential

In many cases, the existence of the osmotic potential (ψ_{Π}) can be neglected. However, ψ_{Π} can play a role in cases where water containing different concentrations of dissolved solutes are separated by a semi permeable membrane (e.g. in the plant-root system). The osmotic potential of a water solution can be calculated with:

$$\psi_{\Pi} = -\frac{R_g T c}{100} \tag{A3.8}$$

where:

ψ_{Π} = osmotic potential (hPa)
c = ionic concentration (mol m^{-3})

Eq. (A3.8) can be used to calculate the osmotic potential that is needed to equilibrate the water potential to desired levels in sediment samples that are stored for incubation experiments. This method was also used in chapter 5 of this thesis.

REFERENCES

Ahmad N, 1983. Vertisols. In: Wilding LP, Smeck NE, Hall GF (Eds.). *Pedogenesis and soil taxonomy, II. The soil orders*. pp 91–123. Elsevier, Amsterdam.

AKWA (Avies- en Kenniscentrum Waterbodems), 1999a. *Fysische rijping van baggerspecie. Modelstudie – Een koppeling tussen Geotechniek en Cultuurtechniek*. AKWA rapport 99.016. DWW, Ministerie van Verkeer en Waterstaat, Delft.

AKWA (Advies- en Kenniscentrum Waterbodems), 1999b. *Inventarisatie waterbodems. Aanbod en bestemming van baggerspecie*. AKWA rapport. RIZA, Ministerie van Verkeer en Waterstaat, Lelystad.

AKWA (Advies- en Kenniscentrum Waterbodems), 2001. *Basisdocument tienjarenscenario waterbodems. Bagger in beeld*. AKWA rapport 01.014. AKWA, Ministerie van Verkeer en Waterstaat, Utrecht.

Allmaras RR, Burwell RE, Voorhees WB, Larson WE, 1965. Aggregate size distribution in the row zone of tillage experiments. *Soil Science Society of America Proceedings* 29:645–650.

Anderson T-H, Domsch KH, 1989. Ratios of microbial biomass carbon to total organic carbon in arable soils. *Soil Biology & Biochemistry* 21:471–479.

Andraski B, Scanlon BR, 2002. Thermocouple psychrometry. In: Dane JH, Topp GC (Eds.). *Methods of soil analysis. Part 4. Physical methods*. No. 5 in the Soil Science Society of America book series, pp 609–642. SSSA, Madison WI.

Arah JRM, Smith KA, 1989. Steady-state denitrification in aggregated soils: a mathematical model. *Journal of Soil Science* 40:139–149.

Arah JRM, Vinten AJA, 1995. Simplified models of anoxia and denitrification in aggregated and simple-structured soils. *European Journal of Soil Science* 46:507–517.

Bakker DM, Bronswijk JJB, 1993. Heterogeneous oxygen concentrations in a structured clay soil. *Soil Science* 155:309–315.

Bakker G, Van der Ploeg MJ, De Rooij GH, Hoogendam CW, Gooren HPA, Huiskes C, Koopal LK, Kruidhof H, *Accepted for publication*. New polymer tensiometers: Measuring matric pressures down to wilting point. *Vadose Zone Journal*.

Bal L, 1982. *Zoological ripening of soils*. Agricultural Research Reports 850. Pudoc, Wageningen.

Basma AA, Al-Homoud AS, Husein Malkawi AI, Al-Bashabsheh MA, 1996. Swelling-shrinkage behavior of natural expansive clays. *Applied Clay Science* 11:211–227.

Baumgartl Th, 1998. Physical soil properties in specific fields of application especially in anthropogenic soils. *Soil & Tillage Research* 47:51–59.

Baumgartl Th, Horn R, 1999. Influence of mechanical and hydraulic stresses on hydraulic properties of swelling soils. In: Van Genuchten, MTh, Leij FJ, Wu L (Eds.). *Characterization and measurement of the hydraulic properties of unsaturated porous media*. Proceedings of an international workshop, 22 – 24 October 1997, Riverside CA, Part 1, pp 449–457. University of California, Riverside CA.

Baver LD, Gardner WH, Gardner WR, 1972. *Soil physics* (4th edition). John Wiley & Sons, New York NY.

Blake GR, Hartge KH, 1986. Particle density. In: Klute A (Ed.). *Methods of soil analysis. Part 1. Physical and mineralogical methods*. Agronomy monograph no. 9 (2nd edition), pp 377–382. American Society of Agronomy, Madison WI.

Bonten LTC, 2001. *Improving bioremediation of PAH contaminated soils by thermal pretreatment*. PhD-thesis Wageningen University. Wageningen.

Bonten LTC, Grotenhuis TC, Rulkens WH, 1999. Enhancement of PAH biodegradation in soil by physicochemical pretreatment. *Chemosphere* 38:3627–3636.

Boudreau BP, Ruddick BR, 1991. On a reactive continuum representation of organic matter diagenesis. *American Journal of Science* 291:507–538.

Bradford JM, Gupta SC, 1986. Compressibility. In: Klute A (Ed.). *Methods of soil analysis. Part 1. Physical and mineralogical methods*. Agronomy monograph no. 9 (2nd edition), pp 479–492. American Society of Agronomy, Madison WI.

Brandsch R, Nowak KE, Binder N, Jastorff B, 2001. Investigations concerning the sustainability of remediation by land deposition of tributyltin contaminated harbour sediments. *Journal of Soils and Sediments* 1:234–236.

Brasher BR, Franzmeier DP, Valassis V, Davidson SE, 1966. Use of Saran resin to coat natural soil clods for bulk-density and water retention measurements. *Soil Science* 101:108.

Braunack MV, Dexter AR, 1989. Soil aggregation in the seedbed: A review. I. Properties of aggregates and beds of aggregates. *Soil & Tillage Research* 14:259–279.

Breteler H, Duijn R, Goedbloed P, Harmsen J, 2001. Surface treatment of polluted sediment in an energy plantation. In: Magar VS, von Fahnestock FM, Leeson A (Eds.). *Ex situ biological treatment technologies*. Proceedings of the sixth International In Situ and On-Site Bioremediation symposium, 4 – 7 June 2001, San Diego CA, Volume 6, pp 59–63. Battelle Press, Columbus OH.

Bronswijk JJB, 1988. Modeling of water balance, cracking and subsidence of clay soils. *Journal of Hydrology* 97:199–212.

Bronswijk JJB, 1990. Shrinkage geometry of a heavy clay soil at various stresses. *Soil Science Society of America Journal* 54:1500–1502.

Bronswijk JJB, 1991. *Magnitude, modeling and significance of swelling and shrinkage processes in clay soils.* PhD-thesis Wageningen Agricultural University. Wageningen.

Bronswijk JJB, Evers-Vermeer JJ, 1990. Shrinkage of Dutch clay soil aggregates. *Netherlands Journal of Agricultural Science* 38:175–194.

Bronswijk JJB, Nugroho K, Aribawa B, Groenenberg E, Ritsema CJ, 1992. Modeling of oxygen transport and pyrite oxidation in acid sulfate soils. *Journal of Environmental Quality* 22:544–554.

Buol SW, McCracken RJ, Hole FD, 1973. *Soil genesis and classification.* The Iowa State University Press, Ames IA.

Burdige DJ, 1991. The kinetics of organic matter mineralization in anoxic marine sediments. *Journal of Marine Research* 49:727–761.

Calmano W, Hong J, Förstner U, 1993. Binding and mobilization of heavy metals in contaminated sediments affected by pH and redox potential. *Water Science & Technology* 28:223–235.

Chan KY, Dexter AR, McKenzie DC, 1999. Categories of soil structure based on mechanical behaviour and their evaluation using additions of lime and gypsum a sodic Vertisol. *Australian Journal of Soil Research* 37:903–911.

Chapman SJ, Gray TRG, 1986. Importance of cryptic growth, yield factors and maintenance energy in models of microbial growth in soil. *Soil Biology & Biochemistry* 18:1–4.

Chertkov VY, 2000. Using surface crack spacing to predict crack network geometry in swelling soils. *Soil Science Society of America Journal* 64:1918–1921.

Conrad R, 1999. Contribution of hydrogen to methane production and control of hydrogen concentrations in methanogenic soils and sediments. *FEMS Microbiology Ecology* 28:193–202.

Cornelissen G, Gustafsson Ö, Bucheli TD, Jonker MTO, Koelmans AA, Van Noort PCM, 2005. Extensive sorption of organic compounds to black carbon, coal, and kerogen in sediments and soils: mechanisms and consequences for distribution, bioaccumulation, and biodegradation. *Environmental Science & Technology* 39:6881–6895.

Cornelissen G, Rigterink H, Ferdinandy MMA, Van Noort PCM, 1998. Rapidly desorbing fractions of PAHs in contaminated sediments as a predictor of bioremediation. *Environmental Science & Technology* 32:966–970.

Cornelissen G, Van Noort PCM, Govers HAJ, 1997a. Desorption kinetics of chlorobenzenes, polycyclic aromatic hydrocarbons, and polychlorinated biphenyls: sediment extraction with Tenax® and effects of contact time and solute hydrophobicity. *Environmental Toxicology & Chemistry* 16:1351–1357.

Cornelissen G, Van Noort PCM, Parsons JR, Govers HAJ, 1997b. Temperature dependence of slow adsorption and desorption kinetics of organic compounds in sediments. *Environmental Science & Technology* 31:454–460.

Crescimanno G, Provenzano G, 1999. Soil shrinkage characteristic curve in clay soils: measurement and prediction. *Soil Science Society of America Journal* 63:25–32.

CUR/NOBIS (Civieltechnisch Centrum Uitvoering Research en Regelgeving / Nederlands Onderzoekprogramma Biotechnologische In-Situ Sanering), 1997. *Definitiestudie biologische reiniging baggerspecie.* NOBIS 96-1-02. CUR/NOBIS, Gouda.

CUR/NOBIS (Civieltechnisch Centrum Uitvoering Research en Regelgeving / Nederlands Onderzoekprogramma Biotechnologische In-Situ Sanering), 1999a. *Kwaliteitsverbetering van baggerspecie op basis van extensieve biorestauratie in combinatie met energieteelt.* NOBIS 96-1-02. CUR/NOBIS, Gouda.

CUR/NOBIS (Civieltechnisch Centrum Uitvoering Research en Regelgeving / Nederlands Onderzoekprogramma Biotechnologische In-Situ Sanering), 1999b. *Reiniging van baggerspecie in een doorgangsdepot. Onderzoek naar de toepasbaarheid van schimmels en elektrische stroom.* NOBIS 96-2-06. CUR/NOBIS, Gouda.

Currie JA, 1965. Diffusion within soil microstructure. A structural parameter for soils. *Journal of Soil Science* 16:279–289.

Cuypers C, 2001. *Bioavailability of polycyclic aromatic hydrocarbons in soils and sediments. Prediction of bioavailability & characterization of organic matter domains.* PhD-thesis Wageningen University. Wageningen.

Cuypers C, Clemens R, Grotenhuis T, Rulkens W, 2001. Prediction of petroleum hydrocarbon bioavailability in contaminated soils and sediments. *Soil & Sediment Contamination* 10:459–482.

Cuypers C, Grotenhuis T, Joziasse J, Rulkens W, 2000. Rapid persulfate oxidation predicts PAH bioavailability in soils and sediments. *Environmental Science & Technology* 34:2057–2063.

Darwin CR, 1881. *The formation of vegetable mould through the action of worms. With observations on their habits.* Murray, London.

Dasog GS, Acton DF, Mermut AR, De Jong E, 1988. Shrink-swell potential and cracking in clay soils of Saskatchewan. *Canadian Journal of Soil Science* 68:251–260.

Dauwe B, Middelburg JJ, Herman PMJ, 2001. Effect of oxygen on the degradability of organic matter in subtidal and intertidal sediments of the North Sea area. *Marine Ecology Progress Series* 215:13–22.

De Glopper RJ, Minten AGM, Winkels HJ, 1992. *Chemische rijping van de bodem in Zuidelijk Flevoland.* Flevobericht 332. Ministerie van Verkeer en Waterstaat, Lelystad.

De Haan W, Otten KJ, Heynen JJM, Folkerts H, Elsman M, 1998. Field monitoring of ripening of dredged material at three sites in The Netherlands (preliminary results). *Water Science & Technology* 37:371–378.

Dekker J, 1981. Grondmechanische aspecten van de toepassing van gerijpt havenslib in dijkbouw. *Polytechnisch Tijdschrift, bouwkunde, wegen- en waterbouw* 36:578–586.

Del'Arco JP, de França FP, 1999. Biodegradation of crude oil in sandy sediment. *International Biodeterioration & Biodegradation* 44:87–92.

De Waard CP, Van de Velde CP, 1981. Het gebruik van gerijpte baggerspecie in dijkverbetering. *Polytechnisch Tijdschrift, bouwkunde, wegen- en waterbouw* 36:575–577.

Dexter AR, 1988. Advances in characterization of soil structure. *Soil & Tillage Research* 11:199–238.

Dexter AR, Bird NRA, 2001. Methods for predicting the optimum and the range of soil water contents for tillage based on the water retention curve. *Soil & Tillage Research* 57:203–212.

Dexter AR, Horn R, Kemper WD, 1988. Two mechanisms for age-hardening of soil. *Journal of Soil Science* 39:163–175.

Dexter AR, Kroesbergen B, Kuipers H, 1984. Some mechanical properties of aggregates of top soils from the IJsselmeerpolders. 1. Undisturbed soil aggregates. *Netherlands Journal of Agricultural Science* 32:205–214.

Dilly O, 2001. Microbial respiratory quotient during basal metabolism and after glucose amendment in soils and litter. *Soil Biology & Biochemistry* 33:117–127.

DWW (Dienst Weg- en Waterbouwkunde), 1999. *Grond uit baggerspecie. Analyse van eisen in relatie tot toepassingen.* Rapport W-DWW-99-002. DWW. Ministerie van Verkeer en Waterstaat, Delft.

Ehlers GAC, Loibner AP, 2006. Linking organic pollutant (bio)availability with geosorbent properties and biomimetic methodology: A review of geosorbent characterisation and (bio)availability prediction. *Environmental Pollution* 141:494–512.

Eijsackers H, Van Gestel CAM, De Jonge S, Muijs B, Slijkerman D, 2001. Polycyclic aromatic hydrocarbon-polluted dredged sediments and earthworms: a mutual interference. *Ecotoxicology* 10:35–50.

Evangelou VP, 1998. *Environmental soil and water chemistry, principles and applications.* John Wiley & Sons, New York NY.

Feng Y, Li X, 2001. An analytical model of soil organic carbon dynamics based on a simple "hocky stick" function. *Soil Science* 166:431–440.

Fick A, 1855. Über Diffusion. *Annalen der Physik (Leipzig)* 94, 59.

Garnier P, Perrier E, Angulo Jaramillo R., Baveye P, 1997. Numerical model of 3-dimensional anisotropic deformation and 1-dimensional water flow in swelling soils. *Soil Science* 162:410–420.

Geerdink MJ, Van Loosdrecht MCM, Luyben KCAM, 1996. Biodegradability of diesel oil. *Biodegradation* 7:73–81.

Gevao B, Semple KT, Jones KC, 2000. Bound residues in soils: a review. *Environmental Pollution* 108:3–14.

Glinski J, Stepniewski W, 1985. *Soil aeration and its role for plants.* CRC Press, Boca Raton FL.

GOBZ (Gemeenschappelijk Orgaan Baggerspecie Zuid-Holland), 1998. *Baggerspecie rijp voor rijping: Monitoring van rijping, uitloging en afbraak van organische verontreinigingen in vier doorgangsdepots voor baggerspecie, Hoofdrapport en meetrapport.* Waterschap De Brielse Dijkring, Brielle.

Grable AR, Siemer EG, 1968. Effects of bulk density, aggregate size, and soil water suction on oxygen diffusion, redox potential and elongation of corn roots. *Soil Science Society of America Proceedings* 32:180–186.

Greenwood DJ, Berry G, 1962. Aerobic respiration in soil crumbs. *Nature* 195:161–163.

Groenevelt PH, Grant CD, 2001. Re-evaluation of the structural properties of some British swelling soils. *European Journal of Soil Science* 52:469–477.

Groenevelt PH, Grant CD, 2002. Curvature of shrinkage lines in relation to the consistancy and structure of a Norwegian clay soil. *Geoderma* 106:235–245.

Grossman RB, 1983. Entisols. In: Wilding LP, Smeck NE, Hall GF (Eds.). *Pedogenesis and soil taxonomy, II. The soil orders.* pp 55–90. Elsevier, Amsterdam.

Grotenhuis T, Smit M, Rulkens W, 2004. Linking bioavailability to environmental technology. In: *Monitoring sediment quality at river basin scale. Understanding the behaviour and fate of pollutants.* Proceedings of a SedNet workhop, 29 – 31 January 2004, Lisbon.

Hadas A, 1990. Directional strength in aggregates as affected by aggregate volume and by a wet/dry cycle. *Journal of Soil Science* 41:85–93.

Haliburton TA, 1979. Best ways to dewater dredged material. *Civil Engineering ASCE* 49(8):57–61.

Harmsen J, 2001. Bioremediation of polluted sediments: a matter of time or effort. In: Leeson A, Foote EA, Banks MK, Magar VS (Eds.). *Phytoremediation, wetlands and sediments.* Proceedings of the sixth International In Situ and On-Site Bioremediation Symposium, 4 – 7 June 2001, San Diego CA, Volume 5, pp 279–287. Battelle Press, Columbus OH.

Harmsen J, 2004. *Landfarming of polycyclic aromatic hydrocarbons and mineral oil contaminated sediments.* PhD-thesis Wageningen University. Wageningen.

Harmsen J, Bouwman L, 2002. Bioremediation of polluted sediments: a matter of time or effort? – Part II. In: Hinchee RE, Porta A, Pallei M (Eds.). *Remediation and beneficial reuse of contaminated sediments.*

Proceedings of the first International Conference on Remediation of Contaminated Sediments, 10 – 12 October 2001, Venice, Volume 3, pp 113–119. Battelle Press, Columbus OH.

Harmsen J, Sims RC, 2004. Height and time in landfarming: from two to four dimensions. In: Magar VS, Kelley ME (Eds.). *In Situ and On-Site Bioremediation – 2003*. Proceedings of the seventh International In Situ and On-Site Bioremediation symposium, 2 – 5 June 2003, Orlando FL, Paper O-02. Battelle Press, Columbus OH.

Heerenklage HK, Woyczechowski H, Bollow S, Stegmann R, 1998. Influence of oxygen on the degradation of diesel fuel in soil bioreactors. *Acta Biotechnologica* 2:109–122.

Hendriks RFA, 1991. *Afbraak en mineralisatie van veen. Literatuuronderzoek*. DLO-SC Rapport 199. DLO-Staring Centrum, Wageningen.

Hendriks RFA, Oostindie K, Hemminga P, 1999. Simulation of bromide tracer and nitrogen transport in a cracked clay with the FLOCR/ANIMO model combination. *Journal of Hydrology* 215:94–115.

Hillel D, Warrick AW, Baker RS, Rosenzweig C, 1998. *Environmental soil physics*. Academic Press, San Diego CA.

Holland EA, Coleman DC, 1987. Litter placement effects on microbial and organic matter dynamics in an agroecosystem. *Ecology* 68:425–433.

Horn R, 1990. Aggregate characterization as compared to soil bulk properties. *Soil & Tillage Research* 17:265–289.

Horn R, 2003. Stress-strain effects in structured unsaturated soils on coupled mechanical and hydraulic processes. *Geoderma* 116:77–88.

Horn R, Baumgartl T, Gräsle W, Richards BG, 1996. Stress induced changes of hydraulic properties in soils. In: Alonso EE, Delage P (Eds.). *Unsaturated Soils*. Proceedings of the first international conference on unsaturated soils / UNSAT'95, 6 – 8 September 1995, Paris, Volume 1, pp 123–127. Balkema, Rotterdam.

Horn R, Dexter AR, 1989. Dynamics of soil aggregation in an irrigated desert loess. *Soil & Tillage Research* 13:253–266.

Horn R, Taubner H, Wuttke M, Baumgartl T, 1994. Soil physical properties related to soil structure. *Soil & Tillage Research* 30:187–216.

Hough BK, 1957. *Basic soils engineering*. The Ronald Press Company, New York NY.

Huesemann MH, Hausmann TS, Fortman TJ, 2003. Assessment of bioavailability limitations during slurry biodegradation of petroleum hydrocarbons in aged soils. *Environmental Toxicology & Chemistry* 22:2853–2860.

Huesemann MH, Truex MJ, 1996. The role of oxygen diffusion in passive bioremediation of petroleum contaminated soils. *Journal of Hazardous Materials* 51:93–113.

Huisman P, 2004. *Water in the Netherlands. Managing checks and balances*. Netherlands Hydrological Society. Utrecht.

Hunt HW, 1978. A simulation model for decomposition in grasslands. In: Innis GS (Ed.). *Grassland simulation model*. pp 155–183. Springer Verlag, New York NY.

Hurst CJ, Sims RC, Sims JL, Sorensen DL, McLean JE, Huling S, 1996. Polycyclic aromatic hydrocarbon biodegradation as a function of oxygen tension in contaminated soil. *Journal of Hazardous Materials* 51:193–208.

Imai G, 1980. Settling behaviour of clay suspensions. *Soils and Foundations* 20:61–77.

Janssen BH, 1984. A simple method for calculating decomposition and accumulation of 'young' soil organic matter. *Plant and Soil* 76:297–304.

Jarvis NJ, Jansson PE, Dik PE, Messing I, 1991. Modelling water and solute transport in macroporous soil. I. Model description and sensitivity analysis. *Journal of Soil Science* 42: 59–70.

Jarvis NJ, Zavattaro L, Rajkai K, Reynolds WD, Olsen PA, McGechan M, Mecke M, Mohanty B, Leeds-Harrison PB, Jacques D, 2002. Indirect estimation of near-saturated hydraulic conductivity from readily available soil information. *Geoderma* 108:1–17.

Johnsen AR, Wick LY, Harms H, 2005. Principles of microbial PAH-degradation in soil. *Environmental Pollution* 133:71–84.

Kalbitz K, Schmerwitz J, Schwesig D, Matzner E, 2003. Biodegradation of soil-derived dissolved organic matter as related to its properties. *Geoderma* 113:273–291.

Kim DJ, Diels J, Feyen J, 1992b. Water movement associated with overburden potential in a shrinking marine clay soil. *Journal of Hydrology* 133:179–200.

Kim DJ, Feyen J, Vereecken H, 1993a. Prediction of dynamic hydraulic properties in a ripening soil. *Geoderma* 57:231–246.

Kim DJ, Feyen J, Vereecken H, Boels D, Bronswijk JJB, 1993b. Quantification of physical ripening in an unripe marine clay soil. *Geoderma* 58:67–77.

Kim DJ, Vereecken H, Feyen J, Boels D, Bronswijk JJB, 1992c. On the characterization of properties of an unripe marine clay soil. I. Shrinkage of an unripe marine clay soil in relation to physical ripening. *Soil Science* 153:471–481.

Kim DJ, Vereecken H, Feyen J, Vanclooster M, Stroosnijder L, 1992a. A numerical model of water movement and soil deformation in a ripening marine clay soil. *Modeling Geo-Biosphere Processes* 1:185–203.

Klute A, 1986. Water retention: laboratory methods. In: Klute A (Ed.). *Methods of soil analysis. Part 1. Physical and mineralogical methods*. Agronomy Monograph no. 9 (2nd edition), pp 635–662. American Society of Agronomy, Madison WI.

Klute A, Dirksen C, 1986. Hydraulic conductivity and diffusivity: laboratory methods. In: Klute A (Ed.). *Methods of soil analysis. Part 1. Physical and mineralogical methods*. Agronomy monograph no. 9 (2nd edition), pp 687–734. American Society of Agronomy, Madison WI.

Koenigsberg S, Sandefur C, 2001. Application of oxygen release compound: a six year review. In: Leeson A, Johnson PC, Hinchee RE, Semprini L, Magar VS (Eds.). *In situ aeration and aerobic remediation*. Proceedings of the sixth International In Situ and On-Site Bioremediation Symposium, 4 – 7 June 2001, San Diego CA, Volume 10, pp 87–94. Battelle Press, Columbus OH.

Konrad JM, Ayad R, 1997. Desiccation of a sensitive clay: field experimental observations. *Canadian Geotechnical Journal* 34:929–942.

Koorevaar P, Menelik G, Dirksen C, 1983. *Elements of soil physics*. Developments in Soil Science 13. Elsevier, Amsterdam.

Kortleven J, 1963. *Kwantitatieve aspecten van humusopbouw en humusafbraak*. Proefschrift Landbouwhogeschool Wageningen. Wageningen.

Kotterman M, Van Lieshout J, Grotenhuis T, Field J, 1999. Development of white rot fungal technology for PAH degradation. In: Leeson A, Alleman BC (Eds.). *Bioremediation technologies for polycyclic aromatic hydrocarbon compounds*. Proceedings of the fifth International In Situ and On-Site Bioremediation Symposium, 19 – 22 April, San Diego CA, Volume 8, pp 69–74. Battelle Press, Columbus OH.

Leffelaar PA, 1979. Simulation of partial anaerobiosis in a model soil in respect to denitrification. *Soil Science* 128:110–120.

Lemon ER, Erickson AE, 1952. The measurement of oxygen diffusion in the soil with a platinum microelectrode. *Soil Science Society of America Proceedings* 16:160–163.

Linkov I, Burmistrov D, Cura J, Bridges TS, 2002. Risk-based management of contaminated sediments: consideration of spatial and temporal patterns in exposure modeling. *Environmental Science & Technology* 36:238–246.

Linn DM, Doran JW, 1984. Effect of water-filled pore space on carbon dioxide and nitrous oxide production in tilled and nontilled soils. *Soil Science Society of America Journal* 48:1267–1272.

Longmuir IS, 1954. Respiration rate of bacteria as a function of oxygen concentration. *Biochemical Journal* 57:81–87.

Löser C, Seidel H, Hoffmann P, Zehnsdorf A, 2000. Remediation of heavy metal-contaminated sediments by solid-bed bioleaching. *Environmental Geology* 40:643–650.

Löser C, Zehnsdorf A, Hoffmann P, Seidel H, 1999. Conditioning of heavy metal-polluted river sediments by Helophytes. *International Journal of Phytoremediation* 1:339–359.

Ma WC, Immerzeel J, Bodt J, 1995. Earthworm and food interactions on bioaccumulation and disappearance in soil of Polycyclic Aromatic Hydrocarbons: studies on phenanthrene and fluoranthene. *Ecotoxicology and Environmental Safety* 32:226–232.

Malina G, Vermeulen J, Kromer M, 2004. Natlenianie zanieczyszczonych osadów dennych podczas tymczasowego składowania. *Engineering and Protection of Environment* 7:401–419.

McGechan MB, Wu L, 2001. A review of carbon and nitrogen processes in European soil nitrogen dynamics models. In: Shaffer MJ, Ma L, Hansen S (Eds.). *Modeling carbon and nitrogen dynamics for soil management*. pp 103–171. Lewis Publishers, Boca Raton FL.

McKenzie BM, Dexter AR, 1988. Radial pressures generated by the earthworm *Aporrectodea rosea*. *Biology and Fertility of Soils* 5:328–332.

Middelburg JJ, 1989. A simple rate model for organic matter decomposition in marine sediments. *Geochimica et Cosmochimica Acta* 53:1577–1581.

Ministerie van VROM, 1992. *Wet Milieubeheer*. Artikel 10.4, Staatsblad 1992, 551. Sdu Uitgeverij, 's-Gravenhage.

Ministerie van VROM, 2000. *Circulaire streefwaarden en interventiewaarden bodemsanering*. Staatscourant 2000, 39. Sdu Uitgeverij, 's-Gravenhage.

Misra RK, Dexter AR, Alston AM, 1986. Penetration of soil aggregates of finite size. I. Blunt penetrometer probes. *Plant and Soil* 94:59–85.

Moldrup P, Olesen T, Rolston DE, Yamaguchi T, 1997. Modeling diffusion in soils: VII. Predicting gas and ion diffusivity in undisturbed and sieved soils. *Soil Science* 162:632–640.

Moldrup P, Olesen T, Yamaguchi P, Schønning P, Rolston DE, 1999. Modeling diffusion and reaction in soils: IX. The Buckingham-Burdine-Campbell equation for gas diffusivity in undisturbed soil. *Soil Science* 164:542–551.

Monod J, 1949. The growth of bacterial cultures. *Annual Review of Microbiology* 3:371–394.

Mulleneers HAE, 2001. *Selective separation of very small particles by flotation. In relation to soil and sediment remediation*. PhD-thesis Wageningen University. Wageningen.

Murayama S, 1984. Decomposition kinetics of straw saccharides and synthesis of microbial saccharides under field conditions. *Journal of Soil Science* 35:231–242.

Nam K, Alexander M, 1998. Role of nanoporosity and hydrophobicity in sequestration and bioavailability: test with model solids. *Environmental Science & Technology* 32:71–74.

NEN (Nederlands Normalisatie Instituut), 1997. *NEN 5733. Bodem. Bepaling van het gehalte aan minerale olie in grond en waterbodem met gaschromatografie*. NEN, Delft.

NEN (Nederlands Normalisatie Instituut), 1999. *NEN 5771. Bodem-Waterbodem. Bepaling van de gehalten aan polycyclische aromatische koolwaterstoffen met hogedrukvloeistofchromatografie*. NEN, Delft.

Nocentini M, Pinelli D, 2001. Biodegradation of PAHs in aggregates of a low permeability soil. *Soil & Sediment Contamination* 10:211–226.

Nocentini M, Pinelli D, Fava F, 2000. Bioremediation of a soil contaminated by hydrocarbon mixtures: the residual concentration problem. *Chemosphere* 41:1115–1123.

Noordkamp ER, 1999. *Remediation of soils, sediments and sludges by extraction with organic solvents*. PhD-thesis Wageningen Agricultural University. Wageningen.

Noordkamp ER, Grotenhuis JTC, Rulkens WH, 1997. Selection of an efficient extraction method for the determination of polycyclic aromatic hydrocarbons in contaminated soil and sediment. *Chemosphere* 35:1907–1917.

Oades JM, 1993. The role of biology in the formation, stabilization and degradation of soil structure. *Geoderma* 56:377–400.

Olsen PA, Haugen LE, 1998. A new model of the shrinkage characteristic applied to some Norwegian soils. *Geoderma* 83:67–81.

Park SS, Jaffé PR, 1996. Development of a sediment redox potential model for the assessment of postdepositional mobility. *Ecological Modelling* 91:169–181.

Parr LF, Gardner WR, Elliot LF, 1981. *Water potential relations in soil microbiology*. Proceedings of a symposium sponsored by Divisions S-1 and S-3 of the Soil Science Society of America, 3–8 December 1978, Chicago IL, SSSA Special Publication No. 9. Soil Science Society of America, Madison WI.

Partheniades E, 1965. Erosion and deposition of cohesive soils. *ASCE Journal of the Hydraulics Division* 91:105–139.

Patrick WH, Gambrell RP, Faulkner SP, 1996. Redox measurements of soils. In: Sparks DL (Ed.). *Methods of soil analysis. Part 3. Chemical methods*. SSSA book series no. 5, pp 1255–1273. Soil Science Society of America, Madison WI.

Penman LH, 1940. Gas and vapour movement in the soil. I. The diffusion of vapours through porous solids. *Journal of Agricultural Science* 30:437–461.

Perrier E, Garnier P, Leclerc C, 2002. ECOUL: an interactive computer tool to study hydraulic behavior of swelling and rigid soils. *Computers & Geosciences* 28:1107–1118.

PHB (Project Hergebruik Baggerspecie), 1995. *Klei uit baggerspecie. Inventarisatie oude rijpingskennis*. Projectbureau Hergebruik Baggerspecie. Rapport W-DWW-95-346. DWW, Ministerie van Verkeer en Waterstaat,. Delft.

PHB (Projectbureau Hergebruik Baggerspecie), 1996. *Klei uit baggerspecie (Deel 2). Chemische aspecten bij rijpen en nuttig toepassen van verontreinigde baggerspecie*. Rapport W-DWW-96-043. DWW, Ministerie van Verkeer en Waterstaat, Delft.

PHB (Projectbureau Hergebruik Baggerspecie), 1997. *Klei uit baggerspecie (Deel 5). Inventarisatie rijpingskennis in het buitenland*. DWW rapport 97.032. DWW, Ministerie van Verkeer en Waterstaat, Delft.

Philip JR, 1969. Moisture equilibrium in the vertical in swelling soils. I. Basic theory. *Australian Journal of Soil Research* 7:99–120.

Poelman JNB, 1975. Dichtheid van de vaste delen van rivierkleigronden. *Boor en Spade* 19:32–38.

Pons LJ, Van der Molen WH, 1973. Soil genesis under dewatering regimes during 1000 years of polder development. *Soil Science* 116:228–235.

Pons LJ, Zonneveld IS, 1965. *Soil ripening and soil classification. Initial soil formation in alluvial deposits and a classification of the resulting soils*. Publication 13, International Institute for Land Reclamation and Improvement. Veenman & Zonen, Wageningen.

POSW (Programma Ontwikkeling Saneringsprocessen Waterbodems), 1995. *Landfarming van baggerspecie: laboratorium- en praktijkonderzoek. Eindrapport (deel 2)*. POSW fase II (1992 – 1996). RIZA rapport 95.013. RIZA, Ministerie van Verkeer en Waterstaat, Lelystad.

POSW (Programma Ontwikkeling Saneringsprocessen Waterbodems), 1997. *Eindrapport Programma Ontwikkeling Saneringsprocessen Waterbodems*. POSW fase II (1992 – 1996). RIZA Rapport 97.026. RIZA, Ministerie van Verkeer en Waterstaat, Lelystad.

POSW (Programma Ontwikkeling Saneringsprocessen Waterbodems), 1997a. *Intensieve landfarming van verontreinigde baggerspecie: ontwatering en afbraak (deel 32)*. POSW fase II (1992 – 1996). RIZA rapport 97.071. RIZA, Ministerie van Verkeer en Waterstaat, Lelystad.

POSW (Programma Ontwikkeling Saneringsprocessen Waterbodems), 1997b. *Mogelijkheden van extensieve landfarming voor biologische reiniging van baggerspecie (deel 33)*. POSW fase II (1992 – 1996). RIZA rapport 97.072. RIZA, Ministerie van Verkeer en Waterstaat, Lelystad.

Press WH, Teukolsky SA, Vetterling WT, Flannery BP, 1992. *Numerical recipes in Fortran 77. The art of scientific computing.* (2nd edition). Cambridge University Press, New York NY.

Priesack E, Achatz S, Stenger R, 2001. Parameterization of soil nitrogen transport models by use of laboratory and field data. In: Shaffer MJ, Ma L, Hansen S (Eds.). *Modeling carbon and nitrogen dynamics for soil management*. pp 459–481. Lewis Publishers, Boca Raton FL.

Quantin C, Joner EJ, Portal JM, Berthelin J, 2005. PAH dissipation in a contaminated river sediment under oxic and anoxic conditions. *Environmental Pollution* 134:315–322.

Radford PJ, Greenwood DJ, 1970. The simulation of gaseous diffusion in soils. *Journal of Soil Science* 21:304–313.

Rappoldt C, 1990. The application of diffusion models to an aggregated soil. *Soil Science* 150:645–661.

Rappoldt C, 1995. Measuring the millimetre-scale oxygen diffusivity in soil using microelectrodes. *European Journal of Soil Science* 46:169–177.

Rappoldt C, Crawford JW, 1999. The distribution of anoxic volume in a fractal model of soil. *Geoderma* 88:329–347.

Rappoldt C, Verhagen JHG, 1999. Equivalent cylinder systems representing the soil matrix in diffusion-reaction models for an aggregated soil. *Transport in Porous Media* 37:1–24.

Reemtsma T, Savric I, Jekel M, 2003. A potential link between the turnover of soil organic matter and the release of aged organic contaminants. *Environmental Toxicology & Chemistry* 22:760–766.

Reid BJ, Jones KC, Semple KT, 2000. Bioavailability of persistant organic pollutants in soils and sediments – a perspective on mechanisms, consequences and assessment. *Environmental Pollution* 108:103–112.

Richards LA, 1931. Capillary conduction of liquids through porous mediums. *Physics* 1:318–333.

Riis V, Babel W, Pucci OH, 2002. Influence of heavy metals on the microbial degradation of diesel fuel. *Chemosphere* 49:559–568.

Rijniersce K, 1983. *Een model voor de simulatie van het fysische rijpingsproces van gronden in de IJsselmeerpolders.* Proefschrift Landbouwhogeschool Wageningen. Wageningen.

Rijniersce K, 1984. Crack formation in newly reclaimed sediments in the IJsselmeerpolders. In: Bouma J, Raats, PAC (Eds.). *Proceedings of the ISSS symposium on water and solute movement in heavy clay soils*. 27 – 31 August 1984, Wageningen, ILRI publication 37, pp 59–62. ILRI, Wageningen.

Rijtema PE, Groenendijk P, Kroes JG, 1999. *Environmental impact of land use in rural regions. The development, validation and application of model tools for management and policy analysis*. Series on environmental science and management. Volume 1. Imperial College Press, London.

Ritchie JT, Adams JE, 1974. Field measurement of evaporation from soil shrinkage cracks. *Soil Science Society of America Proceedings* 38:131–134.

Roels JA, 1983. *Energetics and kinetics in biotechnology*. Elsevier Biomedical Press, Amsterdam.

Rolston DE, 1986. Gas diffusivity. In: Klute A (Ed.). *Methods of soil analysis. Part 1. Physical and mineralogical methods.* Agronomy Monograph no. 9 (2nd edition), pp 1089–1102. American Society of Agronomy, Madison WI.

Ross S, 1989. *Soil processes. A systematic approach.* Routledge, London.

Salanitro JP, Dorn PB, Huesemann MH, Moore KO, Rhodes IA, Rice Jackson LM, Vipond TE, Western MM, Wisniewski HL, 1997. Crude oil hydrocarbon bioremediation and soil ecotoxicity assessment. *Environmental Science & Technology* 31:1769–1776.

Saxena A, Bartha R, 1983. Microbial mineralization of humic acid-3,4-dichloroaniline complexes. *Soil Biology & Biochemistry* 15:59–62.

Scanlon BR, Andraski BJ, Bilskie J, 2002. Miscellaneous methods for measuring matric or water potential. In: Dane JH, Topp GC (Eds.). *Methods of soil analysis. Part 4. Physical methods*. No. 5 in the Soil Science Society of America book series, pp 643–670. SSSA, Madison WI.

Schwaerter S, Søndergaard M, Riemann B, Jensen LM, 1988. Respiration in eutrophic lakes: the contribution of bacterioplankton and bacterial growth yield. *Journal of Plankton Research* 10:515–531.

Selley RC, 1976. *An introduction to sedimentology*. Academic Press, London.

Semple KT, Morriss WJ, Paton I, 2003. Bioavailability of hydrophobic organic contaminants in soils: fundamental concepts and techniques for analysis. *European Journal of Soil Science* 54:809–818.

Sepers AB, 1981. The aerobic mineralization of amino acids in the saline Lake Grevelingen and the freshwater Haringvliet basin (The Netherlands). *Archiv für Hydrobiologie* 92:114–129.

Sextone AJ, Revsbech NP, Parkin TB, Tiedje JM, 1985. Direct measurement of oxygen profiles and denitrification rates in soil aggregates. *Soil Science Society of America Journal* 49:645–651.

Shiel RS, Adey MA, Lodder M, 1988. The effect of successive wet/dry cycles on aggregate size distribution in a clay texture soil. *Journal of Soil Science* 39:71–80.

Sierra J, Renault P, 1995. Oxygen consumption by soil micro-organisms as affected by oxygen and carbon levels. *Applied Soil Ecology* 2:175–184.

Sierra J, Renault P, Valles V, 1995. Anaerobiosis in saturated soil aggregates: modelling and experiment *European Journal of Soil Science* 46:519–531.

Singh SP, Ma LQ, Tack FMG, Verloo MG, 2000. Trace metal leachability of land-deposited dredged sediments. *Journal of Environmental Quality* 29:1124–1132.

Singh SP, Tack FMG, Verloo MG, 1998. Land disposal of heavy metal contaminated dredged sediments: a review of environmental aspects. *Land Contamination & Reclamation* 6:149–158.

Smiles DE, 2000. Hydrology of swelling soils: a review. *Australian Journal of Soil Research* 38:501–521.

Smit M, Grotenhuis T, Rulkens W, 2005. Role of bioavailability and biodegradability to determine emission control options for polluted sediments. In: Uhlmann G, Annokée F, Arendt F (Eds.). *ConSoil 2005*. Proceedings of the ninth international FZK/TNO conference on soil-water systems, 3 – 7 October 2005, Bordeaux, France, pp 638–646. Forschungszentrum Karlsruhe, Eggenstein-Leopoldshafen.

Smith KA, 1980. A model for the extent of anaerobic zones in aggregated soils, and its potential application to estimates of nitrification. *Journal of Soil Science* 31:263–277.

Soil Survey Staff, 1975. *Soil taxonomy. A basic system of soil classification for making and interpreting soil surveys*. Agricultural handbook no. 436, Soil Conservation Service. US Department of Agriculture, Washington DC.

Southard RJ, Buol SW, 1988. Subsoil blocky structure formation in some North Carolina Paleudults and Paleaquults. *Soil Science Society of America Journal* 52:1069–1076.

Sowers GF, 1965. Consistency. In: Black CA, Evans DD, White JL, Ensminger LE, Clark FE (Eds.). Methods of soil analysis. Part 1. No. 9 in the series Agronomy, pp 391–399. American Society of Agronomy, Madison, WI.

Stephens SR, Alloway BJ, Parker A, Carter JE, Hodson ME, 2001. Changes in leachability of metals from dredged canal sediments during drying and oxidation. *Environmental Pollution* 114:407–413.

Stowa (Stichting Toegepast Onderzoek Waterbeheer), 1998. *Karakterisering van met PAK verontreinigde baggerspecie voor biologische reiniging*. Stowa rapport 98.32. Stowa, Utrecht.

Stumm W, Morgan JJ, 1996. *Aquatic chemistry. Chemical equilibria and rates in natural waters* (3rd edition). John Wiley & Sons, New York NY.

Tabak HH, Lazorchak JM, Lei L, Khodadoust AP, Antia JE, Bagchi R, Suidan MT, 2003. Studies on bioremediation of polycyclic aromatic hydrocarbon-contaminated sediments: bioavailability, biodegradability, and toxicity issues. *Environmental Toxicology & Chemistry* 22:473–482.

Tack FM, Lapauw F, Verloo MG, 1997. Determination and fractionation of sulphur in a contaminated dredged sediment. *Talanta* 44:2185–2192.

TAW (Technische Adviescommissie voor de Waterkeringen), 1996. *Technische rapport klei voor dijken*. DWW, Ministerie van Verkeer en Waterstaat, Delft.

Taylor SA, 1949. Oxygen diffusion in porous media as a measure of soil aeration. *Soil Science Society of America Proceedings* 14:55–61.

Terzaghi K, Peck RB, 1967. *Soil mechanics in engineering practice* (2nd edition). John Wiley & Sons, New York NY.

Tichý R, Grotenhuis JTC, Rulkens WH, Nýdl V, 1996. Strategy for leaching of zinc from artificially contaminated soil. *Environmental Technology* 17:1181–1192.

TNO-MEP (Nederlandse organisatie voor toegepast onderzoek - Milieu, Energie en Procesinnovatie), 1997. *Ontwatering, rijping en landfarming van baggerspecie in een doorgangsdepot*. TNO-MEP-R97/053, TNO-MEP, Apeldoorn.

Trapp S, Karlson U, 2001. Aspects of phytoremediation of organic pollutants. *Journal of Soils and Sediments* 1:37–43.

Troeh FR, Jabro JD, Kirkham D, 1982. Gaseous diffusion equations for porous materials. *Geoderma* 27:239–253.

Utomo WH, Dexter AR, 1981a. Tilth mellowing. *Journal of Soil Science* 32:187–201.

Utomo WH, Dexter AR, 1981b. Soil friability. *Journal of Soil Science* 32:203–213.

Van Agteren MH, Keuning S, Janssen DB, 1998. *Handbook on biodegradation and biological treatment of hazardous organic compounds*. Kluwer Academic Publishers, Dordrecht.

Van Breemen N, Buurman P, 1998. *Soil Formation*. Kluwer Academic Publishers, Dordrecht.

Van Dam JC, 2000. Simulation of field-scale water flow and bromide transport in a cracked clay soil. *Hydrological Processes* 14:1101–1117.

Van Doren DM, Erickson AE, 1966. Factors affecting the platinum microelectrode method for measuring the rate of oxygen diffusion through the soil solution. *Soil Science* 102:23–28.

Van Duin RHA, 1976. *Bodemtechniek. Deel B. Aanwinning, rijping en in cultuur brengen van drooggevallen gronden*. Collegedictaat afdeling Cultuurtechniek. Landbouwhogeschool Wageningen, Wageningen.

Van Egmond Th, 1971. Het baggeren in relatie tot toemaken. *Boor en Spade* 17:82–90.

Van Genuchten MTh, 1980. A closed-form equation for predicting the hydraulic conductivity of unsaturated soils. *Soil Science Society of America Journal* 44:892–898.

Van Genuchten MTh, Leij FJ, Yates SR, 1991. *The RETC code for quantifying the hydraulic functions of unsaturated soils*. EPA/600/2-91. U.S. Environmental Protection Agency, Ada OK.

Van Mensvoort MEF, Dent DL, 1997. Acid sulphate soils. In: Lal R, Blum WH, Valentine C, Stewart BA (Eds.). *Methods for assessment of soil degradation*. Advances in Soil Science, pp 301–335. CRC Press, Boca Raton FL.

Van Olphen H, 1977. *An introduction to clay colloid chemistry. For clay technologists, geologists and soil scientists* (2nd edition). John Wiley & Sons, New York NY.

Van Schreven DA, 1962. De microbiologische rijping der gronden in de IJsselmeerpolders. In: Smits H, Zuur AJ, Van Schreven DA, Bosma WA (Eds.). *Van Zee tot Land 32*. pp 34–70. Tjeenk Willink, Zwolle.

Van Schreven DA, Harmsen GW, 1967. Soil bacteria in relation to the development of polders in the region of the former Zuider Zee. In: Gray TRG, Parkinson D (Eds.). *The ecology of soil bacteria*. pp 474–499. Liverpool University Press, Liverpool.

Van Tol AF, 1985. Consolidatie en rijping van baggerspecie. *Bouwkunde en Civiele techniek* 6:35–42.

Van Veen JA, Ladd JN, Amato M, 1985. Turnover of carbon and nitrogen through the microbial biomass in a sandy loam and a clay soil incubated with [^{14}C(U)]glucose and [^{15}N]$(HH_4)_2SO_4$ under different moisture regimes. *Soil Biology & Biochemistry* 17:747–756.

Vermeulen J, Bruning H, Grotenhuis JTC, Rulkens WH, 2004. Modeling oxygen diffusion during ripening of land-deposited clayey dredged sediments. In: Magar VS, Kelley ME (Eds.). *In Situ and On-Site Bioremediation – 2003*. Proceedings of the seventh International In Situ and On-Site Bioremediation symposium, 2 – 5 June 2003, Orlando FL, Paper N-09. Battelle Press, Columbus OH.

Vermeulen J, Grotenhuis T, Joziasse J, Rulkens W, 2003. Ripening of dredged sediments during temporary upland disposal. A bioremediation technique. *Journal of Soils and Sediments* 3:49–59.

Vermeulen J, Grotenhuis JTC, Rulkens WH, 2002. PAH and mineral oil biodegradation in aggregates with anoxic centres. In: Pallei M, Porta A, Hinchee RE (Eds.). *Characterization of Contaminated Sediments*. Proceedings of the first International Conference on Remediation of Contaminated Sediments, 10 – 12 October 2001, Venice, Volume 1, pp 173–180. Battelle Press, Columbus, OH.

Vermeulen J, Van Dijk S, Grotenhuis JTC, Joziasse J, Rulkens WH, 2000. Accelerated physical ripening of PAH and oil contaminated sediment to distinguish critical steps in remediation. In: *Contaminated Soil 2000*. Proceedings of the seventh International FZK/TNO Conference on contaminated soil, 18 - 22 September 2000, Leipzig, Volume 2, pp 1184–1185. Thomas Telford, London.

Vermeulen J, Van Dijk SG, Grotenhuis JTC, Rulkens WH, 2005. Quantification of physical properties of dredged sediments during physical ripening. *Geoderma* 129:147–166.

Vermeulen J, Van Gool MPM, Dorleijn AS, Joziasse J, Rulkens WH, Grotenhuis JTC, Submitted a. Biochemical ripening of dredged sediments during temporary upland disposal. 1 Kinetics of biological soil organic matter mineralization and chemical sulfur oxidation.

Vermeulen J, Van Gool MPM, Mentink GH, Joziasse J, Rulkens WH, Grotenhuis JTC, Submitted b. Biochemical ripening of dredged sediments during temporary upland disposal. 2 Degradation of PAH and TPH in slurried and consolidated sediments.

Vervoort RW, Radcliffe DE, West LT, 1999. Soil structure development and preferential solute flow. *Water Resources Research* 35:913–928.

Visscher PT, Beukema J, Van Gemerden H, 1991. In situ characterization of oxygen and sulfide profiles with a novel combined needle electrode. *Limnology and Oceanography* 36:1476–1480.

Voroney RP, Paul EA, 1984. Determination of k_C and k_N *in situ* for calibration of the chloroform fumugation-incubation method. *Soil Biology & Biochemistry* 16:9–14.

Vulliet L, Laloui L, Harding R, 2002. Environmental geomechanics: an introdution. In: Vulliet L, Laloui L, Schreffer B (Eds.). *Environmental geomechanics* (1st edition), pp 59–68. Presses polytechnique et universitaires romandes, Lausanne, Switzerland.

Watts CW, Dexter AR, 1998. Soil friability: theory, measurement and the effects of management and organic matter content. *European Journal of Soil Science* 49:73–84.

Werkgroep Herziening Cultuurtechnisch Vademecum, 1988. *Cultuurtechnisch vademecum*. Cultuurtechnische vereniging, Utrecht.

White JC, Kelsey JW, Hatzinger PB, Alexander M, 1997. Factors affecting sequestration and bioavailability of phenanthrene in soils. *Environmental Toxicology & Chemistry* 16:2040–2045.

Wichman BGHM, 1999. *Consolidation behaviour of gassy mud: theory and experimental validation.* PhD-thesis Delft University of Technology. Delft.

Wilding LP, Hallmark CT, 1984. Development of structural and microfabric properties in shrinking and swelling clays. In: Bouma J, Raats PAC (Eds.). *Proceedings of the ISSS symposium on water and solute movement in heavy clay soils*. 27 – 31 August 1984, Wageningen, pp 1–18. ILRI, Wageningen.

Willet JR, 1972. Bodemfysisch gedrag van opgespoten baggerspecie uit de Rotterdamse havens (Het begreppelen van de Rotterdamse baggerdepots). *De Ingenieur, Bouw en Waterbouwkunde* 1:B1–B12.

Willet JR, 1985. Nuttig gebruik van slibsoorten. *Heidemijtijdschrift* 96:104–108.

Willet JR, Cavelaars JC, 1981. Milieu-aspecten bij toepassing van 'gerijpte' baggerspecie in dijkbouw. *Polytechnisch Tijdschrift, bouwkunde, wegen- en waterbouw* 36:587–593.

Wilson C, Jones KC, 1993. Bioremediation of soil contaminated with polynuclear aromatic hydrocarbons (PAHs): a review. *Environmental Pollution* 81:229–249.

Wösten JHM, Van Genuchten MTh, 1988. Using texture and other soil properties to predict the unsaturated hydraulic functions. *Soil Science Society of America Journal* 52:1762–1770.

Yaalon DH, Kalmar D, 1984. Extent and dynamics of cracking in a heavy clay soil with xeric moisture regime. In: Bouma J, Raats PAC (Eds.). *Proceedings of the ISSS symposium on water and solute movement in heavy clay soils*. 27 – 31 August 1984, Wageningen, pp 45–48. ILRI, Wageningen.

Yong RN, Siu SKH, Sheeran DE, 1983. On the stability and settling of suspended solids in settling ponds. Part I. Piece-wise linear consolidation analysis of sediment layer. *Canadian Geotechnical Journal* 20:817–826.

Young MH, Sisson JB, 2002. Tensiometry. In: Dane JH, Topp GC (Eds.). *Methods of soil analysis. Part 4. Physical methods*. No. 5 in the Soil Science Society of America Book Series, pp 575–606. SSSA, Madison WI.

Zausig J, Stepniewski W, Horn R, 1993. Oxygen concentration and redox potential gradients in unsaturated model aggregates. *Soil Science Society of America Journal* 57:908–916.

Zevenbergen CW, De Haan W, Peekel AF, Folkerts H, Polderman WM, 1999. Field monitoring of physical and chemical processes during ripening of dredged sediments in transit deposits with emphasis on acidification. In: De Schutter G (Ed.). *Characterisation and treatment of sediments*. Proceedings of CATS 4 conference, 15 – 17 September 1999, Antwerpen, pp 133–142. Technologisch Instituut, Antwerpen.

PUBLICATIONS

Papers in journals

Vermeulen J, Van Dijk SG, Grotenhuis JTC, Rulkens WH, 2005. Quantification of physical properties of dredged sediments during physical ripening. *Geoderma* 129:147–166.

Malina G, Vermeulen J, Kromer M, 2004. Natlenianie zanieczyszczonych osadów dennych podczas tymczasowego składowania. *Engineering and Protection of Environment* 7:401–419.

Vermeulen J, Grotenhuis JTC, Joziasse J, Rulkens WH, 2003. Ripening of clayey dredged sediments during temporary upland disposal. A bioremediation technique. *Journal of Soils and Sediments* 3:49–59.

Steenhuis TS, Van Es HM, Parlange J-Y, Baveye PC, Walter MF, Geohring LD, Hutson JL, Richard TL, Bell JL, Boll J, Gannon J, Liu Y, Sanford WE, Alexander M, Bryant RB, Selker JS, Tan Y, Vandevevere P, Verheyden SML, Vermeulen J, 1991. Hydrology and the environment. *New York's Food & Life Sciences Quarterly* 20:15–19.

Papers in conference proceedings

Vermeulen J, Bruning H, Grotenhuis JTC, Rulkens WH, 2004. Modeling oxygen diffusion during ripening of land-deposited clayey dredged sediments. In: Magar VS, Kelley ME (Eds.). *In Situ and On-Site Bioremediation - 2003*. Proceedings of the seventh International In Situ and On-Site Bioremediation symposium, 2 – 5 June 2003, Orlando FL, Paper N-09. Battelle Press, Columbus OH.

Vermeulen J, Grotenhuis JTC, Rulkens WH, 2002. PAH and mineral oil biodegradation in aggregates with anoxic centres. In: Pallei M, Porta A, Hinchee RE (Eds.). *Characterization of Contaminated Sediments*. Proceedings of the first International Conference on Remediation of Contaminated Sediments, 10 – 12 October 2001, Venice, Volume 1, pp 173–180. Battelle Press, Columbus OH.

Hendriks RFA, Vermeulen J, 2000. Effect of temperature on decomposition of organic matter. In: Rochefort L, Daigle JY (Eds.). *Sustaining our Peatlands*. Proceedings of the 11th International Peat Congress, 6 – 12 August 2000, Québec, Volume I, pp 422–427. Canadian Society for Peat and Peatlands & International Peat Society, Edmonton.

Hendriks RFA, Vermeulen J, 1997. Effect of temperature on decomposition of organic matter in Dutch peat soils. In: Schmilewski, G (Ed.). *Peat in Horticulture – its use and sustainability* –. Proceedings of the International Peat Conference, 2 – 7 November 1997, Amsterdam, pp 163–167. International Peat Society, Jyskä.

Van Es HM, Steenhuis TS, Geohring LD, Vermeulen J, Boll J, 1991. Movement of surface-applied and soil-embodied chemicals to drainage lines in a well-structured soil. In: Gish TJ, Shirmohammadi A (Eds.). *Preferential Flow*. Proceedings of the National Symposium, 16 – 17 December 1991, Chicago IL, pp 59–67. American Society of Agricultural Engineers, St. Joseph MI.

Abstracts

Vermeulen J, Van Dijk S, Grotenhuis JTC, Joziasse J, Rulkens WH, 2000. Accelerated physical ripening of PAH and oil contaminated sediment to distinguish critical steps in remediation. In: *Contaminated Soil 2000*. Proceedings of the seventh International FZK/TNO Conference on contaminated soil, 18 – 22 September 2000, Leipzig, Volume 2, pp 1184–1185. Thomas Telford, London.

Vermeulen J, Grotenhuis JTC, Rulkens WH, Joziasse J, 1999. Clean-up of PAH and mineral oil polluted sediment during temporary disposal. In: Lexmond M (Ed.). *Bodem Breed '99*. Samenvatting van de voordrachten en posters 11e Nationaal Symposium Bodemonderzoek, 29 – 30 november, Lunteren, p 225. Stichting Kennisontwikkeling en kennisoverdracht Bodem, Gouda.

Steenhuis TS, Geohring LD, Van Es HM, Boll J, Vermeulen J, 1990. Fast flow of chemicals in the vadose zone American Geophysical Union Fall 1990 Meeting, 3–7 December 1990, San Francisco CA. *EOS, Transactions, American Geophysical Union 71*(43): 1307.

Research reports

Vermeulen J, Elsman MA, 1999. *Fysische rijping van baggerspecie. Modelstudie – koppeling tussen geotechniek en cultuurtechniek.* AKWA rapport 99.016. Dienst Weg- en Waterbouwkunde, Rijkswaterstaat, Delft.

Vermeulen J, Hendriks RFA, 1996. *Bepaling van afbraaksnelheden van organische stof in laagveen. Ademhalingsmetingen aan ongestoorde veenmonsters in het laboratorium.* DLO-SC Rapport 288. DLO Staring Centrum, Wageningen.

Submitted papers

Vermeulen J, Van Gool MPM, Mentink GH, Joziasse J, Rulkens WH, Grotenhuis JTC. Biochemical ripening of dredged sediments during temporary upland disposal. 2. Degradation of PAH and TPH in slurried and consolidated sediments.

Vermeulen J, Van Gool MPM, Dorleijn AS, Joziasse J, Rulkens WH, Grotenhuis JTC. Biochemical ripening of dredged sediments during temporary upland disposal. 1. Kinetics of biological soil organic matter mineralization and chemical sulfur oxidation.

SUPERVISED MSC-THESES

Van Gool M, 2002. *Afbraakkinetiek van complexe organische stof en PAK en minerale olie in sedimenten.* Sectie Milieutechnologie, Wageningen Universiteit, Doctoraalverslag 02-017. Wageningen.

Kromer M, 2001. *Optimization of oxygenation for bioremediation of polluted sediments in a temporary disposal site.* Sub-department of Environmental Technology, Wageningen University, MSc-thesis 01-15. Wageningen.

Kaziród K, 2001. *Bioremediation of PAH and mineral oil polluted sediment in a temporary disposal site at different oxygenation levels.* Sub-department of Environmental Technology, Wageningen University, MSc-thesis 01-14. Wageningen.

Dorleijn AS, 2000. *Redoxpotentiaalveranderingen tijdens chemische rijping van baggerspecie*. Sectie Milieutechnologie, Wageningen Universiteit, Doctoraalverslag 00-28. Wageningen.

Van Dijk S, 1999. *Diffusie van zuurstof in rijpende baggerspecie.* Sectie Milieutechnologie, Wageningen Universiteit, Doctoraalverslag 99-35. Wageningen.

Mentink G, 1999. *Bepaling van de afbraak van PAK en minerale olie in gedeeltelijk ontwaterde baggerspecie*. Sectie Milieutechnologie, Landbouwuniversiteit Wageningen, Doctoraalverslag 99-26. Wageningen.

DANKWOORD

Toen ik aan dit aio-onderzoek begon hebben veel van mijn vrienden en kennissen mij gewaarschuwd voor allerlei onheil dat ik hierdoor over mij afriep. Terugkijkend op de afgelopen acht jaar moet ik toegeven dat veel van hun waarschuwingen inderdaad zijn uitgekomen en dat mij niet veel reguliere aio-tegenslagen bespaard zijn, maar desondanks heb ik er geen spijt van dat ik de stap richting dit onzekere maar spannende bestaan toch gemaakt heb. Veel grotere spijt zou ik immers hebben als het me nooit gelukt was de door mij lang begeerde aio-aanstelling te krijgen en het hele 'aio-proces' van begin tot eind te doorlopen. Verder ben ik blij dat ik door aio te worden, heb kunnen samenwerken met een heel grote groep mensen die ik anders nooit had leren kennen. Bij mijn onderzoek zijn teveel mensen betrokken geweest om allemaal persoonlijk te bedanken, maar de belangrijkste zal ik hier noemen.

Als eerste bedank ik mijn promotor Wim Rulkens en copromotor Tim Grotenhuis voor het vertrouwen dat zij in mij hebben gesteld bij mijn aanstelling als aio en de vrijheid die ze mij hebben gegeven bij het uitvoeren van mijn promotieonderzoek. Wim en Tim, door jullie oog voor wetenschappelijke diepgang en detail (Tim) en maatschappelijke relevantie en brede kijk (Wim) vormden jullie een perfect begeleidingsteam. Vragen als "wat bedoel je?" en "wat beoog je?" zullen me nog lang bij blijven. Ook bedank ik Jan Joziasse die namens TNO (de bekostiger van mijn salaris), zij het op iets meer afstand, altijd erg betrokken is geweest bij mijn onderzoek en bij het becommentariëren van door mij geproduceerde teksten.

Mijn onderzoek was niet mogelijk geweest zonder verontreinigde bagger. Voor de hulp bij het opsporen ervan bedank ik Marjan Euser (Baggernet). Voor het beschikbaar stellen en hun hulp bij het bemonsteren van geschikt onderzoeksmateriaal bedank ik Valery van den Brand (Gemeentewerken Rotterdam), Jan Ros (Provincie Utrecht), Viktor van Kekum (Adviesbureau Iwaco), Henk Hidding en Uilke Hoekstra (Ingenieursbureau Oranjewoud), Ruud Kampf en Patrick Mensonides (Hoogheemraadschap Uitwaterende Sluizen), Marco Schut (Waterschap Groot-Geestmerambacht), Joop Harmsen en Antonie van den Toorn (Alterra) en Cor Sonneveld (proefboerderij Oostwaardhoeve).

Helemaal onmisbaar was de grote bijdrage van de studenten die in het kader van hun studie een aantal maanden verschillende rijpingsprocessen hebben bestudeerd: Geert, Suzanne, Arne, Magda, Katja en Martine. Alle studenten, aio's, PhD-studenten en postdocs die de afgelopen acht jaar deel uitmaakten van de bodemgroep van de sectie ook hartelijk bedankt. Onmisbaar binnen de bodemgroep was uiteraard de initiatiefnemer Tim, maar ook het rekenwonder Harry. Harry, zeer veel dank voor al die avonden die je hebt gestopt in het schrijven van de Fortran-code voor het zuurstofdiffusiemodel en het versleutelen van SWAP van een 'Euleriaans' in een 'Lagrangiaans' rekenend computermodel. Helaas – of misschien wel gelukkig – is van dit laatste op een paar regels tekst na, uiteindelijk niets terecht gekomen in mijn proefschrift. Martijn, dank voor de tijd die je altijd voor mij nam voor het aanhoren van mijn klachten over Microsoft pakketten.

Tijdens de opstartfase van het experimentele onderzoek heb ik veel gehad aan de hulp van Jan Theunissen (werkplaats), Gert Nieuwboer (glasblazerij), Sjoerd Hobma, Jo Ackerman en Vinnie de Wilde. Voor het mij wegwijs maken op het analytisch laboratorium bedank ik Johannes van der Laan, Ilse Gerrits en Hillion Wegh. Geert Meijer ben ik zeer veel dank verschuldigd voor alle tijd en energie die hij heeft gestopt in het operationeel krijgen van de gaschromatograaf voor de olieanalyses. Albert Boers (leerstoelgroep Bodemtechnologie) en Arjen van de Peppel (leerstoelgroep Tuinbouwproductieketens) ben ik zeer erkentelijk voor hun hulp bij de bepalingen van de aggregaatgroottes en de elementair C- en N-gehalten.

Heleen Vos, Manja Stulen, Anita van de Weerd, Gusta de Kaste bedankt voor jullie administratieve en secretariële ondersteuning. Liesbeth Kesaulya bedankt voor het zijn van het 'vaste baken' op de zevende verdieping. Alle kamergenoten die ik bij de sectie heb versleten, dank voor het dulden van mijn aanwezigheid. In chronologische volgorde waren het volgens mij Tim, Frank, Paula, Jan, Pim, Dale, Gabor, Ghada en Mariela. Alle 'oude' aio's bedank ik voor de erg gezellige lunches en uiteraard voor ons avontuur naar Guise. Deze eclipservaring staat samen met de uitstapjes die ik voor en met de sectie heb gemaakt naar Lunteren, Leipzich, Hannover, Venetië en Orlando voor altijd in mijn geheugen gegrift. En oh ja, voor ik het vergeet, Marjo bedankt dat jij er gewoon bent.

Nico, dank voor je tip actief te worden binnen WIMEK. Naast de contacten die ik al met andere aio's had tijdens de bijeenkomsten van het Kenniscentrum Bodembeheer en Saneringstechnologie (WUR/TNO), leerde ik hierdoor collega's kennen bij andere leerstoelgroepen van Wageningen Universiteit en bij andere universiteiten. Dit weten en voelen dat er 'lotgenoten' waren die ongeveer het zelfde doormaakten als ikzelf, heb ik ervaren als een enorme stimulans. Dat laatste brengt me bij mijn paranimfen. Corine en Carolien, jullie zijn bij elkaar getuige en deelgenoot geweest van veel van mijn wel en wee tijdens mijn volledige academische vorming. Jullie vriendschap heb ik altijd als erg waardevol ervaren en vanwege jullie enorme inlevingsvermogen heb ik jullie gevraagd mij bij te staan op mijn promotiedag. Bedankt dat jullie dit ook wilden doen!

Ten slotte alle andere collega's, vrienden, kennissen en familie bedankt voor de door jullie getoonde belangstelling door de jaren heen.

Hoewel ik er best wat langer van had willen genieten is er recent helaas een abrupt einde gekomen aan mijn formele relatie met Wageningen Universiteit, één van mijn grote liefdes. Nog belangrijker is daarom die andere grote liefde voor mij geworden. Jannie, je kent mij niet anders dan werkend aan mijn proefschrift. Dank voor je geloof in mij en dat je me niet voor gek hebt verklaard tijdens de jaren die je tot nu toe met mij hebt doorgemaakt. Dank ook voor de 'organoleptische' controle van mijn proefschrift. We staan samen voor een periode van wie weet grote veranderingen waarin ik misschien wel meer een 'normaal mens' zal worden. Ik hoop dat je ook dan nog even bij me wilt blijven!

Johan Vermeulen
Wageningen, december 2006

The research described in this thesis was supported by and performed within the Research Centre on Soil, Sediment and Groundwater Management and Remediation, a cooperation of Wageningen University and The Netherlands Organization for Applied Scientific Research

Credits

Printing and cover design: *Pons & Looijen BV, Wageningen*
Cover photo: *Hans Dijkstra*